Substructure Models for Dynamic Analysis of Floating Wind Turbines and the Effect of Hull Flexibility

Chih-Gang Hsu

July 23, 2019

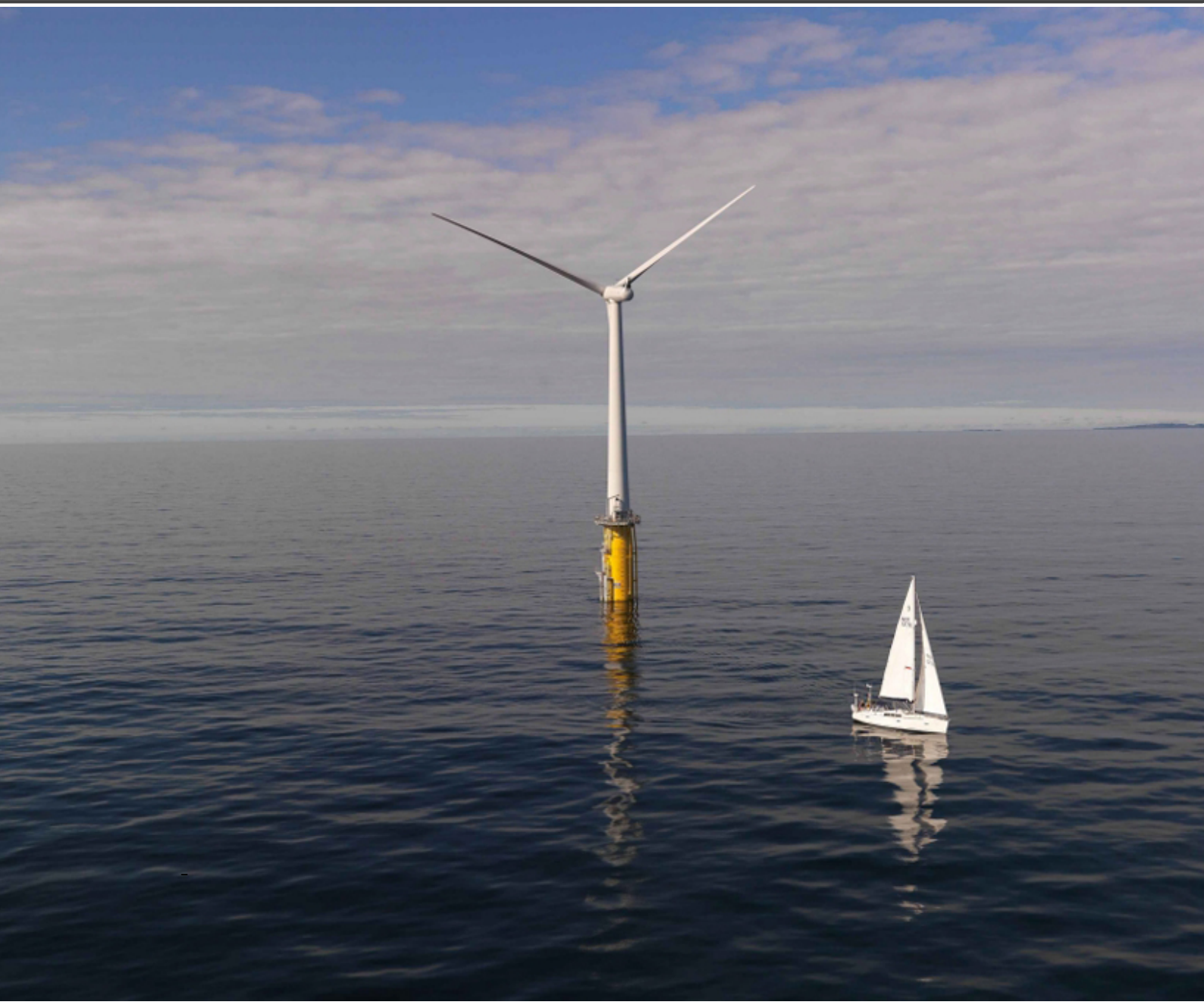

TU Delft NTNU SIEMENS Gamesa RENEWABLE ENERGY

Substructure models for dynamic analysis of floating wind turbines and the effect of hull flexibility

Master of Science Thesis

Author:	Chih-Gang Hsu	
Committee:	Prof. Andrei Metrikine	TU Delft - Chairman
	Dr. Antonio Jarquin Laguna	TU Delft
	Dr. Erin Elizabeth Bachynski	NTNU
	Ir. Nico Maljaars	Siemens Gamesa
	Ir. Corine De Winter	Siemens Gamesa

July 23, 2019

Abstract

In the simulation of floating wind turbines, a traditional rigid floater assumption becomes less valid while pursuing large size floating wind turbines with steel-efficient floaters. Up to date, hull flexibility still cannot be efficiently incorporated into aero-servo-elastic-hydro simulation tools, and the possible influence of hull flexibility has not yet been well-understood. Consequently, it is necessary to identify the significance of hull flexibility and the possible effect of it.

Recent researches have been investigating the influence of hull flexibility on sub-structural internal load, global responses and dynamics of the system. However, little has been done from a tower design perspective. Moreover, tower design for a floating foundation has also been seldom documented. To fill the knowledge gap, two research questions are defined: **What is the difference in tower design with a floating foundation?** and **What is the effect of hull flexibility on tower design?**.

To answer the first research question, a FEM model with rigid hull is built based on four floating concepts designed for DTU 10MW wind turbine[4]. The tower fore-aft bending natural frequencies are compared between fixed foundation and floating foundation. The second research question is answered by developing a FEM model with flexible hull based on a spar-buoy concept. The rigid hull model and the flexible hull model are compared by implementing structural analysis and fatigue damage estimation under waves load.

The result shows that the 1st tower bending natural frequency increases significantly(except for TLP) from a fixed foundation to a floating foundation, making it difficult to achieve a soft-stiff tower design. Furthermore, it is indicated that hull flexibility can decrease the 1st tower bending natural frequency, and the magnitude varies with different tower designs. A stiff-stiff tower decreases more while a soft-stiff decreases less. Lastly, the fatigue damage estimation implies that a soft-stiff design can be lack of fatigue strength to survive from waves load.

In conclusion, a soft-stiff tower design is difficult for large size floating wind turbine partly due to the increase in 1st tower bending natural frequency from fixed foundation to floating foundation, and partly because of strength requirement for fatigue load. As for a stiff-stiff tower design, without considering hull flexibility, there is a high uncertainty in the 1st tower bending natural frequency. As a result, for large size floating wind turbines, inclusion of hull flexibility is necessary for the tower design.

Acknowledgement

This MSc thesis is accomplished under the supervisions of Delft University of Technology(TU Delft), Norwegian University of Science and Technology(NTNU), and Siemens Gamesa Renewable Energy(SGRE). I would like to express my to sincere gratitude to them all to make this thesis possible.

Firstly, I want to thank to the chairman of the committee, Prof. Andrei Metrikine. I appreciate his sharp criticisms and feedback during each progress meeting. In addition, I would like to also thank to my supervisor Dr. Antonio Jarquin Laguna from TU Delft. I am thankful to his help on making all the administrative procedures smooth and easy for me. His feedback and guidance on writing also helped me to produce a better thesis. My appreciation also goes to my supervisors Ir. Nico Maljaars and Ir. Corine De Winter from SGRE. I am grateful for every meeting and discussion we had. Thank you for always pushing me to reflect on my understanding regarding the work I have done. I would like to give my special thanks to my supervisor Dr. Erin Elizabeth Bachynski from NTNU. It has been pleasure and honor to work with her. I am really grateful for her constant guidance and support throughout the whole period of this thesis project. Her feedback and comments are always insightful and straight to the point. Without her knowledge and experience I would have not been able to accomplish this thesis.

Furthermore, I would also like to share my joy and gratitude with every fellow student from EWEM program and from SGRE. Writing a thesis is not easy, but knowing that we are all going through the same thing certainly makes me feel less lonely. This journey has been wonderful because of you all.

Last but not least, I would like to give my biggest appreciation to my family in Taiwan, to my girlfriend, and to all my friends. Thank you for your support, your company, and your love.

謝謝我在臺灣的家人、我的女朋友、還有我所有的朋友們。謝謝你們一直以來的支持、陪伴跟關心，

Nomenclature

Abbreviations

CoG	Center of gravity
DoF	Degree of freedom
FEM	Finite element method
FLS	Fatigue limit state
FWT	Floating wind turbines
KC	Keulegan-Carpenter number
MAC	Modal assurance criterion
MFC	Multifreedom constraint
MSL	Mean sea level
PDE	Partial differential equations
PVD	Principle of virtual displacement
RAO	Response amplitude operator
RNA	Rotor nacelle assembly
Semi-sub	Semi-submersible
TLP	Tension leg platform
ULS	Ultimate limit state

List of Symbols

κ	Curvature
$\mathbf{E}$	Eigenmatrix
$\overline{BM}_x$	Distance between metacenter and buoyancy center
$\overline{GM}$	Distance between metacenter and gravity center
$\overline{KB}$	Distance between keel and buoyancy center
$\overline{KG}$	Distance between keel and gravity center
ϕ	Velocity potential or mode shape
ρ	Density
$\mathbf{A}$	Added mass matrix
$\mathbf{K}_{fl}$	Floater stiffness matrix
$\mathbf{K}_{tb}$	Wind turbine stiffness matrix
$\mathbf{M}_{fl}$	Floater mass matrix
$\mathbf{M}_{tb}$	Wind turbine mass matrix
ξ	Damping ratio
A	Cylinder cross section area or added mass
a	Ratio between T_H and w
a_b	Acceleration of the body
A_{11}	Surge hydrodynamic added mass
A_{15}	Surge hydrodynamic added mass due to pitch motion
A_{51}	Pitch hydrodynamic added mass due to surge motion
A_{55}	Pitch hydrodynamic added mass
B	Damping
C_D	Drag coefficient

C_m	Hydrodynamic mass coefficient
C_T	Thrust force coefficient
C_{55}	Hydrostatic stiffness
D	Cylinder diameter
D_C	Diameter of the platform column
EA	Axial stiffness
EI	Bending stiffness
F_B	Buoyancy force
F_T	Thrust force
g	Gravitational constant
h	Water depth
I_x	Second moment of area of water plane around x axis
I_{fl}	Floater pitch inertia around mass center
k_i	Equivalent stiffness of one mooring line
K_{11}	Surge stiffness of TLP mooring
K_{31}	Heave stiffness of TLP mooring due to surge motion
K_{33}	Heave stiffness of TLP mooring
K_{51}	Pitch stiffness of TLP mooring due to surge motion
K_{55}	Pitch stiffness of TLP mooring
K_{mr}	Equivalent mooring line stiffness
l_s	Arc length of the mooring line
m	Cylinder mass
M_{tot}	Total mass of the floating wind turbine

p	Water pressure
r_o	Radius of the cylinder
s	Arc length of one segment of the mooring line
$S_{\eta\eta}$	Energy spectrum of wave elevation
$S_{\sigma\sigma}$	Energy spectrum of stress
T_0	Line tension of TLP mooring system
T_H	Horizontal tension of mooring line
U	Velocity of water particle
U_b	Velocity of the body
u_i	Degree of freedom(i=1,2,...)
V	Volume
w	Mooring line weight per unit length in water
X	Wave excitation force or response amplitude
z_B	Distance of buoyancy center below MSL
z_b	Location of center of buoyancy
z_G	Distance of gravity center below MSL
z_{fl}	Location of floater center of mass
z_{mr}	Location of fairlead
z_{tb}	Tower base elevation above MSL

Contents

List of Figures

List of Tables

Chapter 1

Introduction

1.1 Background

1.1.1 Floating Wind Turbines

Ever since the first offshore wind farm[55] was built in 1991, it has been proven that offshore wind turbine is not only a feasible technology but also an economic one. However, despite the success over the last few decades, offshore wind energy is still limited to shallow water due to its bottom fixed foundation.

Almost 20 years after the first offshore wind farm, in 2009, a demo project with a floating foundation, Hywind-demo, was tested in Norway. Later on, continuing with the successful test from Hywind-demo, the first floating wind farm in the history Hywind-Scotland was built and started to generate electricity in 2017.

There are undoubtedly many advantages of floating wind turbines over traditional bottom fixed ones. For instance, a floating foundation allows access to the abundant wind resources in the deep water area. Especially for countries like Japan or Norway, the shallow water area are limited and floating wind turbine is one of the solutions to develop offshore wind energy.

In addition, the installation of a floating foundation is more environmental-friendly compared to a bottom fixed foundation. Normally a traditional bottomed fixed foundation requires pile-driving activity, which produces huge noise that could potentially hurt marine mammals nearby[3]. For a floating foundation, only anchors and mooring lines need to be installed and thus pile-driving activity is not required.

1.1.2 Floating Concepts and Design

The design challenge of a floating platform for wind turbines is the difficulty in keeping stability due to the heavy weight(RNA) and the wind force at the top of the wind turbine. Three strategies are often considered to reach stability: ballast stabilized, waterplane stabilized and mooring stabilized. Based on the three methods, a stability triangle can be drawn (Figure 1.1). Every floating concept should fall somewhere in the triangle.

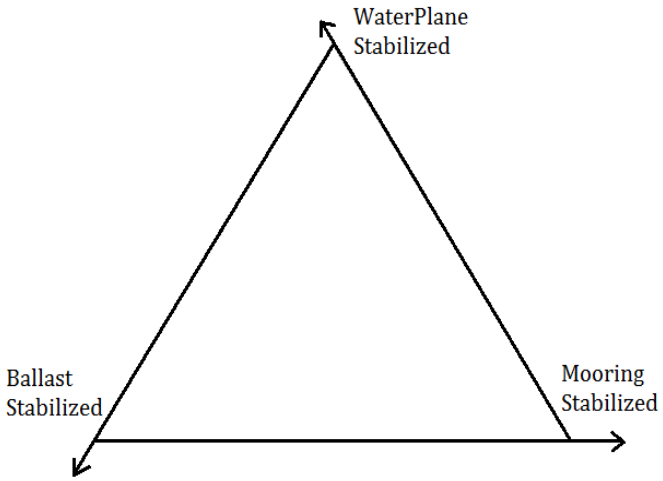

Figure 1.1: Stability triangle

In spite of the variety of floating concepts around the world, most of the concepts rely on one specific stability strategy, meaning most of the them fall at the three corners of the stability triangle. Accordingly three main categories are defined as illustrated in Figure 1.2. They are known as spar-buoy, semi-submersible(semi-sub) and tension leg platform(TLP).

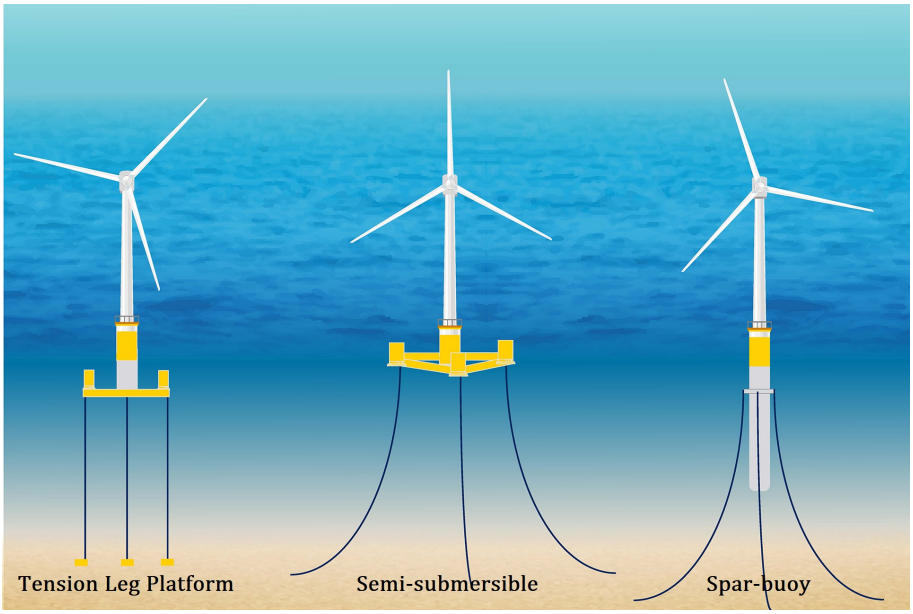

Figure 1.2: Three main floating concepts[10].

Spar-buoy

A typical spar-buoy concept consists of a long cylinder with deep draft, and has heavy ballast at the bottom to keep the center of gravity as low as possible to achieve stability. The simplicity of the design makes it more model-friendly. In addition, another advantage of a spar-buoy concept is its' small heave motion. However, it is only applicable to deep water due to draft requirement.

Semi-sub

A semi-sub concept often comprises of a shallow draft platform with a catenary mooring system. For a semi-sub the stability relies on the large water plane area moment of inertia. One of the advantages of semi-sub is the easier implementation for installation and maintenance. However, having large water plane area can result in large heave motion.

TLP

TLP has been widely used in the oil and gas industry. Unlike the other two concepts, TLP has buoyancy higher than the structural weight, and the extra buoyancy force is balanced out by the tension in the tendon legs. Essentially the system is stabilized by the pulling-down forces from the tendons, which makes the system very stiff and consequently very different dynamic behavior than the other two.

1.1.3 Dynamic Simulation of Floating Wind Turbines

The dynamics of a floating wind turbine is extremely complex due to the interaction between aerodynamics, hydrodynamics, control system and structural dynamics (aero-hydro-servo-elastic). Many nonlinearities exist in a floating wind turbine system, including the interaction between control system and aerodynamic load, the behavior of the mooring lines system, and the interaction between hydrodynamics and structural deformation. In order to capture these nonlinearities, a time domain model is required and it usually involves in several simulation tools coupled together, as shown in Table 1.1.

Historically, aero-servo-elastic time domain simulation tool is first built for onshore wind turbines and is later coupled with a potential flow solver(e.g. WAMIT) to calculate hydrodynamic load for floating wind turbines. The frequency dependent hydrodynamic coefficients from potential flow solver are passed to the time domain model by using convolution. Conventionally, the hydrodynamic coefficients are calculated based on rigid body assumption, which means the interaction between structural deformation and hydrodynamics is usually neglected. Alternatively, it is also possible to have a full time domain model in which the hydrodynamic calculation is also solved in the time domain(e.g. Orcaflex).

In addition, different from typical onshore aero-servo-elastic tool, SIMO-RIFLEX is first developed by MARINTEK specifically for moored offshore structures, and a sub-program AeroDyn(from FAST) is then incorporated by Bachynski[1], resulting in a SIMO-RIFLEX-AeroDyn combination.

Tools combination
FAST(or ADAMS)+AeroDyn+HydroDyn[26]
FAST+Charm3D[49]
FAST+TimeFloat[47]
BHAWC+Orcaflex[38]
SIMO+RIFLEX+AeroDyn[43]
HAWC2+WAMIT[6]
⋮

Table 1.1: Fully coupled non-linear simulation tools

Although a time domain model is able to capture nonlinear behaviors in the system, the downside of using a time domain model is having very computationally-demanding simulation.

In order to reduce the simulation time, it is also possible to have a fully linearized frequency domain model, but the trade-off is the inability to capture nonlinearities. For a linearized frequency domain model, Lupton[39] provided detailed formulations and methods to linearize a floating wind turbine system. Pegalajar-Jurado[44] demonstrated a quick load calculation by using a frequency based model QuLAF incorporated with state-of-art tools. Hegseth and Bachynski[20] developed a semi-analytical frequency domain model and validated it with a time domain model. These developed frequency domain models show the possibility of having a simulation tool for quick assessment of the dynamics of floating wind turbines.

Both time and frequency domain models are useful and they serve for different purposes. A time domain model is often required in a detailed design phase to accurately capture nonlinearities, while a frequency domain model is handy in preliminary design phase because it allows one to have a quick feeling on how the system will respond to any design modification.

1.2 Problem Statement

As mentioned in Sec. 1.1.3, in aero-hydro-servo-elastic floating wind turbine simulations, floater flexibility is rarely included. For small size floating wind turbines, the floater hull is much thicker than the tower due to consideration of hydrostatic pressure and also partly due to conservative design. This means the floater is usually much stiffer than the tower for small size floating wind turbines. As a result, assuming the floater as a rigid body could be a good approximation.

However, as the size of wind turbines gets larger, the tower also becomes thicker due to strength requirement, which means the tower is stiffer for large size floating wind turbines. Consequently, for a steel-efficient floater the conventional rigid body assumption may not be justified anymore. In other words, hull flexibility can be of importance for large size floating wind turbines.

Once hull flexibility is considered in the simulation, the complexity of the system can lead to an unreasonable computational time due to the coupling between several simulation tools. Up to date, simulation tools such as FAST[25] or SIMA[41] still cannot efficiently take into account for hull flexibility. As a result, it is important to identify the significance of hull flexibility and look into the possible effect of it.

The impact of hull flexibility can be roughly separated into a few parts. It might have influence on the global response of the platform rigid motions. It could lead to a change in dynamic properties of the system. It can result in different hydrodynamic load on the structure. Sometimes hull flexibility is important for evaluating the internal loads within the substructure.

In the following section, a literature review is made to identify what has been done in the past regarding the possible influences of hull flexibility mentioned above, and what has been neglected or rarely investigated. Research questions are accordingly defined based upon the identified knowledge gap.

1.3 Literature Review

Hydroelasticity

For a submerged body the hydrodynamic load is very often calculated in frequency domain by using potential flow theory combined with panels method[21] to integrate the pressure on the body surface. Essentially, in a wave-structure dynamic interaction problem the potential can be separated into diffraction and radiation, and for a rigid body the radiation potential only includes contribution from six rigid body motions. However, if structural deformation is considered, not only six rigid body motions but also flexible deformation should be taken into account in the radiation problem. The interaction between structural deformation and hydrodynamics is also known as hydroelasticity.

Although hydroelasticity effect has been studied since late 90s by Newman et al[42], most attention in the past comes from naval architect field and oil and gas industry. Therefore, prior researches mainly focus on structure like vessels or offshore platforms. On the other hand, up to date, offshore wind energy is still a new field, and the effect of hull flexibility on a floating wind turbine has just been noticed in recent years.

In research project LIFES50+[37], it is pointed out that hydroelasticity is a two-ways coupling effect between hydrodynamics and structural dynamics. There is one-way coupling approach by only considering the influence of hydrodynamic pressure on structural deformation but not the other way around, which is also called zeroth-order hydroelastic modeling. If the two-ways coupling effect is considered, it is known as first-order hydroelastic modeling.

Zeroth-Order Hydroelastic Modeling

Most of the potential flow solvers only provide hydrodynamic load and properties corresponding to six rigid body motions. For instance, the output of hydrodynamic added mass and radiation damping are usually six by six matrices. In other words, the outputs from potential flow solvers are the pressure already being integrated along the whole body surface. In order to obtain the sectional hydrodynamic load and properties, unless a potential flow solver can allow one to extract pressure by sections defined by the user, the sectional pressure needs to be recalculated by extracting the panels pressure from the potential flow solver.

As demonstrated by Svendsen[52], it is possible to extract panels pressure from WAMIT[56] and reprocess them in MATLAB to obtain sectional hydrodynamic load and properties which can then be used in FEM model for dynamic analysis. In Svendsen's work, a TLP concept with the NREL 5MW wind turbine[27] was studied, and it was indicated that hull flexibility led to increase in all natural periods. The largest increase was seen in heave(43%) and pitch/bending(18%) modes. In addition, it was also discovered that hull flexibility led to amplification of internal forces within the platform at certain frequencies and increase in RAOs at all frequencies.

Although from Svendsen's work the effect of hull flexibility for a TLP concept is investigated, the approach is based on zeroth-order hydroelastic modeling, which means the effect of structural flexibility on hydrodynamics is missing. Moreover, the size of the investigated floating wind turbine cannot be considered as a large size floating wind turbine.

First-Order Hydroelastic Modeling Implementation

To account for the influence of structural flexibility on hydrodynamics, Borg[6] demonstrated a method to incorporate substructural flexibility into hydrodynamic calculation by coupling aero-elastic tool HAWC2[33] with potential flow solver WAMIT. Essential, the flexible mode shape was obtained in an iterative scheme until the "wet flexible mode shape" converged. The wet flexible mode shape was then included as a new DoF in WAMIT for hydrodynamic calculation. The method is illustrated in Figure 1.3.

This approach was tested by a case study with a spar-buoy carrying the DTU 10MW wind turbine[4]. The case study demonstrated that the flexible mode did not have significant impact on the global response. However, from the substantial excitation of the flexible mode it was concluded that the inclusion of flexible modes can be important for more accurate internal loads within substructure.

The same method was applied to a triple-spar concept[7] carrying the DTU 10MW wind turbine, and it was extended to calculation of sectional load within the substructure. It was concluded that substructural flexible modes can be coupled with tower fore-aft bending mode and affect the bending moments within the structure.

However, from the works done by Borg, the influence of hull flexibility itself and hydroelasticity effect on hydrodynamic load was not clearly distinguished.

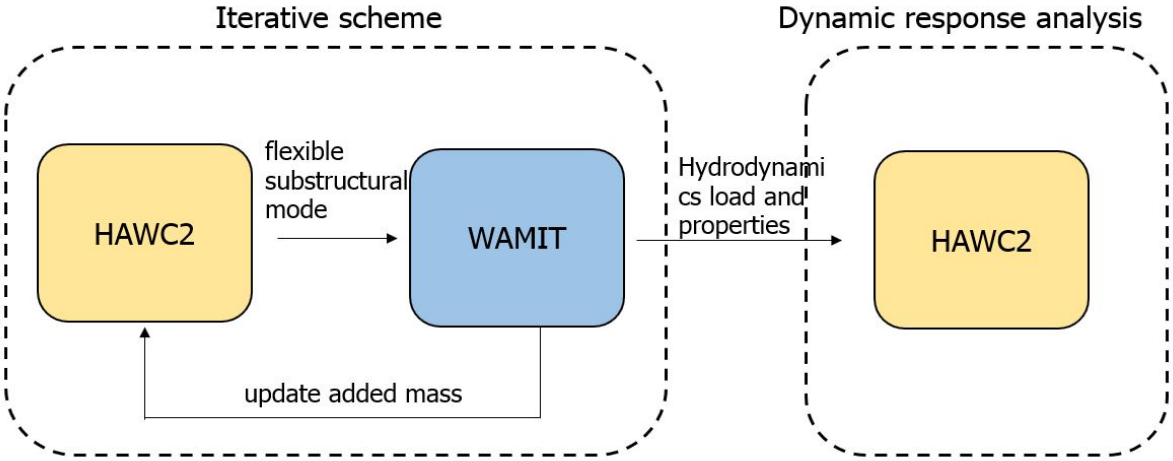

Figure 1.3: Hydroelasticity implementation proposed by Borg[6]

Distinction between hull flexibility and hydroelasticity

The distinction between hull flexibility itself and hydroelasticity effect on hydrodynamic load was quantified by de Souza[50] based on a case study of a TLP concept carrying the NREL 5MW wind turbine. The investigation was separated into two parts as illustrated in Figure 1.4.

Similar to what was found by Svendsen, hull flexibility resulted in increase in all natural periods and a significant increase(50%) in heave was observed. In addition, it was pointed out that a rigid hull assumption was non-conservative in terms of fatigue damage estimation. Lastly, from the study on hydroelasticity, it was concluded that the inclusion of hull flexibility in hydrodynamic load calculation seemed not to be highly important.

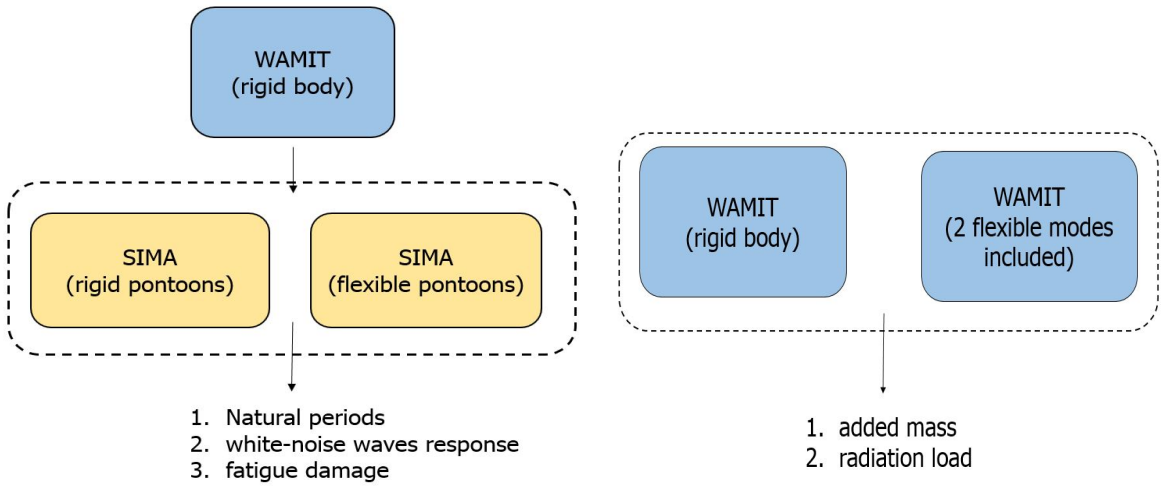

(a) Hull flexibility **(b)** Hydroelasticity

Figure 1.4: Hull flexibility study set up by de Souza[50]

Tower Design with Floating Foundation

Despite the above relevant studies regarding hydroelasticity and hull flexibility, it was found that little has been investigated from a tower design point of view. Nowadays tower design still mainly focuses on fixed foundation and the difference between onshore tower design and floating tower design was seldom documented.

There have been studies presenting tower bending frequencies with different floaters [2][30] but they are never compared with the onshore case. Although from Bir's work[5] the tower bending natural frequencies with different foundation(land-based, mono-pile and floating barge foundation) were documented, there was no discussion and reflection on the results. The effect of floating foundation on tower design is only mentioned briefly in the design code DNVGL-J103 1.10.1[15] with limited explanation.

1.4 Research Questions

As pointed out in Sec. 1.2, the effect of including hull flexibility can be separated into: global responses, internal substructural load, system dynamic properties and hydrodynamic load calculation.

From literature review, it is discovered that the influence on global responses is already discussed from previous works. Method for calculating accurate internal substructural load is proposed. Importance of hull flexibility in hydrodynamic load calculation is also quantified based on a TLP concept. There are also studies documented the influences of hull flexibility on the dynamic properties of the system based on a TLP concept with relatively small size(5MW) wind turbine. However, little has been done regarding the effect of hull flexibility on large size floating wind turbines from a tower design perspective.

Moreover, it is even found that little has been documented regarding the tower design for a floating wind turbine. Therefore, it is important to quantify how a floating foundation can influence the design of a tower before looking into the effect of hull flexibility because nowadays tower design still mainly focuses on fixed bottom foundation.

In order to fill the knowledge gaps mentioned above, two research questions are accordingly defined as follows

- **What is the difference in tower design with a floating foundation?**
- **What is the effect of hull flexibility on tower design?**

1.5 Report Outline

Chapter 1: Introduction

This chapter provides background knowledge on floating wind turbines, including the history, design philosophy and simulation challenges. A problem statement is introduced, followed by a relevant literature study. Two research questions are accordingly defined based on the knowledge gap found in the literature study.

Chapter 2: Theoretical Background

This chapter provides the theoretical background regarding this thesis. It is divided into several fields, including structural dynamics, hydrodynamics, mooring lines and finite element method. Linearization of aerodynamic damping is also introduced.

Chapter 3: Methodology

This chapter explains the methodology taken to answer the defined research questions. The definition of the floating concepts used for the study in this thesis are introduced, followed by the description of the developed FEM models. Two analyses to be implemented for the two research questions are introduced.

Chapter 4: Results and Discussion

This chapter shows the results from the two analyses introduced in chapter 3. Discussion and interpretation on the results are provided. Reflection on the assumptions and the limitation of the developed model are also discussed.

Chapter 5: Conclusion and Future Work

Based on the results and discussion in chapter 4, conclusions are drawn. The answers for two research questions are summarized. In addition, recommendations for the possible future work are also made.

Chapter 2

Theoretical Background

2.1 Structural Dynamics

2.1.1 Modal Analysis

In essence, modal analysis states that a vibration of a structure can be decomposed into uncoupled vibration modes. For a structure with N DoFs, the undamped forced vibration equation of motion can be expressed as

$$\mathbf{M}\underline{\ddot{x}} + \mathbf{K}\underline{x} = \underline{F}(t) \tag{2.1}$$

in which $\mathbf{M}$ and $\mathbf{K}$ are N by N matrices and $\underline{F}$ is a N by 1 vector

The general solution of Equation 2.1 is the summation of the homogeneous solution and a particular solution. The homogeneous solution is found by solving free vibration

$$\mathbf{M}\underline{\ddot{x}} + \mathbf{K}\underline{x} = 0 \tag{2.2}$$

Suppose the solution is a synchronic harmonic vibration

$$\underline{x} = \Phi e^{i\omega t} \tag{2.3}$$

where Φ is the the unknown amplitude and ω is the unknown natural frequency.

By inserting the assumed solution into Equation 2.2

$$(\omega^2\mathbf{M} + \mathbf{K})\Phi = 0 \tag{2.4}$$

The above eigenvalue problem can be solved numerically. The result will be N eigenvalues $\omega_i^2 (i = 1, 2, ..., N)$ and the associated eigenvectors $\Phi_i (i = 1, 2, ..., N)$.

In modal analysis, the square root of the eigenvalue is the natural frequency of each vibration mode and the eigenvector is the associated vibration mode shape. For a forced undamped vibration, the solution can be assumed to be the summation of the vibration mode shapes

$$\underline{x}(t) = \sum_{i=1}^{N} \Phi_i u_i(t) = \mathbf{E}\underline{u}(t) \tag{2.5}$$

where $\mathbf{E}$ is the eigenmatrix containing all the vibration modes and $\underline{u}$(t) is the vector containing the time function of each vibration mode.

By inserting the assumed solution into Equation 2.1

$$\mathbf{ME}\underline{\ddot{u}} + \mathbf{KE}\underline{u} = \underline{F} \tag{2.6}$$

Multiplying Equation 2.6 by the transpose of eigenmatrix $\mathbf{E}^T$

$$\mathbf{E}^T\mathbf{ME}\underline{\ddot{u}} + \mathbf{E}^T\mathbf{KE}\underline{u} = \mathbf{E}^T\underline{F} \tag{2.7}$$

Equivalently

$$\mathbf{M}^*\underline{\ddot{u}} + \mathbf{K}^*\underline{u} = \mathbf{E}^T\underline{F} \tag{2.8}$$

where $\mathbf{M}^*$ is the modal mass and $\mathbf{K}^*$ is the modal stiffness.

$$\mathbf{M}^* = \mathbf{E}^T\mathbf{ME}$$
$$\mathbf{K}^* = \mathbf{E}^T\mathbf{KE}$$

Due to orthogonality, by the use of eigenmatrix, a undamped forced vibration(Equation 2.1) can be transformed into a decoupled system(Equation 2.8). This technique is known as modal analysis.

2.1.2 Modal Assurance Criterion

One of the most popular way to quantitatively compare two mode shapes is the Modal Assurance Criterion(MAC). The MAC is a normalized scalar value which indicates the difference between two mode shapes ϕ_k, ϕ_l. The form of the MAC is a least squares based form of linear regression analysis and it is defined as

$$\text{MAC}(\phi_k, \phi_l) = \frac{|\phi_k^T \phi_l|^2}{||\phi_k||_2^2 ||\phi_l||_2^2} \tag{2.9}$$

The value of the MAC ranges from 0 to 1. The higher it is the closer the two mode shapes are. If MAC $\approx$ 1 it means two mode shapes can resemble to each other very well and if MAC $\approx$ 1 it means two mode shapes are completely different.

2.1.3 Natural Frequency Iteration with Added Mass

As will be explained in Sec. 2.2, hydrodynamic added mass is the hydrodynamic force related to the acceleration of the body and is often moved from the right hand side of equation of motion to the left hand side

$$(\mathbf{M} + \mathbf{A})\underline{\ddot{x}} + \mathbf{B}\underline{\dot{x}} + \mathbf{K}\underline{x} = \underline{F}(t) \tag{2.10}$$

Therefore, when solving the eigen problem in Equation 2.4, added mass should also be included

$$(\omega^2(\mathbf{M} + \mathbf{A}) + \mathbf{K})\Phi = 0 \tag{2.11}$$

However, from potential flow theory it is indicated that hydrodynamic added mass is frequency dependent, which means the calculation of natural frequency of a structure with added mass has to be implemented in an iterative way as shown in Figure 2.1.

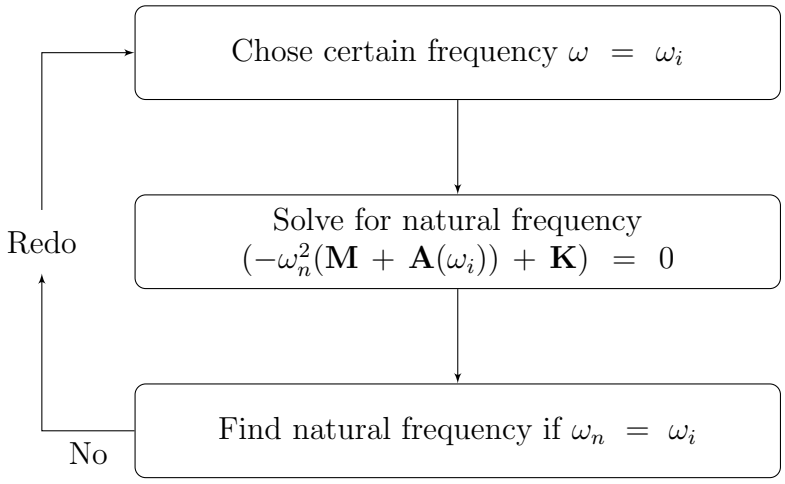

Figure 2.1: Steps to find natural frequency with frequency dependent added mass

2.1.4 Structural Damping

Structural damping mainly comes from the internal friction and sliding in the material and can vary due to many factors such as temperature or stress level and so on, which makes it difficult to evaluate.

A very common way to evaluate structural damping is to assume the damping matrix to be proportional to the mass matrix and stiffness matrix with constant coefficient α and β, which is also known as Rayleigh damping.

$$\mathbf{B} = \alpha\mathbf{M} + \beta\mathbf{K} \tag{2.12}$$

The benefits of Rayleigh damping is that it can guarantee the modal damping matrix will also be a diagonal matrix because both mass matrix and stiffness matrix are symmetric. Therefore, modal analysis can still work and the damping ratio of each mode can be expressed as

$$\xi = \frac{b_i}{2m_i\omega_i} = \frac{\alpha m_i + \beta k_i}{2m_i\omega_i} = \frac{\alpha}{2\omega_i} + \frac{\beta\omega_i}{2} \tag{2.13}$$

Typical values of critical damping ratio ranges from 0.5% to 0.8% in steel structure and 1.2% in concrete material[32].

2.1.5 Frequency Response Function

In structural dynamics, frequency response function(FRF), or amplitude-frequency response matrix, is defined as the ratio of the response amplitude of mode i to the applied force in j DoF

$$\mathbf{H}_{r_iF_j}(\omega) = \frac{r_i}{F_j} \tag{2.14}$$

Frequency response function is useful in structural analysis in frequency domain and it allows one to be able to simply calculate the response of a structure with a input force. A good example of utilizing FRF is response spectrum analysis. Suppose a force spectrum is give S_{FF}, the response spectrum can be easily obtained by

$$S_{rr}(\omega) = |\mathbf{H}_{rF}(\omega)|^2 S_{FF}(\omega) \tag{2.15}$$

A stress response spectrum is often used in a frequnecy domain fatigue damage evaluation and it can be found easily by using frequency response function.

2.2 Hydrodynamics

2.2.1 Hydrostatic Stability

In naval architecture field, the concept of metacenter is commonly used to evaluate the stability of a ship. Metacenter is defined as the intersection of two lines of buoyancy force after a small inclination, as shown in Figure 2.2

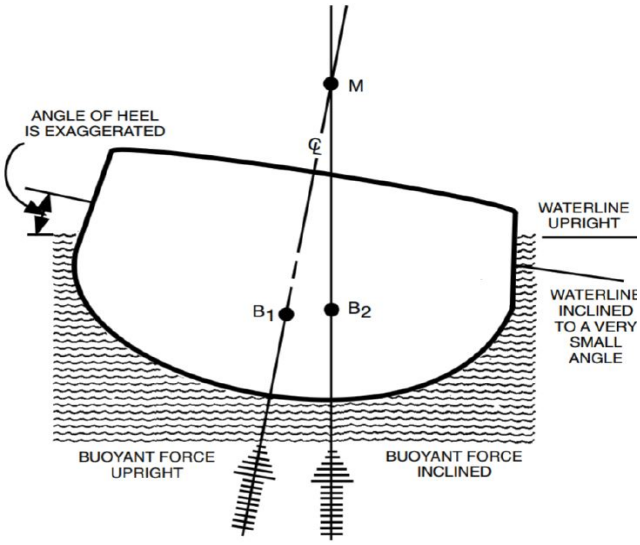

Figure 2.2: Illustration of meatcenter

The distance between metacenter M and buoyancy center B can be calculated as follows

$$\overline{BM}_x = \frac{I_x}{V} \tag{2.16}$$

where I_x is area moment of inertia of the water plane around x axis and V is displacement volume.

To properly estimate the stability of the body, the restoring moment after small inclination has to be formulated. As illustrated in Figure 2.3, the restoring moment τ due to a small inclination angle θ can be written in the following way

$$\tau = F_B \cdot \overline{GM} \cdot \mathrm{Sin}(\theta) \approx F_B \cdot \overline{GM} \cdot \theta \tag{2.17}$$

where F_B is the buoyancy force and $\overline{GM}$ is the distance from gravity center to metacenter. $\overline{GM}$ can be calcuated by

$$\overline{GM} = \overline{KB} + \overline{BM} - \overline{KG} \tag{2.18}$$

in which K represents keel and $\overline{KB}$ is the distance from keel to buoyancy center and $\overline{KG}$ is the distance from keel to gravity center.

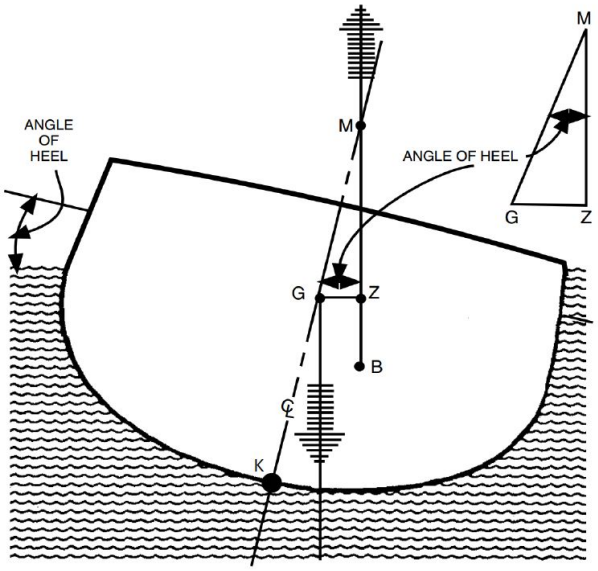

Figure 2.3: Inclined body

Because Equation 2.17 states that restoring moment τ is proportional to the inclination angle θ, the restoring moment can be regarded as a rotational spring with stiffness $F_B \cdot \overline{GM}$, which is also known as hydrostatic stiffness.

Alternatively, hydrostatic stiffness can also be expressed in another form

$$C_{55} = \rho g I_x + \rho g V \cdot z_B - Mg \cdot z_G \tag{2.19}$$

The number 5 denoted in C_{55} follows traditional notation for six rigid body motions and 5 represents the pitch motion. Equation 2.19 indicates that hydrostatic stiffness relies on water plane area, buoyancy force and gravity force.

2.2.2 Morison Equation

Morison equation is well-known for estimating the wave force per unit length on a slender cylindrical body.

$$F = \frac{1}{2}\rho C_D D(U - U_b)|U - U_b| + \rho C_m A(\dot{U} - \dot{U}_b) + \rho A\dot{U} \tag{2.20}$$

where

F	force per unit length[N/m]
ρ	fluid density[kg/m^3]
D	diameter[m]
A	cross section area[m^2]
U	fluid velocity [m/s^2]
U_b	body motion velocity [m/s^2]
C_D	hydrodynamic drag coefficient[-]
C_m	hydrodynamic mass coefficient[-]

Morison equation indicates that the waves force on the body can be separated into drag force and inertia force. The first term in Morison equation is related to the drag force. The second term is the so-called hydrodynamic inertia force and the last term is called Froude-Krylov force. Both hydrodynamic inertia force and Froude-Krylov force are considered as inertia force.

The drag force is induced by the friction between the body and the fluid due to the viscosity of the fluid. The hydrodynamic inertia force can be interpreted as the force related to the acceleration near the surrounding of the body, which means both the acceleration of the body and the acceleration of the surrounding fluid near the body can contribute to hydrodynamic inertia force. Froude-Krylov force is induced by the pressure gradient in the outer-flow region due to the acceleration of the fluid.

Typically, in the dynamic analysis of a submerged body, the hydrodynamic inertia force due to the motion of the body is moved from the right hand side of the equation of motion(external force) to the left hand side(response), and the hydrodynamic inertia force induced by the acceleration of the body is often called hydrodynamic added mass.

Similarly, the drag force caused by the body motion is also often moved to the other side in the equation of motion, and it is known as drag damping because it is related to the velocity of the body.

2.2.3 Keulegan-Carpenter Number

As pointed out in Sec. 2.2.2, Morison equation states that the waves force can be separated into drag and inertia. Keulegan-Carpenter Number, or KC number, is an useful dimensionless value which indicates whether the waves force is dominated by drag or inertia. KC number is defined as follows

$$KC = \frac{UT}{D} \tag{2.21}$$

The higher the KC number is, the more drag dominant the waves force is. The lower the KC number is, the more inertia dominant the waves force is. The following numbers can be used as a rule of thumb

- KC< 3: inertia dominant and drag can be neglected
- 3 <KC< 15: linearized drag is enough
- 15 <KC< 45: full Morison equation is required
- KC> 45: drag dominant and and inertia can be neglected

2.2.4 Linearization of Drag Damping

As mentioned in Sec. 2.2.2, in Morison equation, the drag force related to the velocity of the body is usually considered as drag damping. Morison equation also indicates that drag damping is a quadratic damping.

A time domain model can easily take into account for a quadratic damping, However, for a linearized frequency domain model, a quadratic drag damping has to be linearized. The linearization of a quadratic damping can be achieved by finding the equivalent linearized damping which yields the same energy loss as the real energy loss per cycle in a hysteresis loop[32]. In the case of the drag damping B_{drag} from Morison equation, the linearized form can be expressed as

$$B_{drag} = \frac{1}{2}\rho C_D D \frac{8}{3\pi}\omega \hat{X} \tag{2.22}$$

where

ω	oscillated frequency[rad/s]
$\hat{X}$	response amplitude[-]

The linearized drag damping form in Equation 2.22 implies that the magnitude of the damping is dependent on the response amplitude. Hence, in a linearized frequency domain model, the linearized drag damping need to be evaluated in a iterative way as shown in Figure 2.4.

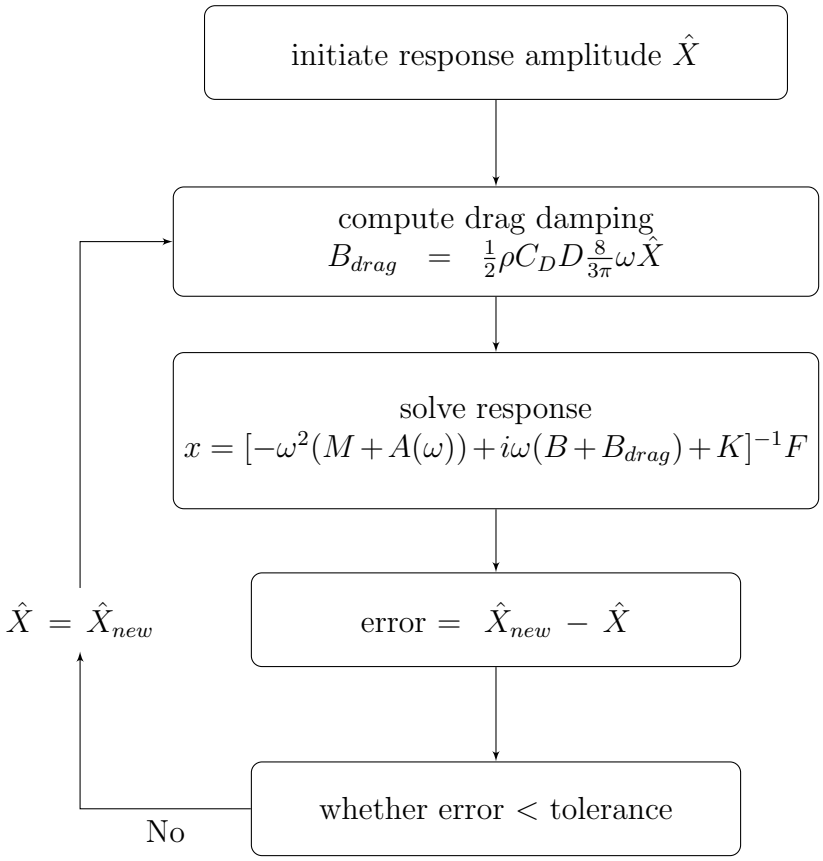

Figure 2.4: Iterative scheme for computing drag damping

2.2.5 First-Order Potential Flow Theory

Apart from Morison equation, another widely used methodology to evaluate the waves force on a body is to integrate the pressure on the body surface directly, and the pressure field around the body is obtained from first-order potential flow theory. The first-order potential flow theory is also known as linear wave theory, which the wave amplitude is assumed to be small.

A potential flow is an incompressible, inviscid and irrotational flow, which means the drag force is not captured from potential flow. For a fluid with a velocity potential ϕ, the pressure in the fluid can be written based on Bernoulli equation

$$p = -\rho(\frac{\partial \phi}{\partial t} + \frac{1}{2}|\nabla^2 \phi| + gz) \tag{2.23}$$

The first term in Equation 2.23 is the linear dynamic pressure. The second term is the quadratic dynamic pressure. The third term is related to hydrostatic pressure.

For a wave-structure interaction problem, the total velocity potential is often separated into diffraction potential ϕ_D and radiation potential ϕ_R.

$$\phi = \phi_R + \phi_D \tag{2.24}$$

The diffraction potential includes the potential of the incident wave ϕ_i and the potential of the scatter wave field ϕ_s due to the existence of the body.

$$\phi_D = \phi_i + \phi_s \tag{2.25}$$

On the other hand, the radiation potential is related to the motions of the body. Suppose only six rigid body motion is taken into account, the radiation potential can be defined as the summation of the contribution form each motion

$$\phi_R = \sum_{j=1}^{6} \xi_j \phi_j \tag{2.26}$$

in which ϕ_j is unit-amplitude radiation potential and the index j denoted to each motion and ξ_j is the amplitude of the motion.

By utilizing the above defined velocity potential and Bernoulli equation, the waves force on a body can be found by integrating the pressure on the body surface. The waves force corresponding to the diffraction potential is the so-called wave exciting force

$$X_i = -i\omega\rho \int\int_{S_B} \phi_D n_i dS \tag{2.27}$$

where S_B stands for body surface and n_i is the unit vector normal to the body surface.

The result of integrated pressure from radiation potential is known as added mass and radiation damping

$$A_{ij} - \frac{i}{\omega} B_{ij} = -\rho \int\int_{S_B} \phi_j n_i dS \tag{2.28}$$

where A_{ij} is the added mass in i DoF due to j motion and B_{ij} is the radiation damping in i DoF due to j motion.

Numerically, in a potential flow solver such as WAMIT[56] or wadam, the surface integration in Equation 2.27 and 2.28 can be done by using panel method. Panel method is basically generating discrete elements on the body surface, and each element contain information of the velocity potential. Typically for low-order panels the velocity potential is assumed as constant, while for higher-order panels the velocity potential is described by functions. Once the panels are generated in a potential flow solved, the surface integration can be achieved by simple summation.

2.3 Mooring Line Analysis

2.3.1 Spread Catenary System

A catenary mooring system utilizes the cable weight in water to provide constraint on the floating structure. The force from the mooring lines can be seen as an equivalent nonlinear spring attached on a floating structure. If a single mooring line is considered as shown in Figure 2.5, a relation between the horizontal line tension T_H and horizontal distance X can be found through a series of simplified formulation.

Since the behavior of the mooring lines is nonlinear, a approximation is made by neglecting the dynamic effect of the lines, which means a quasi-static condition is considered. In addition, to simplified the static analysis, a few assumptions are made. First, The bending stiffness is neglected, which is a good approximation for chains, and also appropriate for wire with large radius of curvature. Second, the effect of elasticity is neglected. These assumptions should be reasonable in a normal condition.

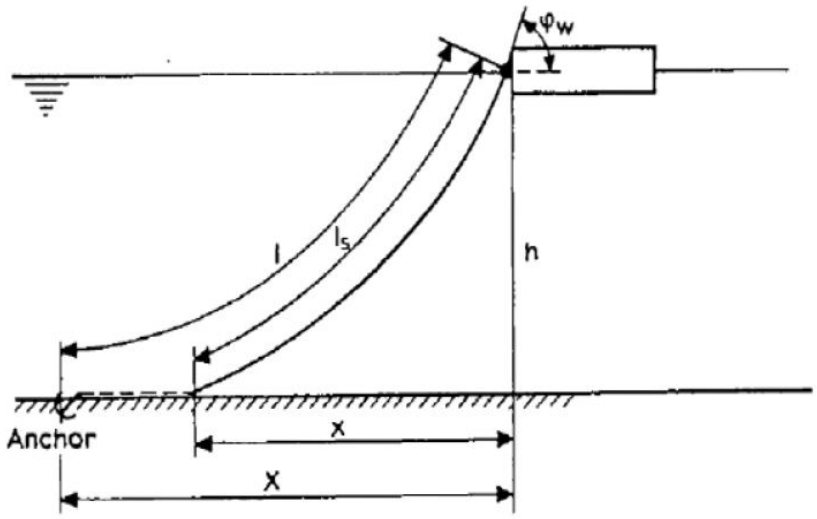

Figure 2.5: Catenary mooring line[16]

Solving two static equilibrium equations for the line can lead to the following results[16]

$$s = \frac{T_H}{w}\sinh(\frac{w}{T_H}x) \tag{2.29}$$

$$z + h = \frac{T_H}{w}(\cosh(\frac{w}{T_H}x - 1)) \tag{2.30}$$

$$T(z) = T_H + wh + (w + \rho g A)z \tag{2.31}$$

where

s	are length of the mooring line [m]
x	horizontal distance of the mooring line [m]
z	distance below MSL [m]
T_H	horizontal tension [N]
w	mooring line weight per unit length in water [kg/m]
h	water depth[m]

For given T_H, w and h, Equation 2.29 tells the relation between s and x and Equation 2.30 shows the relation between z and x. The tension in the line at any position can be found by Equation 2.31.

If the whole mooring line is considered, meaning $s = l_s$ and $z = 0$, Equation 2.29 and 2.30 can be rewritten as

$$l_s = a\text{sinh}(\frac{x}{a}) \tag{2.32}$$

$$h = a(\cosh(\frac{x}{a}) - 1) \tag{2.33}$$

where

$$a = \frac{T_H}{w} \tag{2.34}$$

Combining Equation 2.32 and 2.33 yields a relation between X and T_H as follows

$$X = l - h(1 + \frac{2a}{h})^{0.5} + a\cosh^{-1}(1 + \frac{h}{a}) \tag{2.35}$$

As mentioned earlier, a mooring line can be regarded as an spring with nonlinear stiffness attached to a floating structure. The definition of the stiffness is essentially the derivative of the force w.r.t the displacement, which is $\mathrm{d}T_H/\mathrm{d}X$ in the case of Equation 2.35. Therefore, the equivalent stiffness k_i of a mooring line at a given pre-tension can be written as

$$k_i = \frac{\mathrm{d}T_H}{\mathrm{d}X} = w[\frac{-2}{(1 + \frac{2a}{h})^{0.5}} + \cosh^{-1}(1 + \frac{h}{a})]^{-1} \tag{2.36}$$

For a spread catenary mooring system with several mooring lines, the equivalent stiffness K of the whole system is the summation of each line

$$K = \sum_{i=1}^{n} k_i \cos^2\theta_i \tag{2.37}$$

where θ_i is the angle between the mooring line and the direction of the motion.

2.3.2 Tension Leg System

Another common seen mooring system is tension leg mooring, which usually consists of several high tension cylindrical legs attached to sea bed. Tendons is a name widely used to referred to the high tension slender legs. In addition, TLP is a very common-used abbreviation short for tension leg platform. In a TLP system, buoyancy force is higher than the weight of the platform and the extra buoyancy is balanced out by the tension from the tendons, and the stability of the platform relies on the high tension from the tendons.

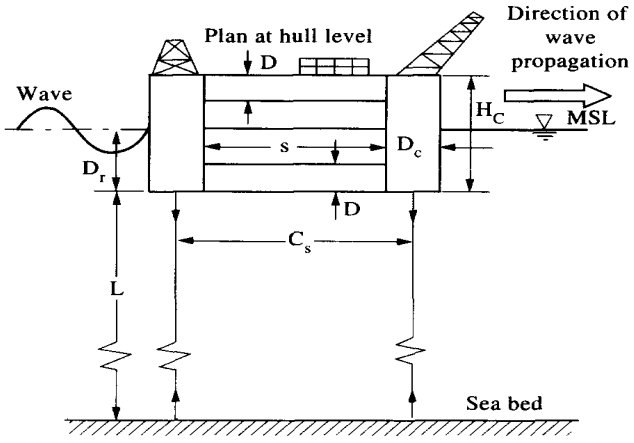

Figure 2.6: Illustration of a TLP system[23]

Suppose a system consists of a platform(rigid body) with 4 high tension tendons is considered as illustrated in Figure 2.6. The tension in the lines is T_0 and the length of tendon is L. The equivalent stiffness can be derived by assigning a unit displacement in the motion of interest, which is also known as displacement method.

For instance, if the equivalent stiffness in surge motion is of interest, one can assign a surge displacement x to the platform as shown in Figure 2.7. By formulating static

force equilibrium in horizontal and vertical direction and static moment equilibrium, three equations can be written as

$$K_{11} = \frac{4(T_0 + \Delta T)\sin\theta_x}{x} \tag{2.38}$$

$$K_{31} = \frac{4[T_0(\cos\theta_x - 1) + 4\Delta T\cos\theta_x]}{x} \tag{2.39}$$

$$K_{51} = \frac{-4\bar{h}(T_0 + \Delta T)\sin\theta_x}{x} = -hK_{11} \tag{2.40}$$

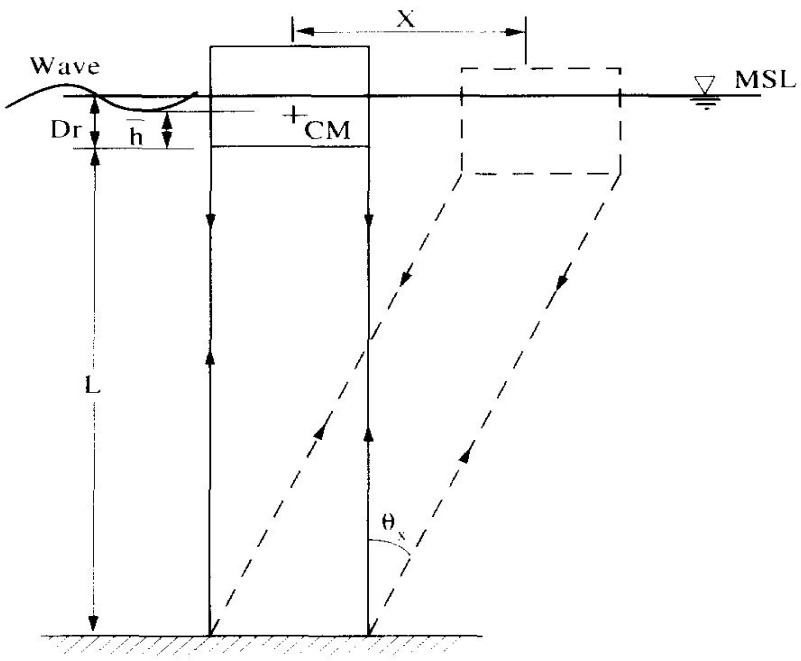

Figure 2.7: TLP with surge displacement[23]

The number denoted in K_{11}, K_{31} and K_{51} follows traditional notation for referring to six rigid body motions, which {1,2,3,4,5,6} refer to {surge, sway, heave, roll, pitch, yaw}.

Similarly, the equivalent stiffness in heave and pitch motions be formulated by using displacement method

$$K_{33} = \rho\pi g D_c^2 + \frac{4EA}{L} \tag{2.41}$$

$$K_{55} = \rho\pi g a^2 D_c^2 + 4(T_0\bar{h}\frac{\sin\theta_5}{\theta_5} + EAa^2\frac{\cos\theta_5}{L}) \tag{2.42}$$

where

D_c	diameter of the platform columns [m]
ρ	fluid density[kg/m^3]
a	horizontal distance from platform center to tendons [m]
$\bar{h}$	vertical distance from platform center to tendons [m]
EA	tendons axial stiffness [N]
θ_5	assigned pitch rotation angle [rad]

Suppose there are n_t number of tendons. If the rotation angle θ_x and θ_5 are small, the equivalent stiffness from Equation 2.38 to 2.42 can be reduced to the following forms[1]

$$K_{11} \approx \sum_{j=1}^{n_t} k_{11} \tag{2.43}$$

$$K_{31} \approx 0 \tag{2.44}$$

$$K_{51} \approx \sum_{j=1}^{n_t} -k_{11}\bar{h} \tag{2.45}$$

$$K_{33} \approx \sum_{j=1}^{n_t} k_{33} \tag{2.46}$$

$$K_{55} \approx \sum_{j=1}^{n_t} [k_{11}\bar{h}^2 + k_{33}a^2]\cos^2\theta_j \tag{2.47}$$

where

k_{11}	$= T_0/L$
k_{33}	$= EA/L$
θ_j	tendons angle along z-axis[rad]

2.4 Finite Element Method

Finite element method is a numerical method for solving partial differential equations(PDE) and has been widely used in many fields such as structural vibration, fluid dynamics, electromagnetism and so on. In essence, the idea of finite element method is to discretize a mathematical model into a numerical model.

In the case of structural vibration, the PDE to be solved is the well-known equation of motion. Finite element method can be used to discretize a structure into elements. There are different types of elements and each oh them suits for different condition. One of the most popular element type used in structural vibration analysis is beam element and it can be either Euler-Bernoulli beam or Timoshenko beam depending on whether shear deformation is considered or not.

For a 4-DoFs Euler-Bernoulli beam element(Figure 2.8) without considering axial displacement, the degree of freedoms can be defined as

$$\mathbf{u} = \begin{bmatrix} \mathrm{v}_{z1} \\ \mathrm{v}_{\theta 1} \\ \mathrm{v}_{z2} \\ \mathrm{v}_{\theta 2} \end{bmatrix} \tag{2.48}$$

which v_{z1} and $\mathrm{v}_{\theta 1}$ represent the transverse displacement and rotation at node 1, while v_{z2} and $\mathrm{v}_{\theta 2}$ are the transverse displacement and rotation at node 2, and the displacement between node 1 and node 2 are described by shape(interpolation) functions based on the displacements at two nodes.

Figure 2.8: 4-DoFs Euler-Bernoulli beam element

The mass matrix and stiffness matrix of the beam element are then found by utilizing the shape functions together with principle of virtual displacement(PVD)

based on energy equilibrium. The expression of mass and stiffness matrices of the element are as follows

$$\mathbf{m}^e = \frac{\rho AL}{420}\begin{bmatrix} 156 & -22L & 54 & 13L \\ -22L & 4L^2 & -13L & -3L^2 \\ 54 & -13 & 156 & 22L \\ 13L & -3L^2 & 22L & 4L^2 \end{bmatrix} \tag{2.49}$$

$$\mathbf{k}^e = \frac{EI}{L^3}\begin{bmatrix} 12 & -6L & -12 & -6L \\ -6L & 4L^2 & 6L & 2L^2 \\ -12 & 6L & 12 & 6L \\ -6L & 2L^2 & 6L & 4L^2 \end{bmatrix} \tag{2.50}$$

where

ρ	material density[kg/m^3]
A	cross section area[m^2]
L	element length [m]
E	Young's modulus [Pa]
I	area moment of inertia[m^4]

The numerical way of utilizing element matrices to model a structure can be demonstrated by taking a tower-like structure as an example(Figure 2.9). Suppose the structure is modeled by beam elements, the mass and stiffness matrices of the structure can be found by assembling the element matrices to form banded diagonal matrices as follows

$$\mathbf{M}_{tw}, \mathbf{K}_{tw} = \begin{bmatrix} \square & & \mathbf{0} \\ & \square\square & \\ & \square & \\ \mathbf{0} & & \ddots \end{bmatrix} \tag{2.51}$$

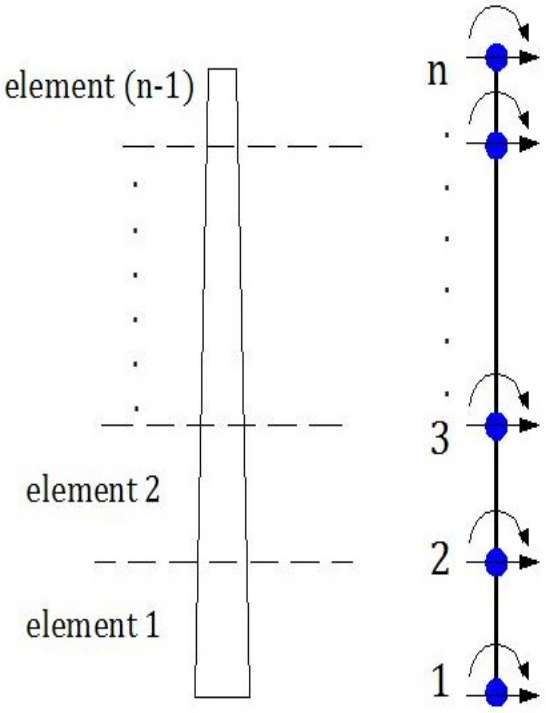

Figure 2.9: Illustration of tower beam elements and node numbering

2.4.1 Axes Rotation

The formulation of mass and stiffness matrices of an element from finite element theory is based on local coordinate from element point of view. However, it is often more convenient to express the matrices based on global coordinate. As a result, transformation from local coordinate to global coordinate is very common when building a FEM model and it can be achieved by utilizing axes rotation matrix.

$$R_x = \begin{bmatrix} 1 & 0 & 0 \\ 0 & c & -s \\ 0 & s & c \end{bmatrix} \qquad R_y = \begin{bmatrix} c & 0 & -s \\ 0 & 1 & 0 \\ s & 0 & c \end{bmatrix} \qquad R_z = \begin{bmatrix} c & -s & 0 \\ s & c & 0 \\ 0 & 0 & 1 \end{bmatrix} \tag{2.52}$$

where

R_x	Rotation along x-axis
R_y	Rotation along y-axis
R_z	Rotation along z-axis
c	short for cos
s	short for sin

Suppose the element need to rotate along x-axis, the relation between local coordinate (x,y...) and global coordinate ($\bar{x}$,$\bar{y}$...) can be described by

$$\begin{bmatrix} x \\ y \\ z \\ \theta_x \\ \theta_y \\ \theta_z \end{bmatrix} = \underbrace{\begin{bmatrix} R_x & 0 \\ 0 & Rx \end{bmatrix}}_{\mathbf{T}_0} \begin{bmatrix} \bar{x} \\ \bar{y} \\ \bar{z} \\ \bar{\theta_x} \\ \bar{\theta_y} \\ \bar{\theta_z} \end{bmatrix} \tag{2.53}$$

Based on rotational matrix $\mathbf{T}_0$ the mass and stiffness matrices of an element can be expressed in the global coordinate as follows

$$\bar{\mathbf{k}}^e = \mathbf{T}_g^T \mathbf{k}^e \mathbf{T}_g \tag{2.54}$$

$$\bar{\mathbf{m}}^e = \mathbf{T}_g^T \mathbf{m}^e \mathbf{T}_g \tag{2.55}$$

where

$$\mathbf{T}_g = \begin{bmatrix} \mathbf{T}_0 & 0 \\ 0 & \mathbf{T}_0 \end{bmatrix} \tag{2.56}$$

2.4.2 Multifreedom Constraints

In a finite element model, multifreedom constraints(MFCs) is widely used to describe either compatibility condition or force equilibrium at the interface between substructures. For compatibility constrains it can be written down as a function mathematically as follows

$$f(u_i, u_j, \ldots) = c \tag{2.57}$$

where u_i and u_j are the constrained degree of freedom and c is a constant.
The constraint is called homogeneous if the constant $c = 0$ and non-homogeneous otherwise. The constraint can also be linear or non-linear depends on how the nodes are related to each other.

The schematics of MFCs application[17] is shown in Figure 2.10. Simply put, MFCs can change the equation with the assembled mass and stiffness matrices to a modified system of equation:

$$\mathbf{M\ddot{u} + Ku = F} \quad \xrightarrow{MFC} \quad \mathbf{\hat{M}\ddot{\hat{u}} + \hat{K}\hat{u} = \hat{F}} \tag{2.58}$$

There are three methods to apply MFCs and only detailed description on Master-Slave elimination will be provided.

1. **Master-Slave Elimination**: Each MFC separtaed into master and slave nodes. The modified equations do not contain the slave degree of freedoms.

2. **Penalty Augmentation(Penalty function method)**: Each MFC is seen as the presence of a fictitious elastic element(penalty element) that enforces it approximately. The penalty element is parametrized by a numerical weight. The MFCs are imposed by augmenting the finite element method with the penalty elements.

3. **Lagrange Multiplier Adjunction**: For each MFC, an additional unknown is adjoined to the master stiffness equations. The set of unknowns physically represent the constraint forces which would enforce the constraints as they should be applied to the unconstrained system.

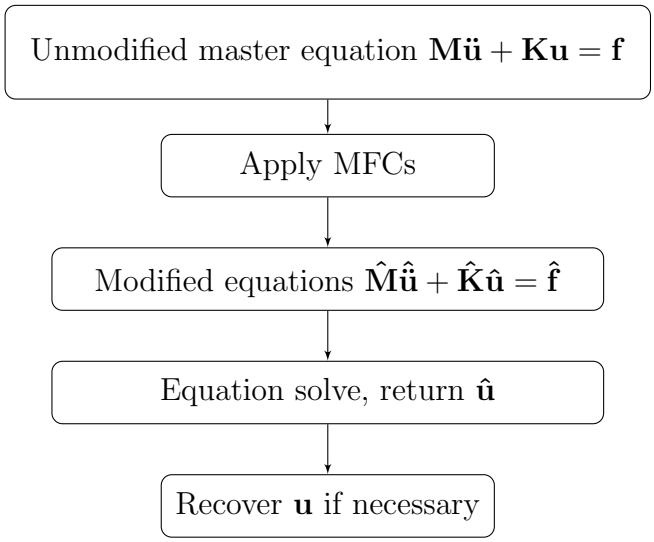

Figure 2.10: Steps for implementing MFC[17]

2.4.2.1 Master-Slave Elimination

From the framework of substructuring technique[31], Master-Slave elimination is also defined as primal assembly in physical domain. Nevertheless, they are both describing the same technique.

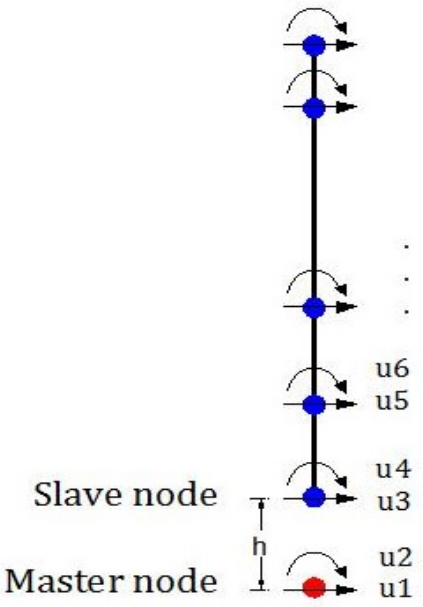

Figure 2.11: Master node and slave node

The implementation of Master-Slave elimination will be explained by providing an example. Suppose a tower-like structure is rigidly connected to a free-moving rigid body at the bottom as shown in Figure 2.11 and if the rotation of the free-moving rigid body is assumed to be small, the compatibility condition can be formulated as

$$u_3 = u_1 + h \cdot u_2$$
$$u_4 = u_2$$

To include the compatibility condition into the system in a matrix form, equivalently, it can be written down as follows

$$\begin{bmatrix} u_1 \\ u_2 \\ u_3 \\ u_4 \\ u_5 \\ u_6 \\ \vdots \end{bmatrix} = \begin{bmatrix} 1 & 0 & 0 & 0 & \cdots \\ 0 & 1 & 0 & 0 & \cdots \\ 1 & h & 0 & 0 & \cdots \\ 0 & 1 & 0 & 0 & \cdots \\ 0 & 0 & 1 & 0 & \cdots \\ 0 & 0 & 0 & 1 & \cdots \\ \vdots & \vdots & \vdots & \vdots & \ddots \end{bmatrix} \begin{bmatrix} u_1 \\ u_2 \\ u_5 \\ u_6 \\ \vdots \end{bmatrix} \tag{2.59}$$

or in a compact form

$$\mathbf{u} = \mathbf{T}\hat{\mathbf{u}} \tag{2.60}$$

where $\mathbf{u}$ contains two redundant DoFs($u_3 and u_4$) from the slave node while $\hat{\mathbf{u}}$ does not. The transformation matrix $\mathbf{T}$ which describes the compatibility condition is also known as Boolean matrix under the framework of substructuring technique.

The governing equation describing the responses of the structure is the well-known equation of motion

$$\mathbf{M}\ddot{\mathbf{u}} + \mathbf{B}\dot{\mathbf{u}} + \mathbf{K}\mathbf{u} = \mathbf{F} \tag{2.61}$$

by simply inserting Equation 2.60 into 2.61 it yields

$$\mathbf{M}\mathbf{T}\ddot{\hat{\mathbf{u}}} + \mathbf{B}\mathbf{T}\dot{\hat{\mathbf{u}}} + \mathbf{K}\mathbf{T}\hat{\mathbf{u}} = \mathbf{F} \tag{2.62}$$

By multiplying the transpose of the transformation matrix $\mathbf{T}^T$ the system can be expressed as

$$\mathbf{T}^T\mathbf{M}\mathbf{T}\ddot{\hat{\mathbf{u}}} + \mathbf{T}^T\mathbf{B}\mathbf{T}\dot{\hat{\mathbf{u}}} + \mathbf{T}^T\mathbf{K}\mathbf{T}\ddot{\hat{\mathbf{u}}} = \mathbf{T}^T\mathbf{F} \tag{2.63}$$

The governing equation of the modified system can then be described as

$$\hat{\mathbf{M}}\ddot{\hat{\mathbf{u}}} + \hat{\mathbf{B}}\dot{\hat{\mathbf{u}}} + \dot{\mathbf{K}}\dot{\mathbf{u}} = \dot{\mathbf{F}} \tag{2.64}$$

where

$$\hat{\mathbf{M}} = \mathbf{T}^T\mathbf{M}\mathbf{T}$$
$$\hat{\mathbf{B}} = \mathbf{T}^T\mathbf{B}\mathbf{T}$$
$$\hat{\mathbf{K}} = \mathbf{T}^T\mathbf{K}\mathbf{T}$$
$$\hat{\mathbf{F}} = \mathbf{T}^T\mathbf{F}$$

2.5 Linearization of Aerodynamic Damping

Aerodynamic damping is the consequence of having relative wind speed due to the movement of the rotor. When the rotor moves forward, the relative wind speed is higher and result in larger wind force to against the movement. When the rotor is movies backwards, the relative wind speed decreases and results in a smaller wind force.

The thrust force on a wind turbine is typically expressed as

$$F_T = \frac{1}{2}\rho A C_T(\bar{U} + u - \dot{x})|\bar{U} + u - \dot{x}| \tag{2.65}$$

where

ρ	air density[kg/m^3]
A	rotor plane area[m^2]
C_T	thrust force coefficient[-]
$\bar{U}$	mean wind speed[m/s]
u	stochastic wind speed variation[m/s]
$\dot{x}$	speed of the rotor motion[m/s]

The summation of every term related to $\dot{x}$ in Equation 2.65 can be regarded as the aerodynamic damping force. Clearly, Equation 2.65 tells that aerodynamic damping is nonlinear and it is wind speed dependent. In addition, the thrust coefficient C_T is also wind speed dependent and it is also related to the pitch control system of the blades. Therefore, a closed-form derivation for aerodynamic damping can be a challenging task.

Without a closed form, aerodynamic damping can still be incorporated into aero-elastic simulation tool because the wind force can be solved based on the relative wind speed and C_T at each time step, and the nonlinear behavior can be captured.

However, for a linearized frequency domain model, aerodynamic damping must be linearized. Van der Tempel[53] summarize three possible ways to account for aerodynamic damping into a linearized model, which are a closed-form linearization from Garrad's derivation[18], numerical linearization, or using an engineering number.

Among three methods, numerical linearization is more popular due to the simplicity of implementation if an aero-elastic-servo time domain simulation tool is available.

Essentially, numerical linearization is to utilize the time domain tool to find the aerodynamic damping B_{aero} by the derivative of thrust force F_T w.r.t wind speed U.

$$B_{aero} = \frac{\mathrm{d}F_T}{\mathrm{d}U} \tag{2.66}$$

For each mean wind speed $\bar{U}$, a corresponding aerodynamic damping B_{aero} can be found. The aeordynamic damping ratio ξ_{aero} at each wind speed can accordingly be found. Usually the critical damping is based on the 1st tower bending mode and the aerodynamic damping ratio ξ_{aero} is then calculated by

$$\xi = \frac{B_{aero}}{2m_1\omega_1} \tag{2.67}$$

where

m_1	1st tower bending modal mass[kg]
ω_1	1st tower bending natural frequency[rad/s]

Chapter 3

Methodology

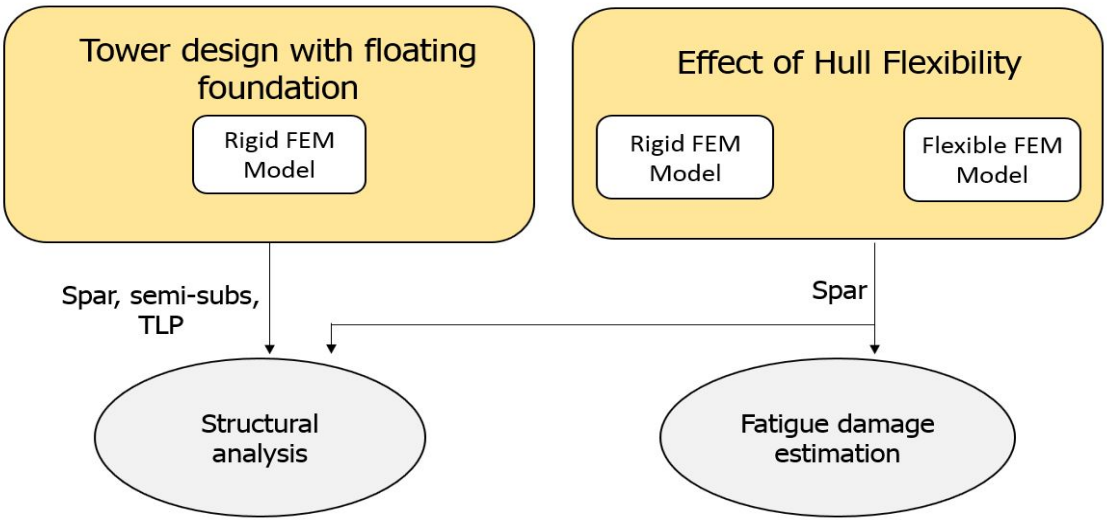

Figure 3.1: Overview of methodology

The methodology is illustrated in Figure 3.1. The first research question **"What is the difference in tower design with a floating foundation?"** is answered by implementing structural analysis based on four different floating concepts with the developed rigid hull FEM model.

The second research question **"What is the effect of hull flexibility on tower design?"** is answered by comparing the difference in dynamic properties of the tower and waves load fatigue damage between rigid hull FEM model and flexible hull FEM model based on a spar-buoy concept.

3.1 Public Available Large Size Floating Concepts

In order to implement the analyses shown in Figure 3.1, it requires description of large size floating concepts for each type, namely spar, semi-sub and TLP. Therefore, for the cases study, the used floating concepts are based on public available definition as follows

Spar-buoy

In Xue's master thesis[57], a large size spar is designed to carry the DTU 10MW wind turbine[4] by upscaling OC3-Hywind spar[28]. The spar designed by Xue is named Xue-10 in this thesis.

Semi-submersible

In research project LIFES50+[35], two semi-sub(OO-star and NAUTILUS-10) designed to carry the DTU 10MW wind turbine are described. It should be noted that the tower design of OO-star and NAUTILUS-10 are modified and they are different from the original land-based DTU 10MW wind turbine.

TLP

From Tian's master thesis[54], a upscaled version of the TLP designed by Bachynski[1] is made to carry the DTU 10MW wind turbine. The TLP designed by Tian is named Tina-10 in this thesis.

The study on tower design with floating foundation is based on four public available floating concepts mentioned above, while the effect of hull flexibility is studied based on Xue-10 spar. The geometry and properties of four floating concepts are described in Appendix A.

3.2 Model Description

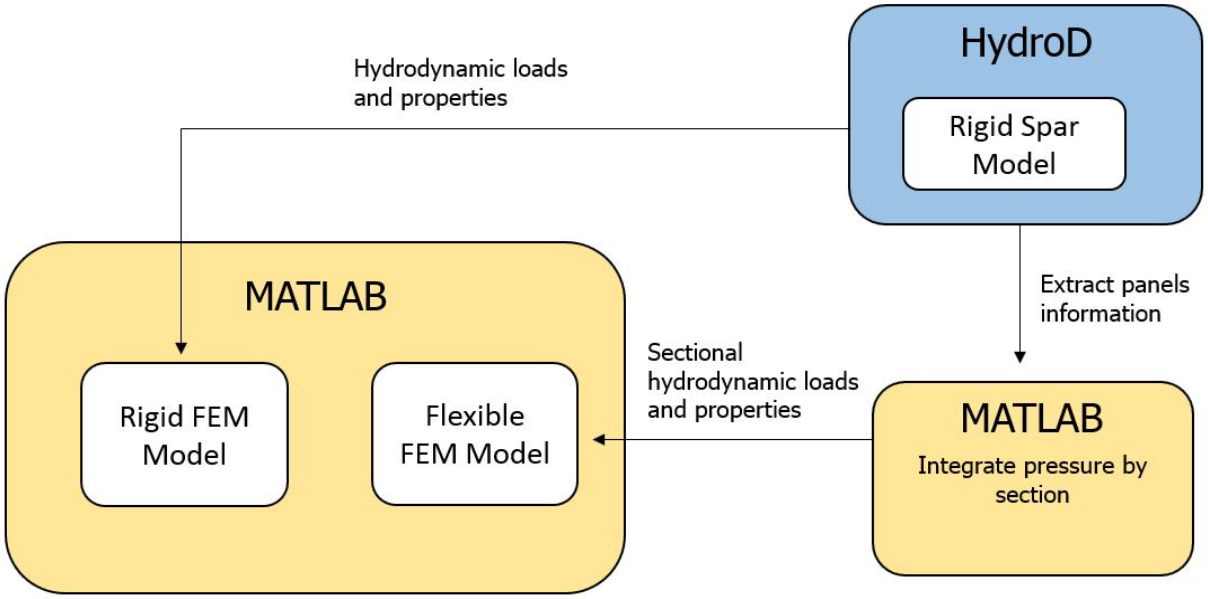

Figure 3.2: Illustration of model set up

The developed FEM models are 2-D in-plane model with each node contains only 2 DoFs(one translation and one rotation) which correspond to surge and pitch rigid body motion of the platform.

The FEM models are built in MATLAB and the hydrodynamic properties is calculated by HydroD as shown in Figure 3.2. However, it should be noted that **only a spar model is built in HydroD** because of the need to have sectional hydrodynamic properties for the flexible model. For the study "tower design with a floating foundation" the hydrodynamic properties of other floaters are extracted from the corresponding literature.

A separate MATLAB algorithm is made to process the panels information from HydroD and re-calculate the sectional hydrodynamic loads and properties. More detail about the implementation is provided in Sec. 3.3

3.2.1 Rigid FEM Model

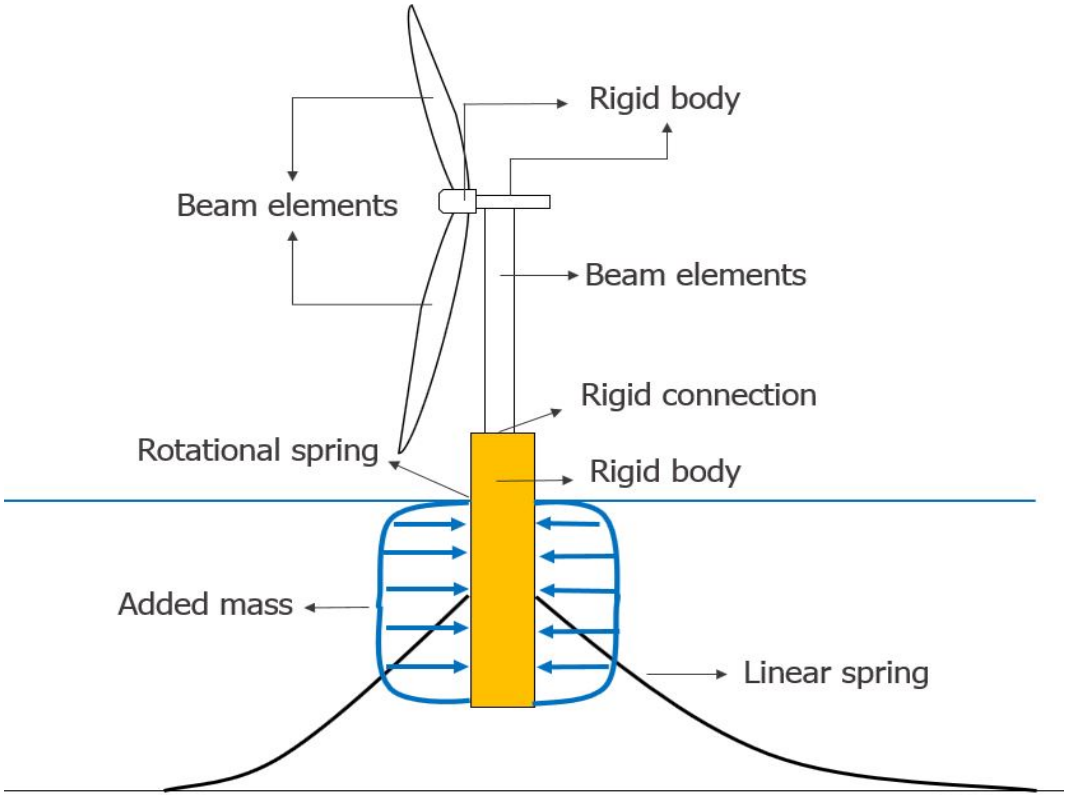

Figure 3.3: Rigid model illustration

An overview of rigid model based on a spar-buoy is illustrated in Figure 3.3. As mentioned previously, four different floaters are modeled by the rigid model. Illustration of the FEM model for each concept can also be found in Figure 3.4.

The model description starts with the assumptions made in the model, followed by the modeling approach for each component indicated in Figure 3.3. Numerical values used in the model are also provided.

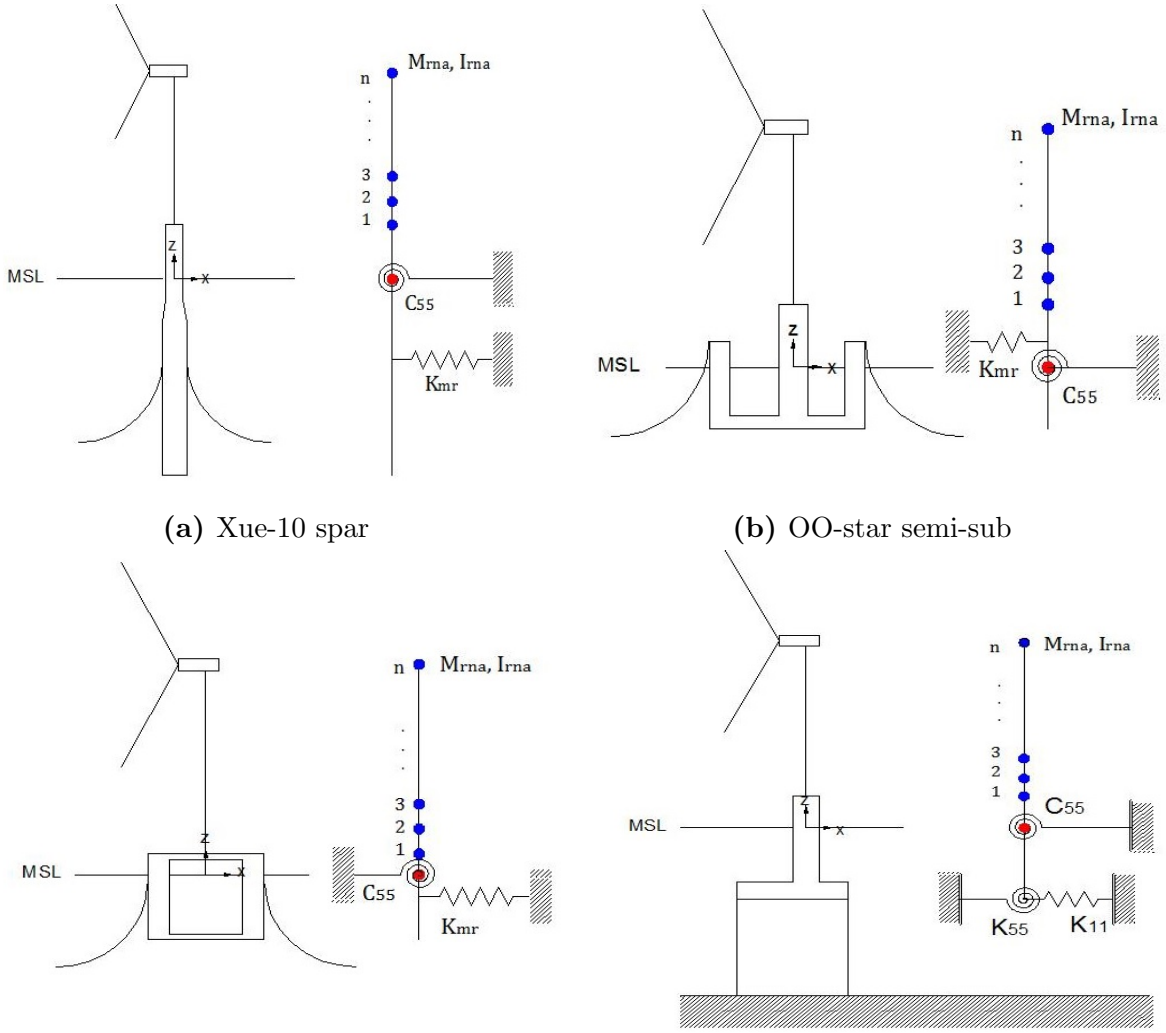

(a) Xue-10 spar

(b) OO-star semi-sub

(c) NAUTILUS-10 semi-sub

(d) Tian-10 TLP

Figure 3.4: Illustration of the rigid FEM model

Assumptions

- The tower and the floater are rigidly connected.
- Structural deformation has small influence on restoring moment.
- The nonlinear behavior of the mooring lines can be neglected.
- Nacelle, hub and floater are assumed as rigid body.
- Blades are directly connected to the tower top.

Tower

4 DoFs Euler-Bernoulli beam elements are used to described the tower. The tower is divided into 10 sections with linear varied diameter and thickness. The assembly of each elements to form the whole tower is demonstrated in Sec. 2.4.

RNA

Nacelle and hub are modeled by a point mass located at the tower top while the blades are modeled by 4 DoFs Euler-Bernoulli beam elements. The sectional properties of the blades such as mass and bending stiffness are extracted from the definition of DTU 10MW wind turbine[4]. The flap-wise sectional bending stiffness is used for the blades.

Since the developed model is a 2-D model includes only in-plane(x-z plane) motions as shown in Figure 3.5a, the inclusion of the blades means that the beam elements for the blades have to rotate out of the plane(y-z plane). The blades location for the model is chosen as one straight up and two with $\pm$ 120 $^\circ$ rotation as shown in Figure 3.5b.

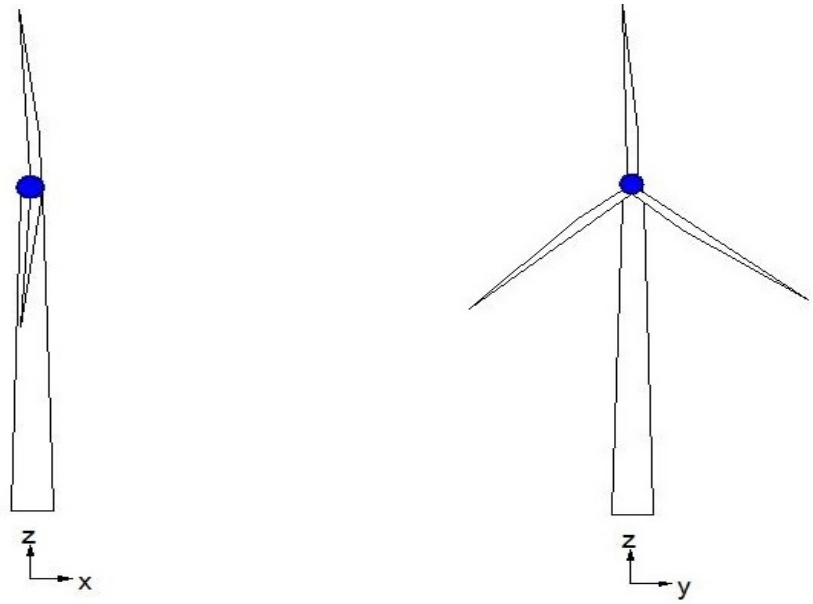

(a) x-z plane **(b)** y-z plane

Figure 3.5: Illustration of blades in two planes

Axes rotation for each beam element can be implemented by using rotation matrix as explained in Sec. 2.4.1. In the case of blades shown in Figure 3.5b, the beam elements should rotate ± 120 ° along y-z plane and rotation matrix R_x should be used

$$R_x = \begin{bmatrix} 1 & 0 & 0 \\ 0 & \cos \pm 120^\circ & -\sin \pm 120^\circ \\ 0 & \sin \pm 120^\circ & \cos \pm 120^\circ \end{bmatrix} \tag{3.1}$$

Since the DoFs in the model are translation and rotation in y-z plane, which means the considered DoFs in Equation 2.53 should be x and θ_y

$$\begin{bmatrix} x \\ \theta_y \end{bmatrix} = \begin{bmatrix} 1 & 0 \\ 0 & \cos \pm 120^\circ \end{bmatrix} \begin{bmatrix} \bar{x} \\ \bar{\theta}_y \end{bmatrix} = \mathbf{T}_0 \begin{bmatrix} \bar{x} \\ \bar{\theta}_y \end{bmatrix} \tag{3.2}$$

which lead to transformation matrix

$$\mathbf{T}_g = \begin{bmatrix} 1 & 0 & 0 & 0 \\ 0 & \cos \pm 120^\circ & 0 & 0 \\ 0 & 0 & 1 & 0 \\ 0 & 0 & 0 & \cos \pm 120^\circ \end{bmatrix} \tag{3.3}$$

In addition to blades, the remaining part of RNA (hub and nacelle) are included as point mass at the tower top and the numerical numbers of mass and moment of inertia of each RNA components are provided in Table 3.1.

	Blades	**Hub**	**Nacelle**	**Total**
Mass [kg]	1.25E+5	1.06E+5	4.46E+5	6.77E+5
Inertia [kgm^2]	9.11E+7	6.07E+6	5.90E+6	1.03E+8

Table 3.1: Mass and moment of inertia (around tower top y-axis) of RNA components

Floater

The representative point of the floater is selected at MSL and it is assumed that the pitch angle of the floater is small. The small pitch angle assumption should be valid because in the design of a floater there is a limitation(i.e. 7°)[15] in pitch angle under maximum mean wind speed for stability reason, which means for most of the time the pitch angle is small.

If the floater has mass M_{fl}, center of mass of z_{fl}, and moment of inertia around center of mass I_{fl}, by using parallel axis theorem, the mass matrix can be written as

$$\mathbf{M}_{fl} = \begin{bmatrix} M_{fl} & M_{fl} \cdot z_{fl} \\ M_{fl} \cdot z_{fl} & I_{fl} + M_{fl} \cdot z_{fl}^2 \end{bmatrix} \tag{3.4}$$

Hydrodynamic Added Mass

As explained in Sec. 2.2, hydrodynamic added mass can be obtained from either Morison equation or potential flow solvers. For the developed model, since four floating concepts have different geometry and the calculation of added mass can be a repetitive work, it is decided to use the added mass appeared in the corresponding literature for each floater, and the extracted values are zero-frequency added mass.

However, due to the necessity of using potential flow solver to obtain sectional added mass for flexible FEM model, the added mass used for Xue-10 is frequency dependent as shown in Figure 3.6. The zero-frequency added mass of the other three floaters are listed in Table 3.2.

	OO-star	NAUTILUS-10	Tian-10
A_{11}[kg]	1.7E+7	5.7E+6	1.51E+7
A_{15}, A_{51}[kgm]	-2.0E+8	-2.46E+7	-5.82E+7
A_{55}[kgm^2]	1.4E+10	1.07E+10	1.08E+10

Table 3.2: Zero-frequency added mass of three floaters

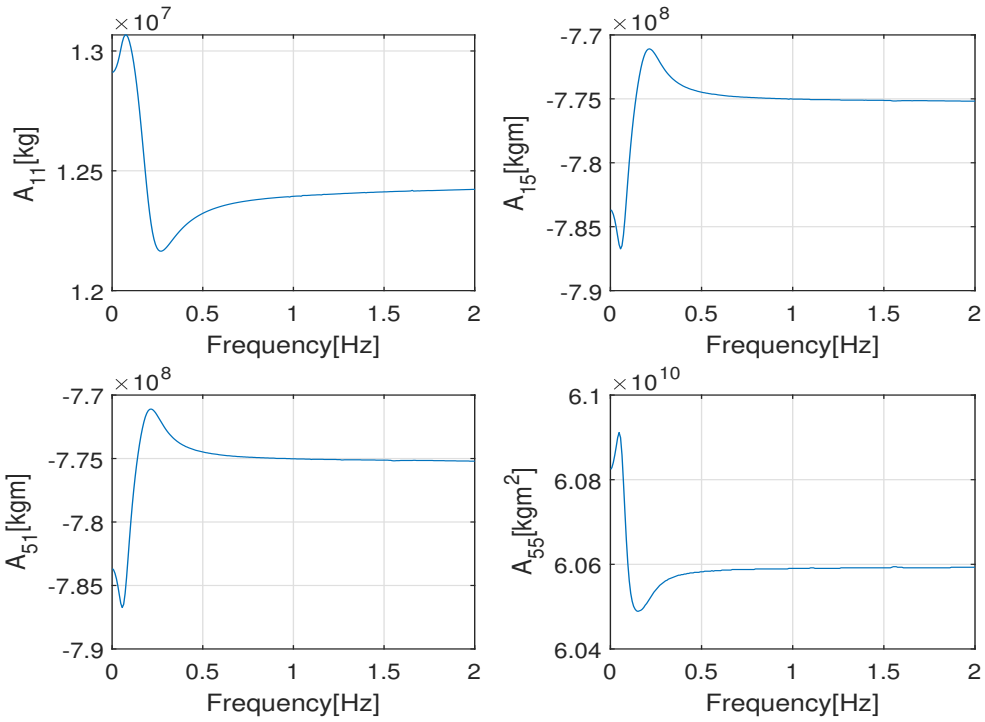

Figure 3.6: Frequency dependent added mass of Xue-10 spar

Hydrostatic Stiffness

Restoring moment due to the pitch motion of the floater is modeled by a rotational spring at MSL. The stiffness of the rotational spring is calculated based on Equation 2.19 from conventional hydrostability theory. It has to be addressed that using Equation 2.19 implies the effect of tower deformation on restoring moment is neglected, which means the shift of center of mass caused by tower deformation is

neglected. Because tower has much smaller mass than the floater, the magnitude of the shift should be small enough to be ingnored.

	Xue-10	**OO-star**	**NAUTILUS-10**	**Tian-10**
C_{55}[Nm/rad]	1.64E+9	1.44E+9	1.37E+9	-2.82E+9

Table 3.3: Hydrostatic stiffness in pitch motion for four floaters

Linearized Mooring Lines(Catenary)

The whole mooring lines system is represented by a linear spring with stiffness K_{mr} linearized at the equilibrium position. Since the study of this thesis mainly focuses on the dynamics of the wind turbine rather than mooring lines, it is considered sufficient to use a linear spring for the study.

The linearized stiffness of a catenary mooring lines system can be calculated by the closed form solution(Equation 2.36). However, due to the presence of a clump weight in Xue-10's and OO-star's mooring system, the closed form solution is not applicable. Therefore, the linearized stiffness is obtained numerically for Xue-10 and OO-star(see Appendix B).

Suppose the fairlead of the mooring lines is located at z_{mr}, the stiffness matrix due to the mooring lines can be written as

$$\mathbf{K}_{mr} = \begin{bmatrix} K_{mr} & K_{mr}z_{mr} \\ K_{mr}z_{mr} & K_{mr}z_{mr}^2 \end{bmatrix} \tag{3.5}$$

Linearized Mooring Lines(TLP)

For the TLP, as shown in Figure 3.4 a rotational spring and a translational spring are placed at the fairlead elevation. However, it should be noted that the illustration in Figure 3.4 is not fully representative to what it is implemented in the model. Based on the illustration the stiffness matrix from mooring lines should be

$$\mathbf{K}_{mr} = \begin{bmatrix} K_{11} & K_{11}z_{mr} \\ K_{11}z_{mr} & K_{11}z_{mr}^2 + K_{55} \end{bmatrix} \tag{3.6}$$

However, the stiffness matrix used in the model is

$$\mathbf{K}_{mr} = \begin{bmatrix} K_{11} & K_{11}z_{mr} \\ K_{11}z_{mr} & K_{55} \end{bmatrix} \tag{3.7}$$

The reason for such difference is because the calculation of rotational stiffness K_{55} from Equation 3.7 already accounts for the contribution from K_{11}. In addition, despite that the developed model does not include heave motion, the rotational stiffness K_{55} still includes the contribution from K_{33} as shown in Equation 3.7.

An overview of the linearized mooring stiffness for four floating concepts are listed in Table 3.4. The order of the values indicates that the TLP mooring system provides much higher pitch stiffness constraint than the others.

	Xue-10	**OO-star**	**NAUTILUS-10**	**Tian-10**
K_{mr}[N/m]	9.00E+4	2.75E+4	4.46E+4	
$K_{mr}z_{mr}^2$[Nm]	4.41E+8	3.72E+6	1.77E+6	
K_{11}[N/m]				4.99E+5
K_{55}[Nm]				2.20E+12

Table 3.4: Linearized mooring line stiffness

Implementation of Rigid Connection

Once the mass and stiffness matrices of the wind turbine and the floater are formulated, they can be assembled as follows

$$\mathbf{M} = \begin{bmatrix} \mathbf{M}_{fl} + \mathbf{A} & 0 \\ 0 & \mathbf{M}_{tb} \end{bmatrix} \tag{3.8}$$

$$\mathbf{K} = \begin{bmatrix} \mathbf{K}_{fl} & 0 \\ 0 & \mathbf{K}_{tb} \end{bmatrix} \tag{3.9}$$

where

$\mathbf{M}_{fl}$	floater mass matrix
$\mathbf{A}$	hydrodynamic added mass matrix
$\mathbf{M}_{tb}$	wind turbine mass matrix
$\mathbf{K}_{fl}$	hydrostatic and mooring stiffness matrix
$\mathbf{K}_{tb}$	wind turbine stiffness matrix

Suppose the wind turbine has m number of DoFs, the size of the system matrices should be $m + 2$ as shown

$$\mathbf{M}, \mathbf{K} = \begin{bmatrix} 2 \times 2 & \mathbf{0} \\ \mathbf{0} & m \times m \end{bmatrix} \tag{3.10}$$

Clearly from the matrices above the relation between the wind turbine and the floater has not yet been described(not coupled). Since the tower and the floater are assumed to be rigidly connected, a compatibility condition should be applied. The compatibility condition can be achieved by using Master-Slave elimination technique. The detail on the implementation of Master-Slave elimination technique is well described in Sec. 2.4.2.1.

3.2.2 Flexible FEM Model

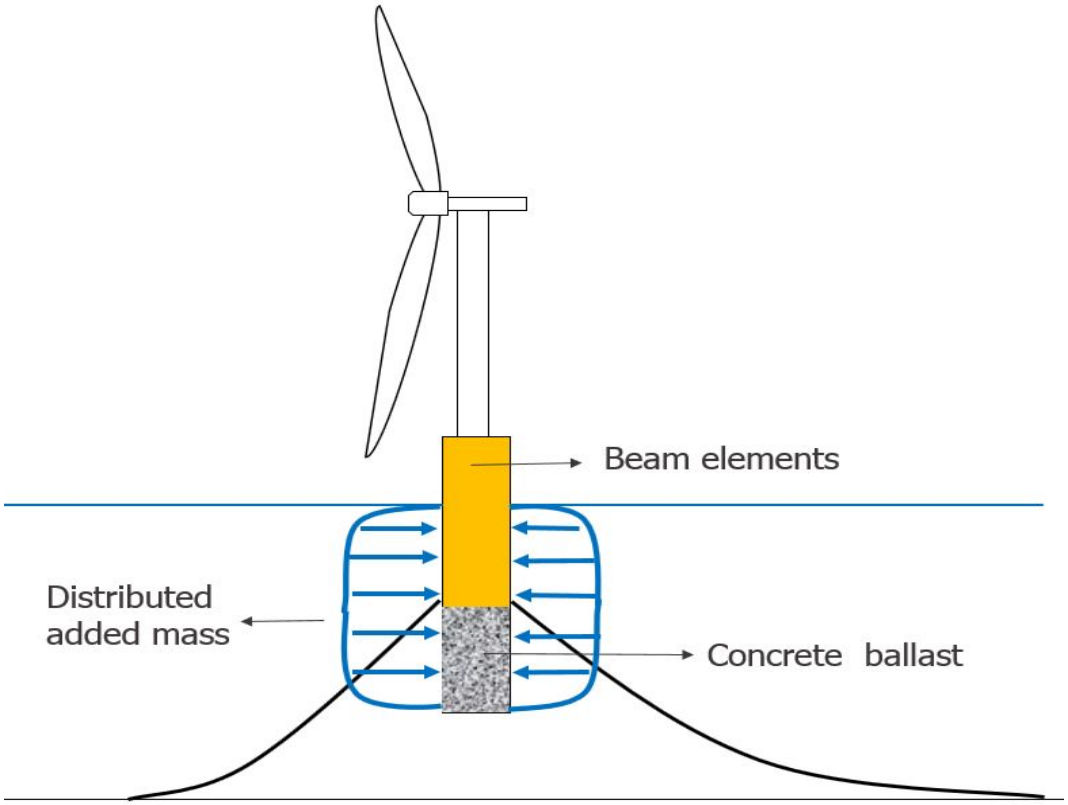

Figure 3.7: Flexible model illustration

The flexible model is built by describing the steel hull of the spar as beam elements, and the ballast is calculated by having the same floater weight and weight distribution as the rigid model. The sectional hydrodynamic added mass is obtained by building a spar model in HydroD. Panels mesh is created and the pressure on each panel is calculated in HydroD. The information of each panel is extracted from the HydroD. The pressure is re-integrated in MATLAB for each section defined in the FEM model. The hydrodynamic added mass is computed based on rigid body assumption and therefore the approach is zeroth-order hydroelasticity modeling.

Assumptions

- The tower and the floater are rigidly connected.
- Structural deformation has small influence on restoring moment.
- The nonlinear behavior of the mooring lines can be neglected.
- Nacelle, hub and floater are assumed as rigid body
- The ballast is filled with concrete(constant density) at the bottom of the spar.

Steel Hull

The steel hull is modeled by 4-DoFs Euler-Bernoulli beam elements. The density of the steel is assumed 7,850kg/m^3 and the Young's modulus is assumed 210GPa.

Distributed Added Mass

For the flexible model, added mass should be distributed into each element below MSL. The distributed added mass is generated by reprocessing the panels pressure from HydroD. Detail about the implementation is provided in Sec. 3.3.

Concrete Ballast

The reference thesis[57] of Xue-10 spar states that the ballast is filled with only concrete at the bottom of the spar. Therefore, the ballast distribution is calculated based on the assumption of fully concrete ballast at the bottom, and it is calculated by having a consistent weight and center of gravity.

First, the ballast mass is calculated by subtracting the mass of the steel from the total floater mass. Once the ballast mass is found, the height of the ballast is then computed by matching the center of gravity(Figure 3.9) based on the assumption of a constant ballast density. From the computed concrete height, the ballast density can be obtained by dividing the mass by the volume. The resultant concrete density is found to be 2,135kg/m^3.

In addition, the concrete ballast is also modeled by 4 DooF Euler-Bernoulli beam element. The Young's modulus of the concrete is assumed to be 30GPa.

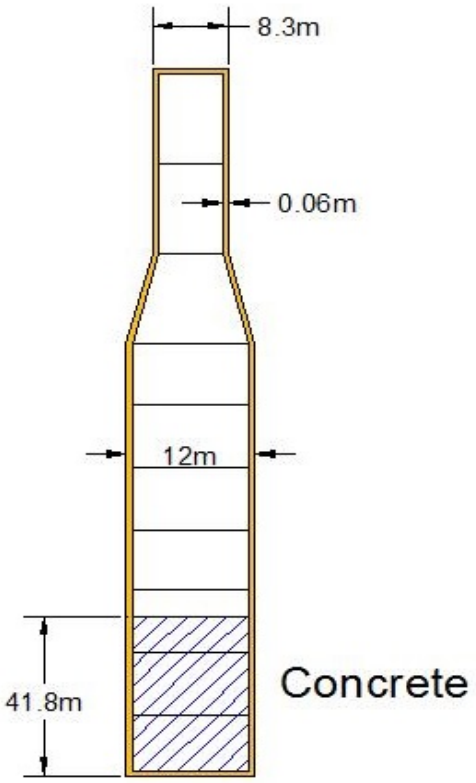

Figure 3.8: Bottom concrete ballast

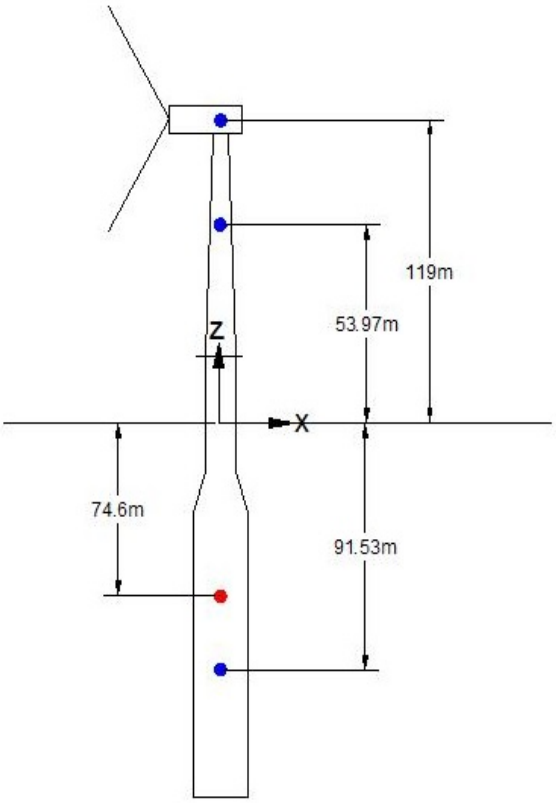

Figure 3.9: Center of gravity. RNA, tower and spar(blue). Whole structure(red)

3.3 Sectional Hydrodynamic Load and Properties

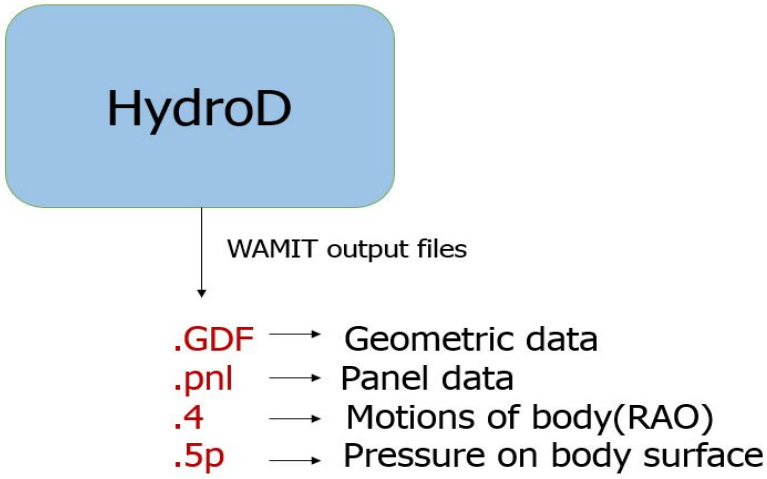

Figure 3.10: WAMIT files output from HydroD

To re-integrate panels pressure, it requires WAMIT output files generated by HydroD as shown in Figure 3.10. These data files are processed in MATLAB and sectional hydrodynamics load(added mass, radiation damping and wave excitation force) and can be reproduced.

Added mass and radiation damping can be calculated from radiation pressure, while wave excitation force can be calculated from diffraction pressure. From WAMIT user manual[56] the pressure from .5p file is defined as

$$\bar{p} = \bar{\varphi_D} + KL \sum_{j=1}^{6} \bar{\xi}_j \bar{\varphi}_j \tag{3.11}$$

where

KL	non-dimensional infinite depth wave number[-]
$\bar{\xi}_j$	non-dimensional RAO in j motion[-]
$\bar{p}$	non-dimensional total pressure[-]
$\bar{\varphi_D}$	non-dimensional diffraction potential[-]
$\bar{\varphi}_j$	non-dimensional radiation potential in j motion[-]

Because .5p file only gives total pressure without separation of diffraction and radiation, and it is difficult to change the configuration in HydroD to give separated diffraction and radiation pressure, some tricks are required to separate the total pressure into diffraction and radiation pressure.

Firstly, it is possible to set the structure as fixed position in HydroD, which means the pressure from radiation potential can be excluded and the output pressure will be diffraction pressure.

Secondly, to separate radiation pressure into 6 components(each rigid body motion), constraints are applied to all rigid body motions except the one that is of interest. For example, if radiation pressure due to surge motion is of interest, it can be found by applying constraints to other five motions. The constraint can be achieved by assigning extremely high stiffness to the motion.

It should also be noted that the radiation pressure in WAMIT is defined as

$$\bar{p_j} = KL\bar{\varphi_j} \tag{3.12}$$

which means the radiation pressure from from .5p file should normalized by non-dimensional RAO $\bar{\xi_j}$(from .4 file).

Once diffraction and radiation pressure are separated, they can be used to generate sectional hydrodynamic load and properties.

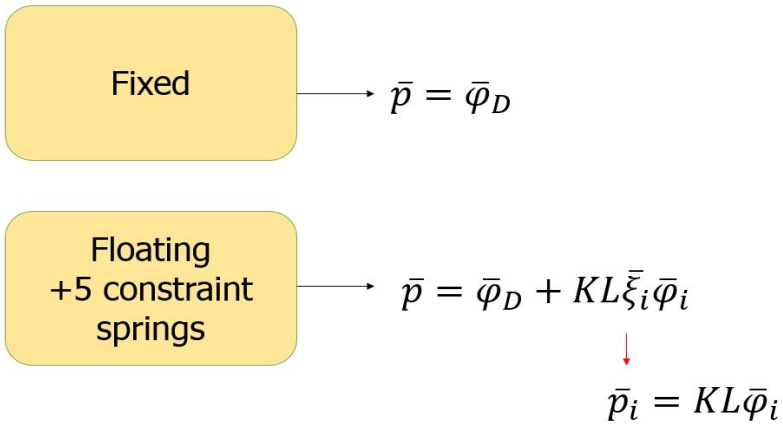

Figure 3.11: Tricks to separate diffraction and radiation

Added Mass and Radiation Damping

Sectional added mass and radiation damping can be obtained by numerically integrating radiation pressure on the body surface

$$A_{ij} - \frac{i}{\omega} B_{ij} = \rho \int \int p_j n_i dS \tag{3.13}$$

where

A_{ij}	added mass in i direction due to j motion[kg]
B_{ij}	radiation damping in i direction due to j motion[Ns/m]
n_i	panels normal vector in i direction [-]
p_j	radiation pressure due to j motion [Pa]
ρ	water density [kg/m^3]

The resultant added mass and radiation damping distribution are plotted in Figure 3.12 and 3.13. The added mass distribution shows that added mass is almost constant in the middle and becomes smaller at two ends. Since added mass is not real mass but the resistance from water particles to the body acceleration, they have more space to escape at two ends. Therefore, the resultant distribution can be expected. On the other hand, the radiation damping distribution implies that energy dissipation from radiation mostly happens at water surface as oscillating frequency goes higher(for the case of a deep-draft spar).

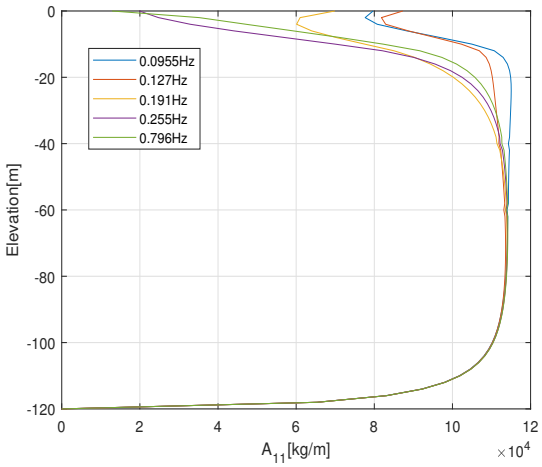

Figure 3.12: Added mass distribution

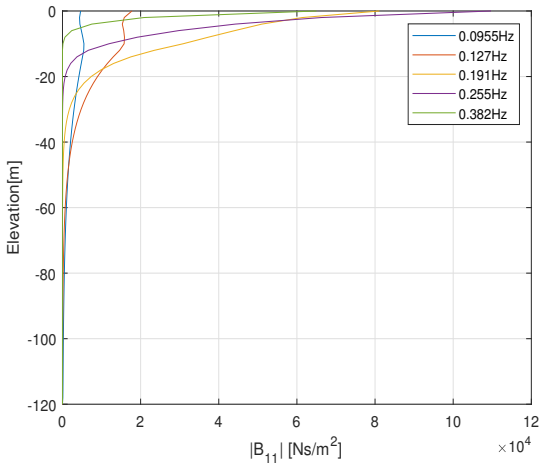

Figure 3.13: Radiation damping distribution

The algorithm to process the panels is validated by comparing the summation of sectional added mass and radiation damping with the original output from HydroD. As shown in Figure 3.14, the algorithm can yield to the same results as the ones from HydroD.

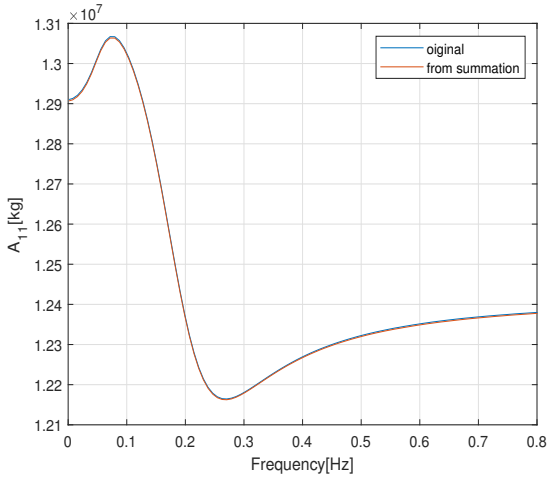

Figure 3.14: A_{11} comparison

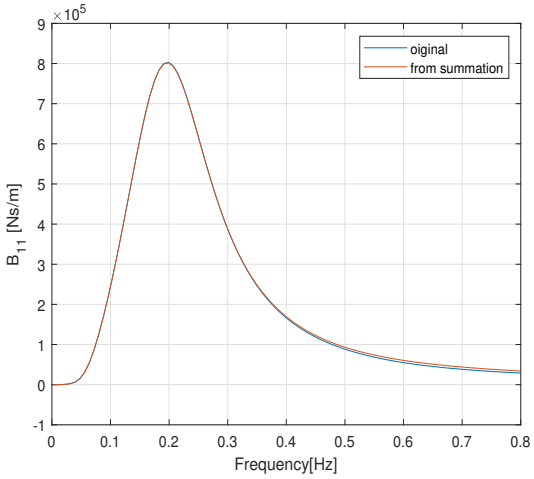

Figure 3.15: B_{11} comparison

Wave Excitation Force

Sectional wave excitation force can be found by numerically integrating diffraction pressure on the body surface

$$X_i = -i\omega\rho \int\int p_D \cdot \vec{n}_i dS \tag{3.14}$$

where

X_i	wave excitation force in i direction[N]
p_D	diffraction pressure[Pa]
n_i	normal vector in i direction[-]
ρ	water density[kg/m^3]

The resultant wave excitation force distribution is plotted in Figure 3.16. The result shows that the water particles movement only appears near the surface at high frequency(shorter wave length), which is aligned with linear wave theory. The sudden jump of the wave force at around 16m below MSL is due to the tapered section of the spar, where the diameter of the spar varies from 8.3m to 12m.

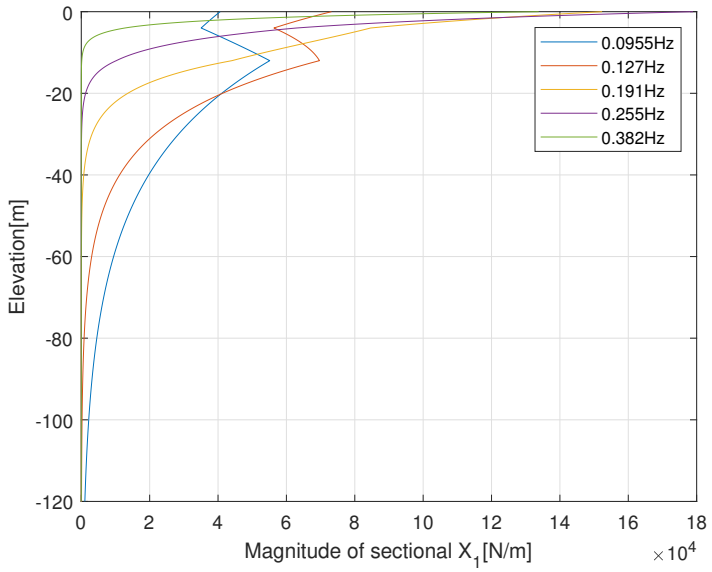

Figure 3.16: Wave excitation force per unit length along the depth

3.4 Tower Design with Floating Foundation

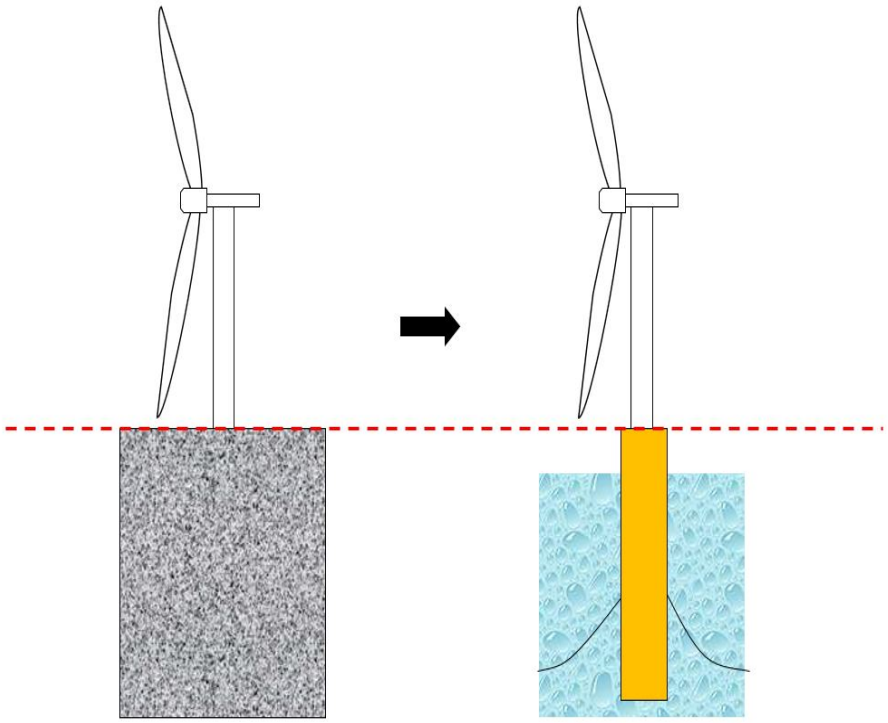

Figure 3.17: From bottom fixed foundation to floating foundation

As mentioned in Sec 1.3 the tower design nowadays still mainly focuses on bottom fixed foundation and very few literature have discussed the possible consequence of using a land-based tower design directly to a floating wind turbine. Therefore, to answer the research question **"What is the difference in tower design with a floating foundation?"**, the dynamic properties of the tower with a fixed foundation and with a floating foundation are compared as shown in Figure 3.17.

Four floating concepts(1 spar, 2 semi-subs and 1 TLP) are examined. In addition, it should be noted that due to freeboard requirement of a floating foundation, the original land-based DTU 10MW tower is truncated at the bottom to keep the hub height unchanged. In other words, the tower put on the floaters has different length than the original land-based tower. In order to be comparable for the study, the tower with a fixed foundation is based on the truncated tower length.

3.5 Effect of Hull Flexibility

To answer the second research question **"What is the effect of hull flexibility on tower design?"**, two analyses based on a spar-buoy are implemented. First, the dynamic properties of the tower from rigid hull to flexible hull is examined. Second, the fatigue damage at the tower bottom in 20 years life time under waves load is evaluated for both rigid hull model and flexible hull model.

3.5.1 Dynamic Properties of Tower

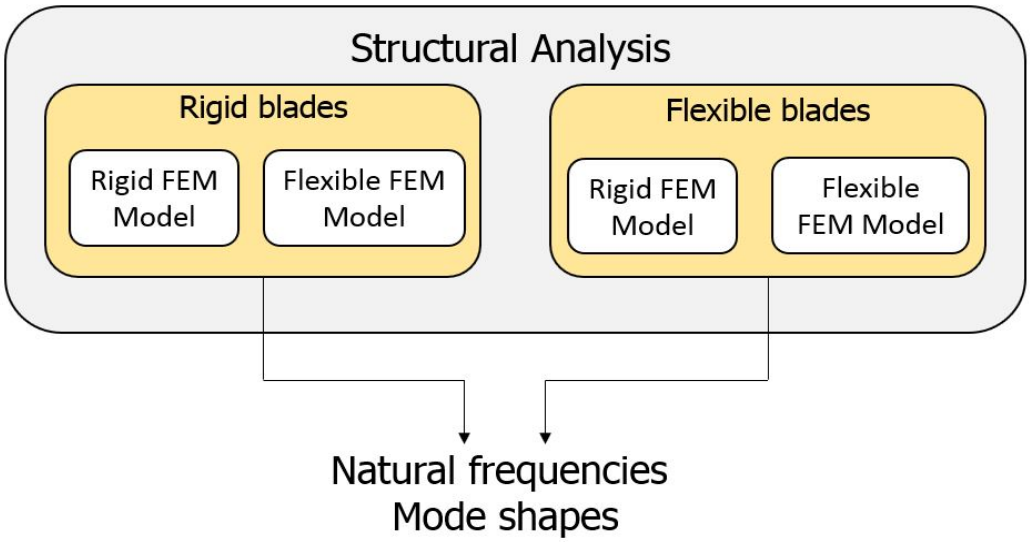

Figure 3.18: Investigation on the effect of hull flexibility on tower dynamic properties

The dynamic properties of the tower is first examined by using rigid blades in both models in order to avoid blades flexibility involved. The 1st tower bending natural frequency is evaluated together with consideration of 1P-3P frequency ranges. Moreover, two tower designs are made for sensitivity study on the effect of hull flexibility. The second part of the investigation will also include the flexibility of the blades and an overview of the dynamic properties of the system is assessed.

3.5.2 Life Time Fatigue Damage in Frequency Domain

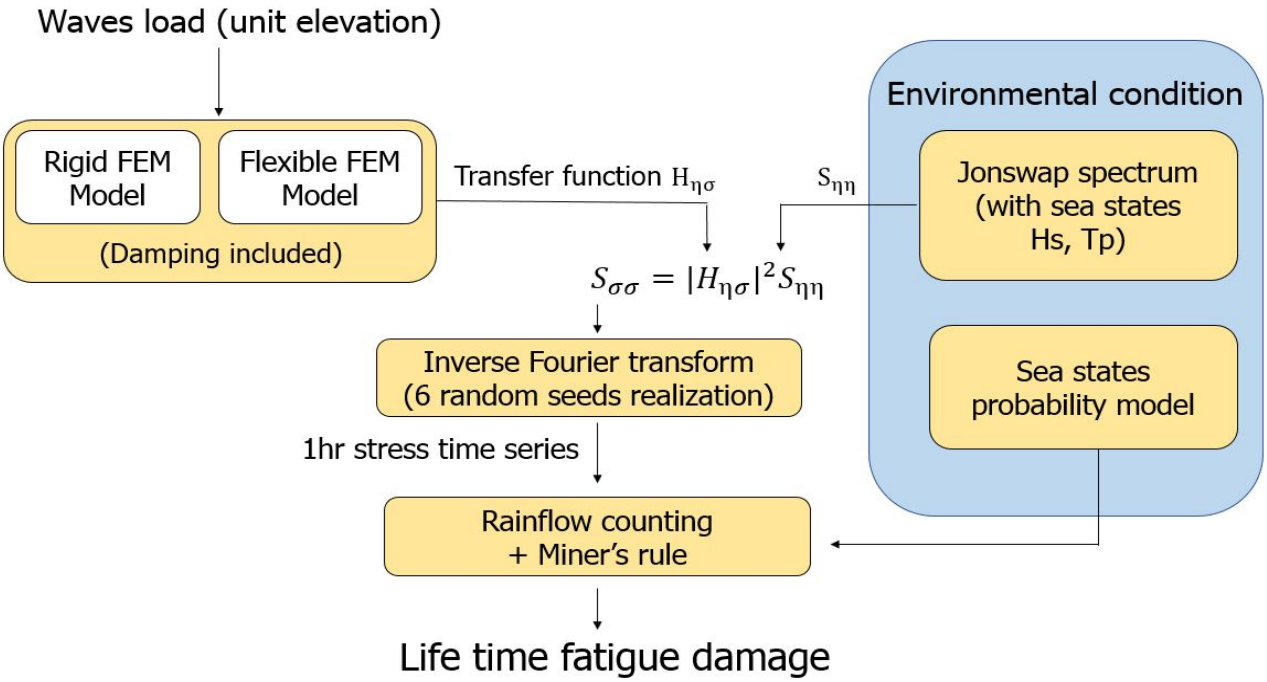

Figure 3.19: Steps for fatigue damage calculation

The life time fatigue damage under waves load is evaluated followed by the steps described in Figure 3.19. The fatigue damage is evaluated based on the **axial stress at the tower bottom**. 20 years life time is assumed. The frequency response function under waves load is obtained by applying a unit amplitude wave load to the two FEM models with damping included. The stress spectrum can be obtained from frequency response function together with wave spectrum. An one hour stress time series is then generated by inverse Fourier transform with assigned random phases. The fatigue damage from the one hour time series is evaluated by rainflow counting and Palmgren-Miner rule. For each sea state the simulation uses six realizations. The life time damage caused by each sea state is obtained by using the one-hour fatigue damage multiplying by 175,200(20years/1hour) with the corresponding sea state probability. The total life time damage is then the summation of the damage from each sea state.

Damping

The considered damping sources are drag damping, radiation damping, structural damping and aerodynamic damping, as illustrated in Figure 3.20.

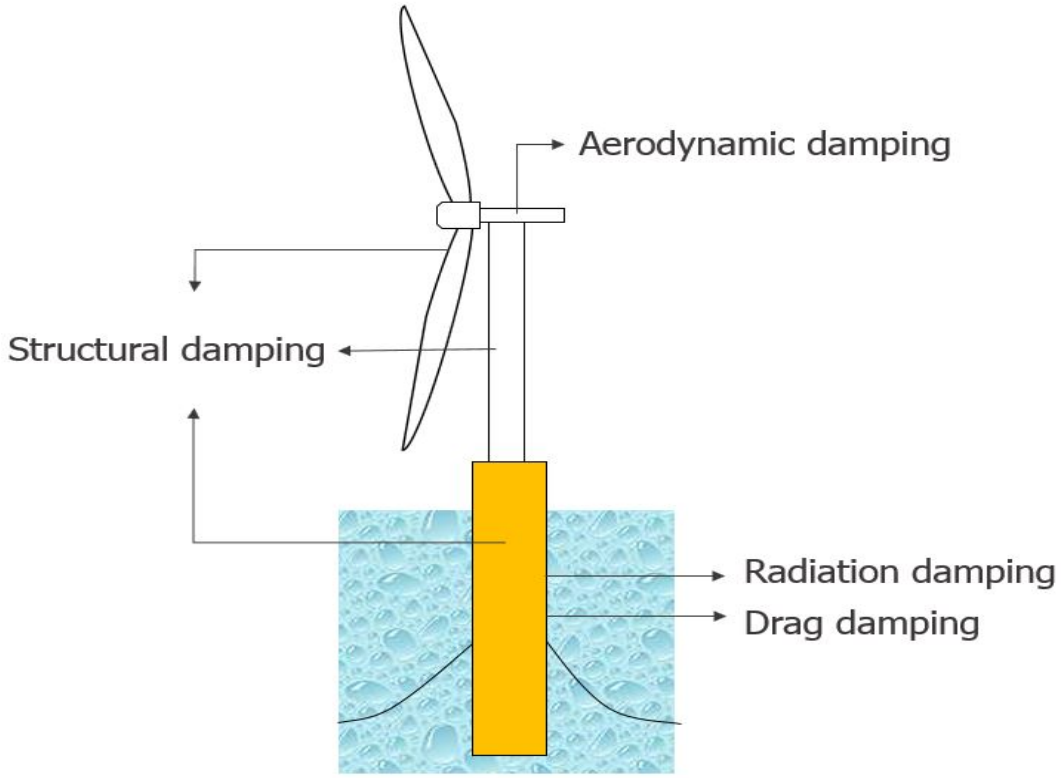

Figure 3.20: Damping sources in the system

Drag damping is evaluated in an iterative scheme as described in Sec. 2.2.4. Radiation damping is extracted from HydroD and the sectional radiation damping is recalculated for the flexible model(see Sec. 3.3).

Structural damping is included by using stiffness proportional damping(Rayleigh damping). The proportional coefficients are calculated based on the damping ratio of the 1st bending mode. 0.8% damping ratio is used for the tower and 1.2% for the blades. The stiffness proportional coefficient β for the tower are calculated as 0.0058 and 0.0071 for rigid model and flexible model respectively, while blades has β=0.0062 based on 1.2% damping ratio.

As for aerodynamic damping, the linearization of aerodynamic damping can be a challenging task without a time domain model in hand, as explained in Sec. 2.5. Therefore, in this study, the aerodynamic damping is based on the 1st tower bending mode of the **onshore DTU 10MW with a constant** 6% **damping ratio**. The 6% damping ratio is purely an engineering guess and the reason for using the onshore 1st tower bending mode is to avoid rewarding a higher aerodynamic damping for the stiffer system. The aerodynamic damping is introduced into the model as a dashpot at the tower top as shown in Figure 3.21.

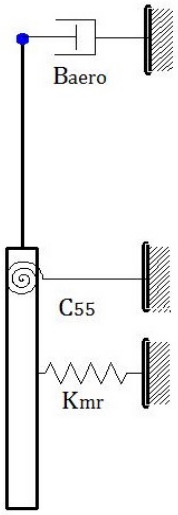

Figure 3.21: Dashpot at tower top for aerodynamic damping

Waves Load

The waves load with unit amplitude is directly extracted from HydroD as shown in Figure 3.22. For the flexible model, the sectional waves load is generated by re-integrating the pressure on the body surface as described in Sec. 3.3. In addition, the drag force from waves excitation is neglected because the KC number at the water surface is generally smaller than 3, which means waves load is inertia dominant.

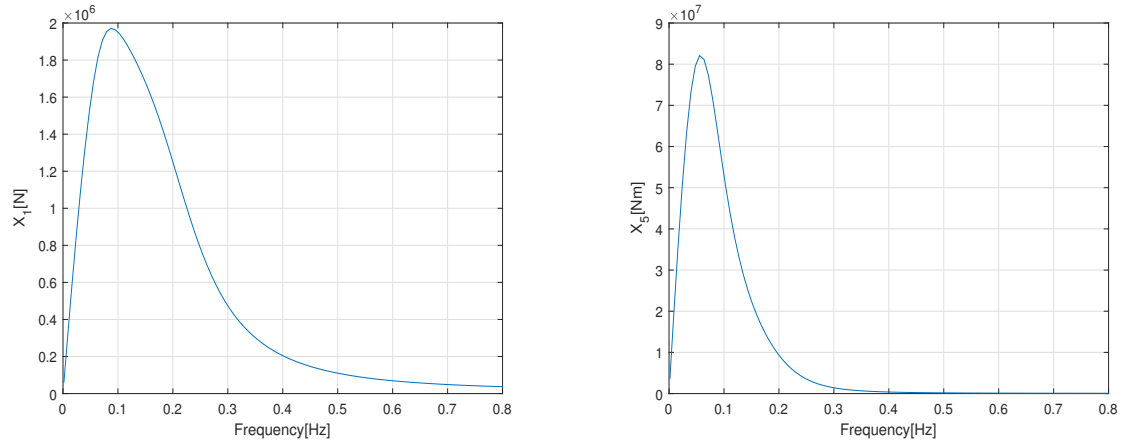

(a) Magnitude of X_1 (wave force in surge) **(b)** Magnitude of X_5 (wave force in pitch)

Figure 3.22: Wave excitation force with unit wave amplitude

Frequency Response Function

The frequency response function from unit wave elevation to axial stress at the tower bottom is obtained through three steps.

The first step is to calculate the structural response by applying unit amplitude waves load to the FEM models

$$\mathbf{r} = [-\omega^2(\mathbf{M} + \mathbf{M}_A(\omega)) + i\omega\mathbf{B} + \mathbf{K}]^{-1} \cdot \mathbf{F}_{wave} \tag{3.15}$$

The second step is to compute the bending moment response M at the tower bottom by utilizing the stiffness matrix for beam element from finite element theory. The last step is to compute the axial stress due to the bending moment. The axial stress caused by axial force is assumed to be insignificant because a spar-buoy has very minor heave motion. Therefore, the axial stress is computed from

$$\sigma = \frac{My}{I} \tag{3.16}$$

where

M	bending moment at tower bottom [Nm]
y	distance from neutral axis to the point [m]
I	area moment of inertia[m^4]

The frequency response function is then obtained by repeating the above steps for each frequency. The result can be seen in Figure 3.23.

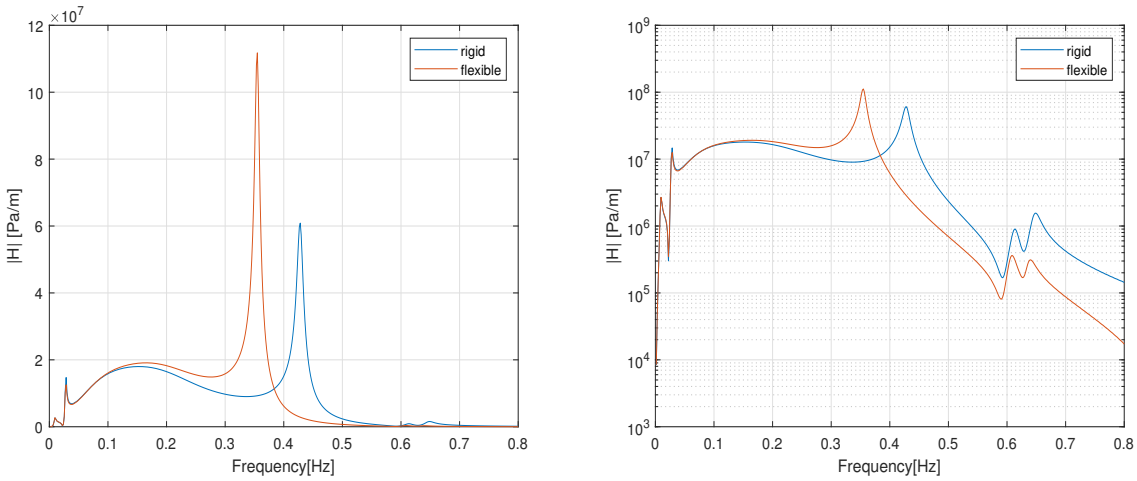

(a) Normal scale **(b)** Log scale

Figure 3.23: $H_{\eta\sigma}$, transfer function from unit wave elevation to axial stress at the tower bottom

The difference appears in Figure 3.23 suggests that the response under waves load is different in two models. Later structural analysis will show that the main difference is caused by the different tower bending natural frequency in two models. Discussion on tower dynamic properties change from rigid hull to flexible hull will be discussed in Sec. 4.2.

S-N Curve

The chosen S-N curve is based on DNV-RP-C203[14] 2.4 class D, which is defined as circumferential butt weld from both sides. The corresponding material and parameters are K=$10^{12.64}$ and m=3.

Environmental condition

In order to estimate the fatigue damage in life time, environmental condition is required. A joint wind wave model built by K.Johannessen[24] is used.

The wind turbine fatigue load case estimation is chosen as **fully operational condition**, which corresponds to wind speed from cut-in to cut-out(4m/s to 25m/s).

However, because only waves load is considered, wind speed is lumped. In other words, the original wind-wave probability model should result in a three dimensional matrix with each dimension as wind speed, wave height and peak period. Lumping wind speed means that the wind speed dimension is compressed, leading to a two dimensional matrix(Hs-Tp scatter diagram). The result is illustrated in Figure 3.24.

For each sea state, the selected wave spectrum is based on JONSWAP spectrum[19] and the peak enhancement parameter γ is decided based on the combination of H_s and T_p. According to DNVGL C205[13] 3.5.5.5:

$$\gamma = \begin{cases} 5, & \text{for} \quad \frac{T_p}{\sqrt{H_s}} \leq 3.6 \\ \exp(5.75 - 1.15\frac{T_p}{\sqrt{H_s}}) & \text{for} \quad 3.6 < \frac{T_p}{\sqrt{H_s}} < 5 \\ 3, & \text{for} \quad 5 \geq \frac{T_p}{\sqrt{H_s}} \end{cases}$$

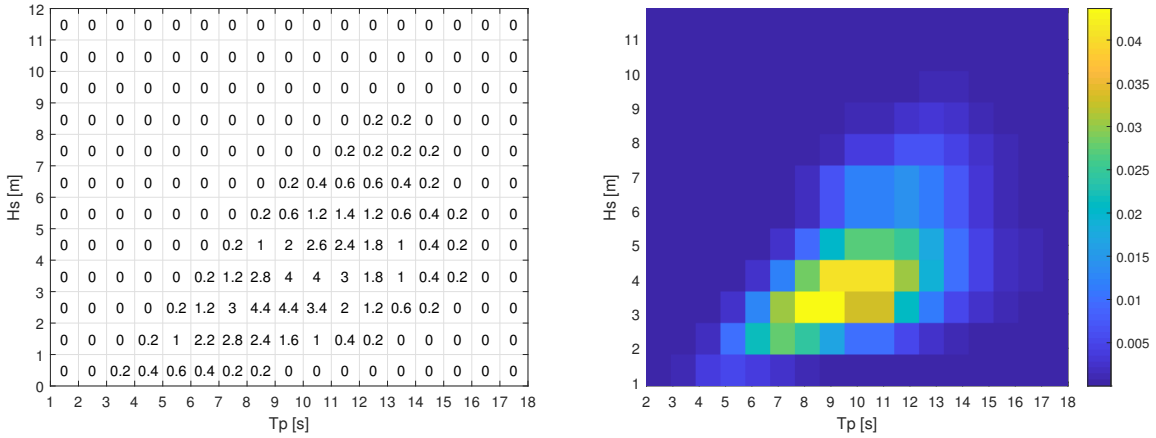

(a) Probability[%] **(b)** Colorized

Figure 3.24: Hs-Tp scatter diagram

Chapter 4

Results and Discussion

4.1 Tower Design with Floating Foundation

As explained in Sec. 3.4 four types of floating wind turbines are examined based on rigid model. The tower natural frequencies with fixed foundation and floating foundation are listed in Table 4.1 and 4.2. The resultant 1st tower bending natural frequency are also plotted in 1P-3P diagram as shown in Figure 4.1.

Natural Period[s] /Frequency[Hz]	**Xue-10**	**OO-star**	**NAUTILUS-10**	**Tian-10**
Clamped Tower	3.34/0.3	1.89/0.53	2.50/0.4	3.34/0.3
Floating Platform	2.34/0.43	1.37/0.73	1.80/0.56	3.31/0.3

Table 4.1: 1st tower bending natural period/frequency

Natural Period[s] /Frequency[Hz]	**Xue-10**	**OO-star**	**NAUTILUS-10**	**Tian-10**
Clamped Tower	0.57/1.75	0.42/2.38	0.44/2.27	0.57/1.75
Floating Platform	0.55/1.82	0.41/2.44	0.43/2.33	0.59/1.69

Table 4.2: 2nd tower bending natural period/frequency

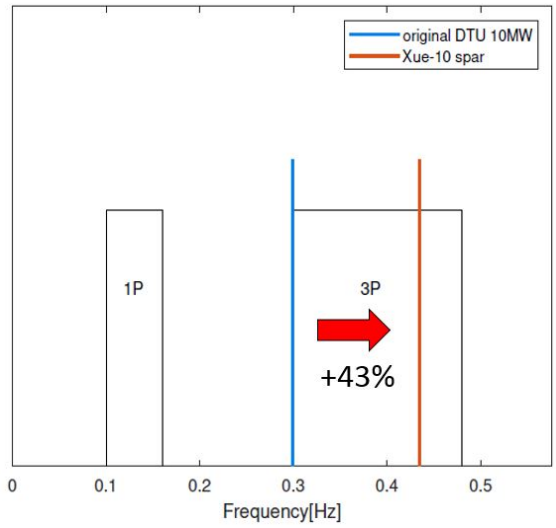

(a) Xue-10 spar

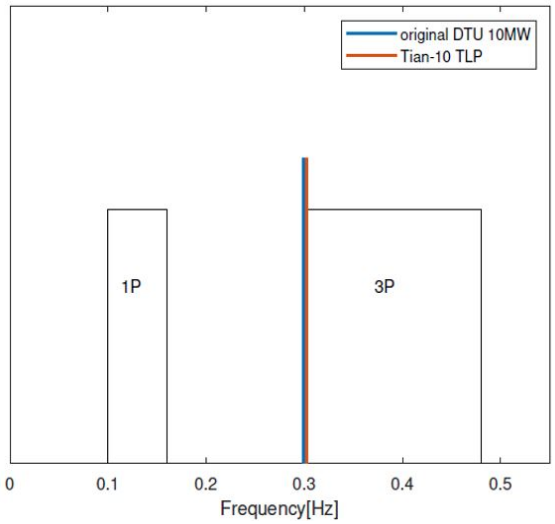

(b) Tian-10 TLP

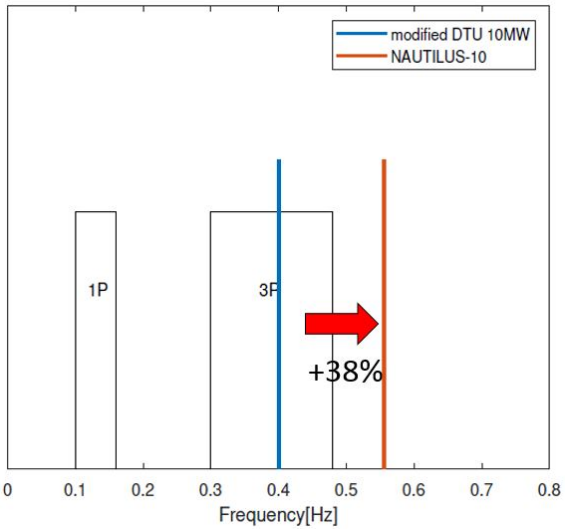

(c) NAUTILUS-10 semi-sub

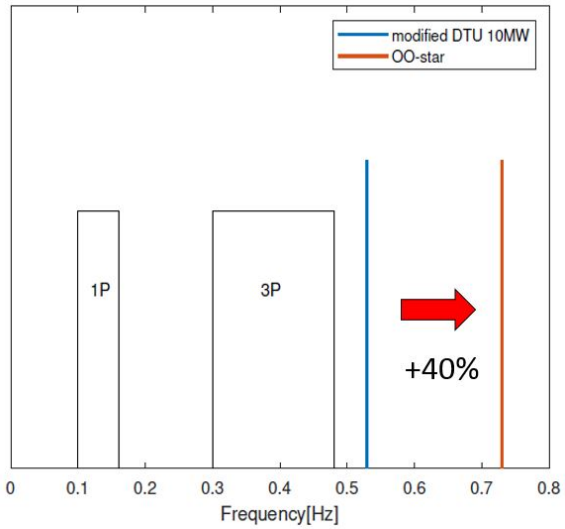

(d) OO-star semi-sub

Figure 4.1: 1P-3P diagram of four floaters

4.1.1 Spar and Semi-Sub

In the case of floaters with catenary mooring system(Xue-10, OO-star and NAUTILUS-10), it is shown that **the presence of the floater results in a higher 1st tower bending natural frequency** but has little influence on the 2nd tower bending natural frequency.

From the mode shapes shown in Figure 4.2 it is seen that the 1st tower bending is highly coupled with the floater pitch motion. On the other hand, the 2nd tower bending mode has less coupling with the floater pitch motion.

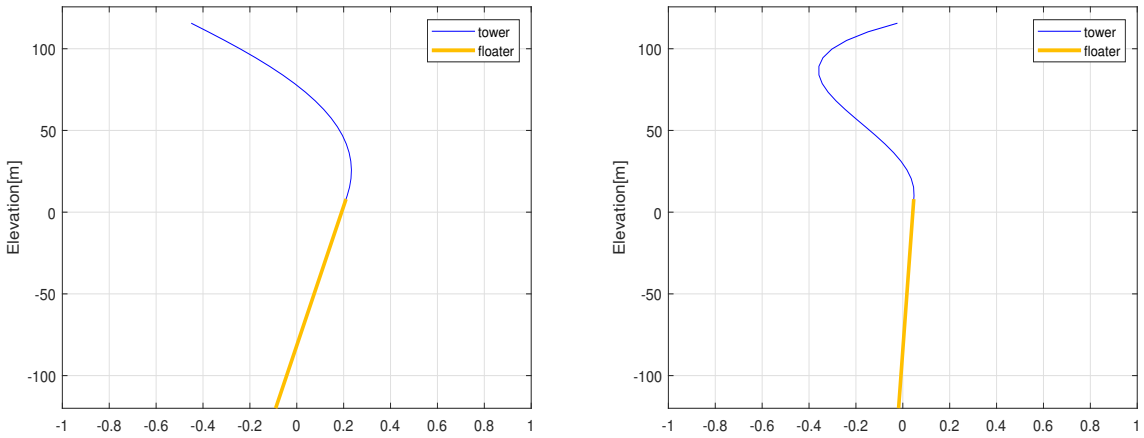

(a) 1st bending mode **(b)** 2nd bending mode

Figure 4.2: Tower bending mode shapes of Xue-10 spar

In order to understand the natural frequency change from fixed foundation to floating foundation, it can be helpful to first look into the difference in boundary conditions for the two cases. From the tower point of view, a land-based foundation can be regarded as having clamped-free boundary conditions, while with a floating platform it can be seen as having inertial-elastic-free boundary conditions, as shown in Figure 4.3.

For the floating foundation case, because there are inertia and elasticity involved at the boundary, it will be useful to identify whether the change in 1st tower bending is dominated by the inertial boundary or the elastic boundary.

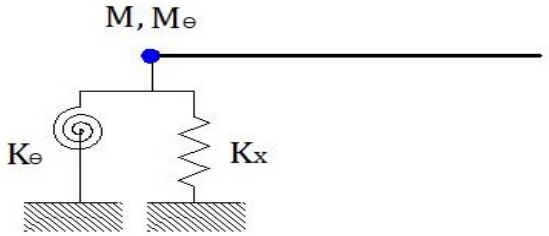

Figure 4.3: beam with inertial-elastically-free boundary

For a catenary mooring system, the rigid body modes(in the case of this thesis, surge and pitch) are usually low frequency modes, which means the springs at the tower bottom boundary only function as restricting the rigid body motions and cannot have a big influence on the structural modes. Therefore, it can be inferred that **the difference in the 1st tower bending is related to the inertia boundary**, namely the large inertia of the floater.

If the tower is regarded as a beam, the natural frequency difference from a clamped-free beam to a inertia-free beam can be understood by looking at the solution of bending natural frequencies with different boundary conditions. From beam theory the natural frequency of a beam can be written as

$$\omega_n = \frac{C_n}{L^2}\sqrt{\frac{EI}{\rho A}} \tag{4.1}$$

where

ω_n	bending natural frequency of the beam[1/rad]
C_n	natural frequency coefficient[-]
L	beam length [m]
EI	bending stiffness[Nm^2]
ρ	density of the beam[kg/m^3]
A	cross section area[m^2]

The natural frequency coefficient C_n can be found by solving natural vibration of a beam analytically with corresponding boundary conditions. For the first bending mode, a clamped-free boundary condition has $C_n = 3.52$, while a free-free boundary condition has $C_n = 22.4$. This implies that there will be an increase in bending natural

frequency if a clamped boundary(kinematic) is changed to a free boundary(dynamic).

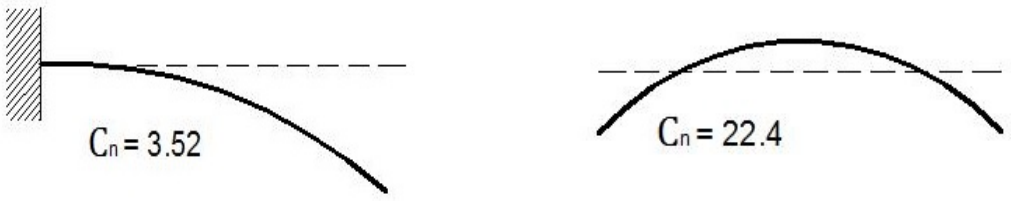

(a) clamped-free **(b)** free-free

Figure 4.4: beam with different boundary conditions

Since it is found that for a floater with catenary mooring system the boundary condition at the tower bottom is inertia-dominant, the following discussion is based on inertial-free boundary condition.

For a Euler-Bernoulli beam with inertial-free boundary condition, the dynamic boundary conditions(shear force and bending moment equilibrium) at the inertia end can be written as

$$EI\frac{\partial^3 w}{\partial x^3} = M\ddot{w} \tag{4.2}$$

$$EI\frac{\partial^2 w}{\partial x^2} = \frac{\partial}{\partial x}(M_\theta \ddot{w}) = M_\theta \ddot{\theta} \tag{4.3}$$

where

x	longitudinal displacement [m]
w	transverse displacement[m]
θ	rotational displacement[-]
M	mass at the boundary [kg]
M_θ	moment of inertia at the boundary[kgm^2]

Suppose the inertia at the boundary is zero, it will be equivalent to have a free end. On the other hand, if the inertia is approaching to infinity, from Equation 4.2 and 4.3

the only possible solution it to have a zero displacement($0 = M(\rightarrow \infty) \cdot 0$), which means the boundary will approach to a zero displacement kinematic condition(clamped) as the inertia approaches to infinity. In other words, it can be inferred that a beam with inertial-free boundary conditions should have C_n ranges from 3.52(clamped-free) to 22.4(free-free).

In order to prove the above argument, a numerical experiment with a simple beam is implemented. The properties of the tested beam is listed as follows.

L	40 [m]
EI	1.86E+12[Nm^2]
ρ	8,500 [kg/m^3]
A	1.04 [m^2]

Springs with low stiffness are attached to restrict rigid body motions for numerical calculation reason. The rigid body modes are low frequencies compared to the bending frequencies to assure the springs at the boundary do not have influence on the bending modes. Inertia boundary with different magnitudes are applied and the resultant 1st bending natural frequency is calculated accordingly.

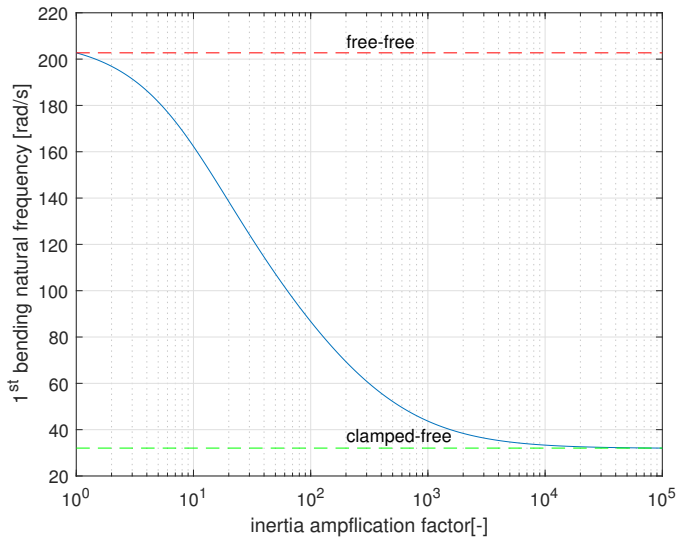

Figure 4.5: 1st bending natural frequency of a simple beam with different magnitude of inertia boundary

As shown in Figure 4.5 the natural frequency converges with large and small inertial boundary. The converged values are aligned with the values calculated from Equation 4.1 with clamped-free and free-free conditions respectively.

For higher bending modes the same logic can be applied. Table 4.2 shows that the increase of 2nd tower natural frequency is not significant, which implies that the inertia at the boundary is sufficiently large such that the second mode starts to converge to a clamped boundary condition. The mode shape shown in Figure 4.2 also agrees with the argument(similar to clamped boundary).

To conclude, the increase of 1st tower natural frequencies from bottom fixed foundation to floating foundation is the consequence of having boundary condition changed from clamped to free, and the large inertia of the floater provide the constraint to reduce the amount of increase.

For low frequency mode(i.e. 1st tower bending) the inertia at the boundary is not sufficient enough to provide constraint such that the boundary can resemble as a clamped condition so the frequency increase due to free boundary is still significant. On the other hand, for the higher modes(i.e. 2nd tower bending) the boundary starts to converge to a clamped condition and thus less increase is observed.

4.1.2 TLP

In the case of TLP, it is completely different from a catenary mooring system. The platform-mooring system is very stiff due to the high tension in the tendon legs. Hence the boundary at the tower bottom is more elasticity-dominant than inertia-dominant.

Due to the high pitch stiffness in the platform motion, it is highly coupled with 2nd tower bending mode as shown in Figure 4.6, and it is not possible to identify a mode as rigid body pitch mode anymore.

From a tower design point of view, directly applying a land-based tower design to TLP should be less problematic than a platform with catenary system considering less change in 1st tower bending frequency. However, the higher bending modes can be influenced by the stiff platform system and the high frequency pitch/bending modes should be carefully evaluated.

Moreover, for a TLP system the focus is often not only on the tower but rather more on the whole structure, including tendons, platform and the tower together. The limitations of the developed model is that the tendons are simply modeled as two linear springs, and the heave motion is not included.

Although the developed rigid model provides an easy modeling approach to account for the platform coupling effect with the tower, the analysis can be done for a TLP floater is very limited. If necessary, further improvement can be made by modeling the tendon legs as beam elements so that the flexibility of the tendon legs can also be included in the model.

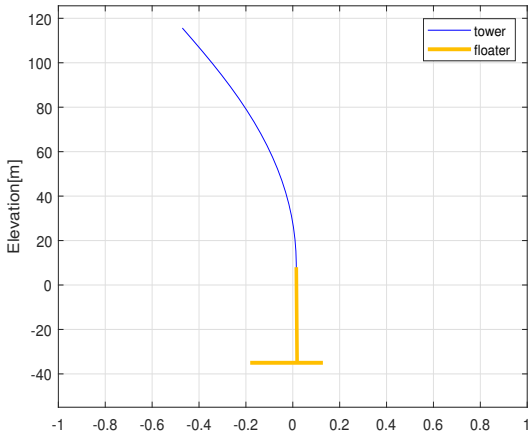

(a) 1st bending mode

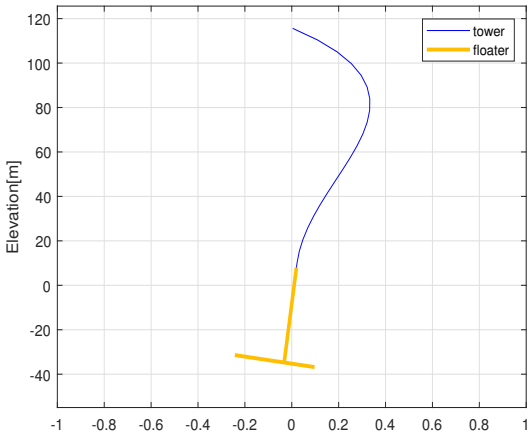

(b) 2nd bending/pitch mode

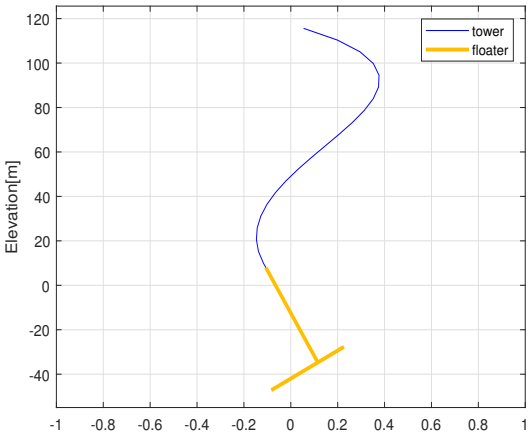

(c) 2nd bending/pitch mode

Figure 4.6: Tower bending mode shapes of Tian-10 TLP

4.2 Effect of Hull Flexibility

As explained in Sec. 3.5 the investigation on the effect of hull flexibility is based on structural analysis and fatigue damage estimation. In structural analysis the effect of hull flexibility on dynamic properties of the tower is discussed. The influence on 1st tower bending natural frequency with consideration of 1P-3P frequency ranges is addressed. Two two different tower designs(relatively soft and stiff) are made for study purpose. Fatigue damage estimation of two models are compared. Reflection on the results and possible impact on the design of a tower are also be discussed.

4.2.1 Dynamic Properties of Tower

4.2.1.1 Rigid Blades

The natural periods/frequencies from rigid and flexible model with rigid blades are shown in Table 4.3. The reason of using rigid blades is to avoid having blades modes involved so that the effect of hull flexibility on the tower can be studied. Results with flexible blades are provided later in Sec. 4.2.1.2.

Table 4.3 shows that barely any difference appears in surge and pitch modes, which is the result of using the same mooring stiffness and hydrostatic stiffness in both models, and it does not necessarily reflect to reality.

On the other hand, the tower bending natural frequencies are significantly affected by hull flexibility. Based on the design of Xue-10 spar, hull flexibility leads to 16% decrease in the 1st tower bending natural frequency and 24% decrease in 2nd tower bending natural frequency.

Natural Period[s] /Frequency[Hz]	**Rigid Floater**	**Flexible Floater**	**Difference**
Surge	107	107	0%
Pitch	38.0	38.4	− 1.1%
1st tower bending	2.31/0.43	2.8/0.36	+21%/−16%
2nd tower bending	0.55/1.82	0.72/1.39	+31%/−24%

Table 4.3: Natural periods/frequencies comparison(with rigid blades)

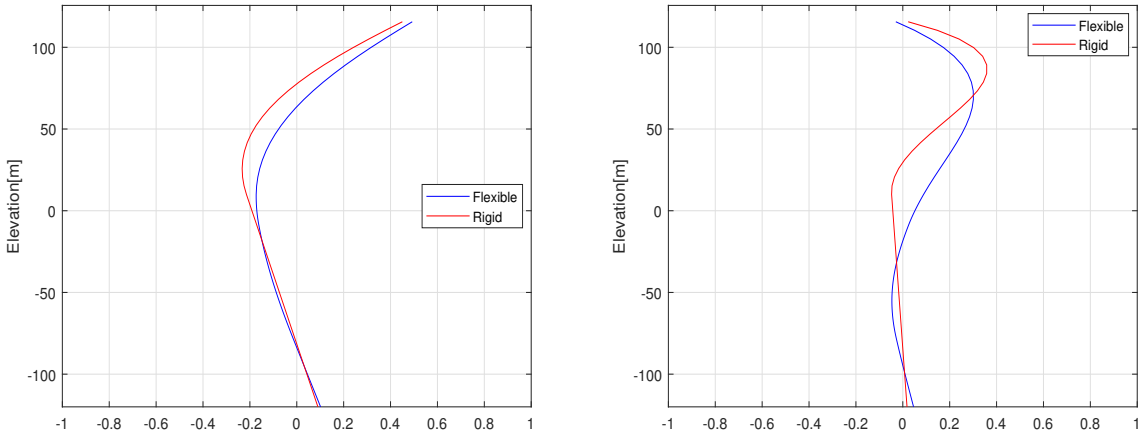

(a) 1st tower bending mode (MAC= 0.94) **(b)** 2nd tower bending mode (MAC= 0.64)

Figure 4.7: Mode shapes from and rigid model and flexible model(with rigid blades)

In addition, differences in the mode shapes(see Figure 4.7) are also observed. In the 1st tower bending mode, flexible model shows extra bending roughly from tower bottom to MSL, while below MSL the bending of the spar is minor. It can be interpreted as if the tower is extended to MSL, which is exactly the idea of "semi-flexible approach" proposed in LIFES50+[36]. This implies that a semi-flexible approach for a spar-buoy concept might be a good approximation.

As for the 2nd tower bending modes, a bigger difference appears. The 2nd tower bending mode from flexible model looks more like a 2nd bending mode of the whole structure rather than just a tower bending mode, which means the name of 2nd tower bending might not be justified anymore.

Clearly, for a large size floating wind turbine, a rigid body assumption is not valid anymore because hull flexibility has significant influence on the dynamic properties of the tower. For instance, it can lead to significant decrease in tower bending natural frequency as shown in Figure 4.8.

From a fatigue design view point, not only 1P and 3P wind load can cause fatigue damage, but waves can also lead to significant fatigue damage for large size floating wind turbines. If the bending natural frequency is too close to where waves have the most energy, which it typically from 0.04Hz to 0.2Hz(according to DNV-OS-J103[15]), the high fatigue load from waves might lead to structural failure. Therefore, an overestimation of the tower bending frequency may lead to an underestimation of fatigue damage from waves excitation.

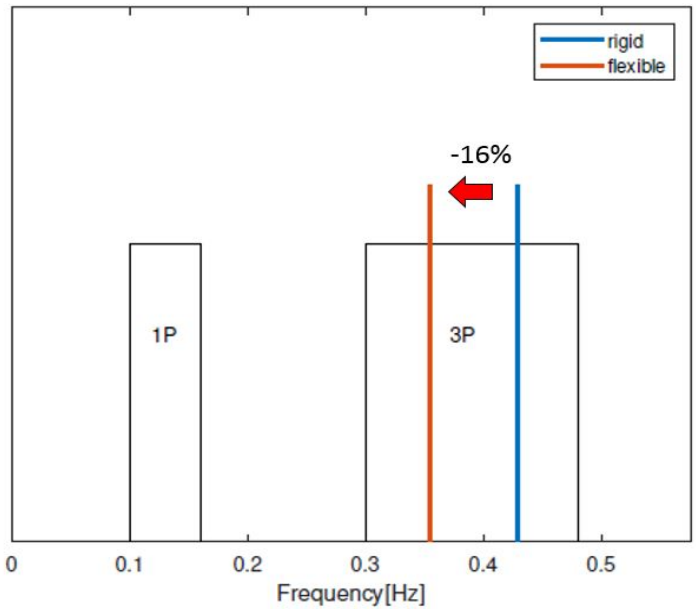

Figure 4.8: Xue-10 1P-3P diagram with 1st tower bending natural frequency

4.2.1.2 Flexible Blades

Previous section the study is based on rigid blades. In this section, blades flexibility is included and the effect of hull flexibility on tower and blades are discussed. The natural frequencies calculated from two models are shown in Table 4.4. Only the natural modes which have natural frequencies lower than 1.5Hz are listed.

Natural Period[s] /Frequency[Hz]	**Rigid Floater**	**Flexible Floater**	**Difference**
Surge	107	107	0%
Pitch	38.0	38.4	+ 1.1%
1st tower bending	2.34/0.43	2.82/0.36	+21%/−16%
1st blade bending	1.63/0.61	1.65/0.61	0%
	1.62/0.62	1.62/0.62	0%
	1.56/0.64	1.58/0.63	0%
2nd system bending		0.66/1.5	

Table 4.4: Natural periods/frequencies from rigid and flexible model with flexible blades

The 1st blade modes are identified by the mode shapes(see Figure 4.9). Three blade modes appear when blades flexibility is included. Table 4.4 shows that hull flexibility has no influence on the 1st blade modes. In addition, it should be noted that the 1st blade bending natural frequency of an isolated blade with a clamped bottom is also 0.6Hz, which is the same as the 1st blade bending natural frequencies shown in Table 4.4. This implies that neither tower flexibility nor hull flexibility affect the 1st blade modes.

On the other hand, by comparing results from Table 4.4 with Table 4.7, it is found that the 1st tower mode is barely affected by the flexibility of the blades, while the 2nd system bending increase 7% from 1.39Hz to 1.5Hz. In addition, the 2nd system bending mode shape in Figure 4.10 indicates that the blades are coupled together with the tower and the spar, which means part of the dynamic behavior of the blades will be missing if hull flexibility is not included.

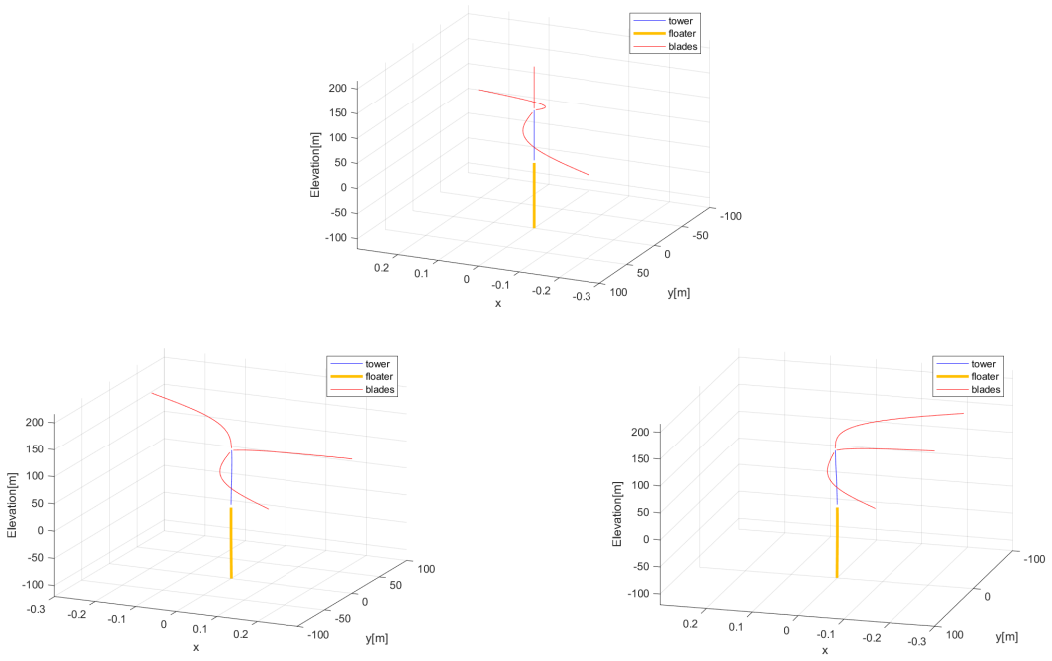

Figure 4.9: 1st blade modes

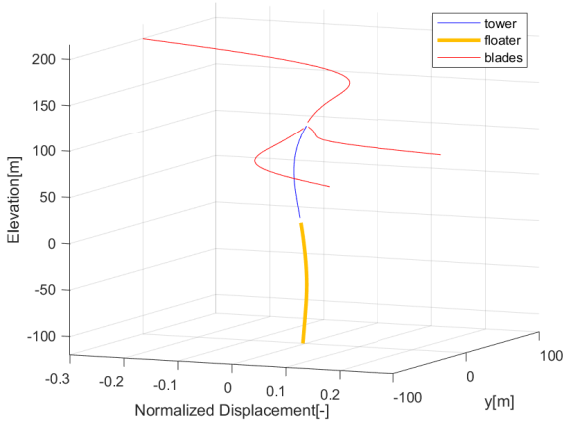

Figure 4.10: 2nd system bending mode from flexible model

4.2.1.3 Different Tower Design

In order to have more insights on the effect of hull flexibility from a tower design point of view, a soft-stiff tower design and a stiff-stiff tower design are made **based on the rigid model with flexible blades**.

For the soft-stiff case, the 1st tower bending natural frequency is adjusted to be slightly lower than 3P range by reducing the tower thickness, while the stiff-stiff design is achieved by increasing the tower thickness such that the 1st tower bending frequency can be above 3P range. The modified tower thickness are listed in Table 4.5.

It must be noted that these two tower design are only for study purpose and the reason of modifying the tower thickness is certainly not justified. In real design process, the tower thickness should be checked with load cases such as ULS or FLS to see whether the structure could fail. In addition, buckling strength requirement should also be considered. Nevertheless, because the purpose of the study is to see the effect of hull flexibility on different tower design, **none of the above strength requirement are considered**.

	Original Tower	**Soft Tower**	**Stiff Tower**
Tower top thickness[mm]	20	7	34
Tower bottom thickness[mm]	38	16	60

Table 4.5: Tower thickness of different tower design

It should also be pointed out that when the tower thickness is changed, the mass of the wind turbine will accordingly change, leading to a different draft. One can chose to either keep the floater unchanged and recalculate the new draft, which can lead to different center of mass and different hydrodynamic added mass, or keep the total weight and the center of mass unchanged by adjusting the ballast. For the study in this thesis, the latter approach is chosen, meaning the ballast is adjusted based on the different tower thickness.

Figure 3.9 shows that the center of mass of the whole structure is 74.6m below MSL and the center of mass of the floater is 91.52m below MSL. If the tower thickness is changed, to keep the center of mass to be still at 74.6m below MSL, the mass distribution of the floater should change, which means the amount of ballast and its

density should be recalculated. The outcome of having different tower thickness are listed in Table 4.6

	Original Tower	**Soft-Stiff Tower**	**Stiff-Stiff Tower**
Spar CoG below MSL[m]	91.52	87.47	95.04
Ballast density[kg/m^3]	2,135	1,765	2,810
Ballast height[m]	41.8	52.3	30.6

Table 4.6: Modification for different tower design

The resultant 1st tower bending natural frequency from two different tower designs are listed in Table 4.7 and 4.8 and they are plotted in 1P-3P diagram as shown Figure 4.11.

Natural Period[s] /Frequency[Hz]	**Rigid**	**Flexible**	**Difference**
Surge	107	107	0 %
Pitch	36.3	36.1	+ 0.5 %
1st tower	3.62/0.28	3.85/0.26	+ 6.0 % / − 7.1%

Table 4.7: Natural periods/frequencies of the soft-stiff design

Natural Period[s] /Frequency[Hz]	**Rigid**	**Flexible**	**Difference**
Surge	108	108	0%
Pitch	41.1	40.9	+ 0.5%
1st tower	2.01/0.5	2.54/0.39	+ 26.4 %/− 22 %

Table 4.8: Natural periods/frequencies of the stiff-stiff design

The resultant 1st tower natural frequencies suggest that the effect of hull flexibility are very different for two tower designs. For the soft-stiff design, rigid model only yields to 7.1% error in 1st tower bending natural frequency, while for the stiff-stiff design the error from rigid model rises to 22%.

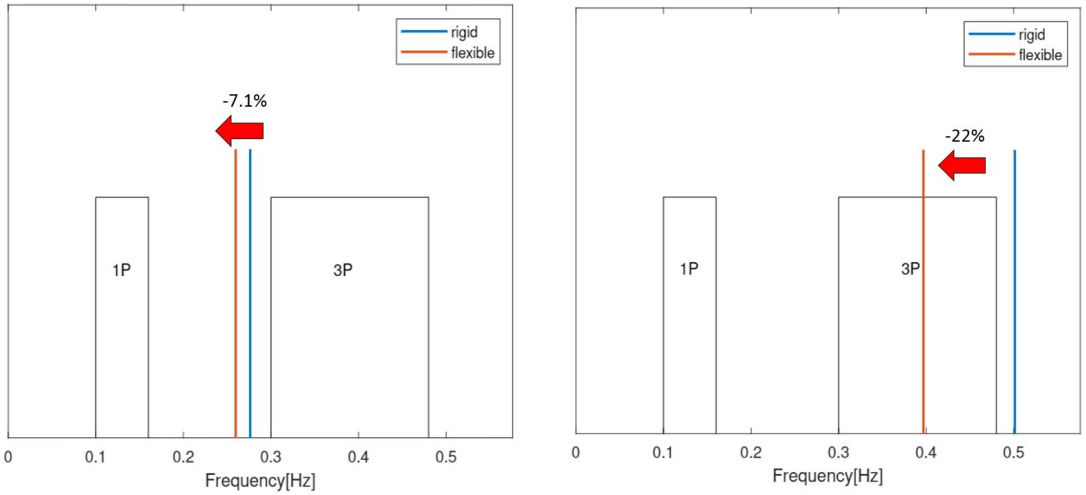

(a) Soft-stiff design **(b)** Stiff-stiff design

Figure 4.11: 1P-3P diagram

The result implies that **the effect of hull flexibility is smaller for a relatively soft tower and becomes more significant when the tower becomes stiffer**. The difference appeared in different tower design can be understood by the relative stiffness between the tower and the floater.

Essentially, a rigid body assumption is to assume a structure to be infinitely stiff. For a relatively soft tower, the spar is stiffer compare to the tower, which means assuming the spar as a rigid body may be a good approximation. However, on the other hand, for a relatively stiff tower the stiffness difference between the tower and the floater is much less, and assuming the floater as a rigid body can lead to a larger error.

Although rigid model can predict the 1st tower bending natural frequency better for a soft-stiff tower design, for large size floating wind turbine a soft-stiff tower design may be unfeasible because a large size floater means large waves load, which can make it difficult to achieve required strength to overcome extreme load or fatigue load.

For the case of fatigue strength, a soft-stiff design has the 1st bending natural frequency located closer to where waves has the most energy(0.04Hz to 0.2Hz) and the resonant excitation can lead to tremendous fatigue damage. Therefore, despite the fact that rigid model gives less error in 1st tower natural frequency estimation for a soft-stiff tower design, in reality a soft-stiff tower design for a large size floating wind turbine might not be a good design choice.

On the other hand, the challenge for a stiff-stiff tower design is the much higher uncertainty in tower bending natural frequency if one only has rigid model. The consequence can be an over-designed tower which has the 1st bending natural frequency far away from 3P to account for the effect of hull flexibility. However, a too conservative tower design might end up with having 1st bending natural frequency within 6P range, which can also lead to some fatigue damage.

To conclude, from the study with different tower design, it is found that the design of the tower can be difficult without considering hull flexibility. Therefore, for a large size floating wind turbine with a steel-efficient floater, it seems to be necessary to account for the flexibility of the hull in preliminary design.

A Stiff-Stiff Tower Design with Hull Flexibility Included

Figure 4.11 implies that a stiff-stiff tower design based on a rigid model is still a poor design because the 1st tower bending natural frequency is still within 3P ranges when hull flexibility is included. Therefore, a stiff-stiff tower design based on the flexible model is necessary. However, as one can see in Table 4.5, the thickness of the tower at the bottom is already 60mm, which is the same as the thickness of the spar, and keeping increasing the tower thickness to achieve a stiff-stiff design is not realistic anymore.

Alternatively, to increase the 1st tower bending frequency, one can also change the length of the tower, which means the hub height should be changed. However, the capacity of a turbine is related to the rotor swept area, accordingly the length of the blades. If the hub height is reduced, the blades might end up hitting the sea surface. Therefore, changing the hub height is not an idea option to increase the 1st tower bending natural frequency.

From above discussion, it seems that there is a limitation in the spar design of Xue-10 concept and the spar should be modified in order to achieve a stiff-stiff tower

design. Several possible options to improve the design of the spar are provided and discussed:

- **Reduce the draft:** If the whole floating wind turbine is regarded as a beam with free-free boundaries(not true but can be resembled), reducing the draft means a shorter length of the beam and hence can increase the bending natural frequency (according to Equation 4.1). However, simply reducing the draft may lead to a higher CoG. A possible solution to compensate the rise of CoG is to have a larger space at the bottom of the spar to fill more ballast.

- **A Hybrid solution:** In addition to reduce the draft and fill more ballast at the bottom, it is also possible to reduce the draft and increase the water plane area to gain more stability. Therefore, a hybrid solution which uses both ballast and large water plane for stability can also be a possibility. An good example is the triple spar concept[8]. However, a triple spar concept can lead to other problems such as having substructural modes' natural frequency fall within 1P and 3P[7].

- **Use different material:** Because the design of Xue-10 spar is a steel-efficient approach(steel with thin wall), the effect of hull flexibility is significant and as a result a stiff-stiff design is more difficult to achieve. However, the design of a spar is not bound to steel-efficient approach. Other materials such as concrete is also possible. If the spar is made of solid concrete without any thin wall, the effect of hull flexibility will be much less, but the challenge might be how to keep CoG as low as possible for desired stability.

4.2.2 Life Time Fatigue Damage

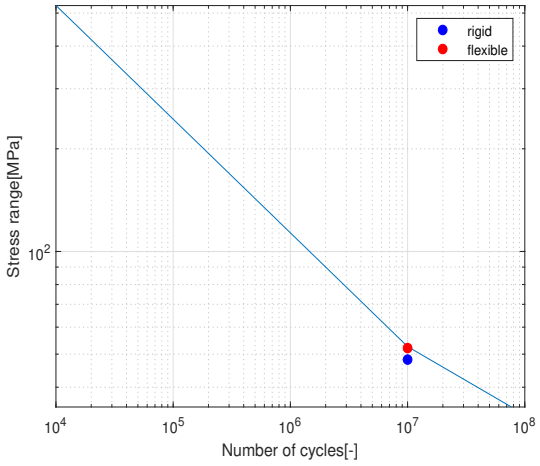

Figure 4.12: DEL and S-N curve

	Rigid	Flexible	Diff-
Damage[-]	0.770	0.970	-26.0%
DEL[MPa]	48.2	52.1	-8.09%

Table 4.9: Damage and DEL from two models

The estimated fatigue damage and damage equivalent load(DEL) in 20 years life time are listed in Table 4.9. The result shows that the fatigue damage from two models are already very close to failure without considering 3P wind load, and it can be expected that the tower will fail once 3P wind load is included due to the fact that both models have 1st tower bending natural frequency within 3P ranges(as shown in Sec. 4.2.1.1).

In addition, the result also shows that rigid model underestimates DEL by 8.09% compare to the flexible model. Although a 8.09% error might not be regarded as significant, one should be keep in mind that the result is only based on waves excitation. Because the 1st tower bending natural frequency is away from the wave energy spectrum, the small difference is expected.

In reality, there are many unexpected excitation sources and if one excitation source contains high narrow banded energy which happen to be close to the 1st tower bending natural frequency of either rigid or flexible model, it can possibly lead to large difference in fatigue damage estimation between two models.

In addition, the life time fatigue damage of the two tower designs(soft-stiff and stiff-stiff) made in Sec 4.2.1.1 are also calculated. The results are shown in Table 4.10 and 4.11.

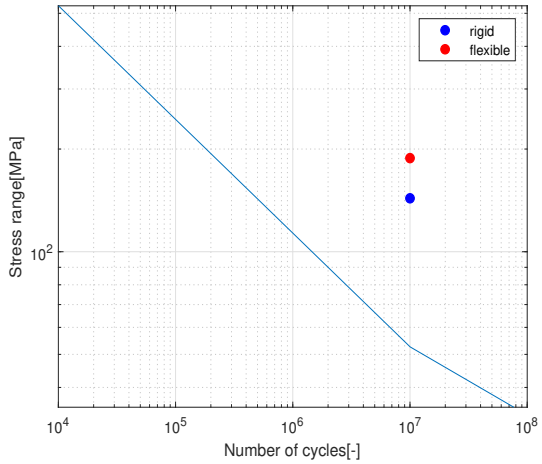

	Rigid	Flexible	Diff-
Damage[-]	20.2	45.6	-126%
DEL[MPa]	143	188	-31.2%

Table 4.10: Fatigue damage and DEL of soft-stiff tower

Figure 4.13: DEL and S-N curve(soft-stiff tower)

The extreme high fatigue damage appears in the soft-stiff tower design proves the fact that for a large size wind turbine, a soft-stiff tower design is not realistic because of the large waves load. In order to minimize the fatigue damage from waves, the better way is to move 1st tower bending natural frequency away from most of the waves energy(typically from 0.04Hz to 0.2Hz), which means a stiff-stiff tower is inevitable for the case of a large size floating wind turbine with a steel-efficient spar floater.

Furthermore, because there are more resonant excitation from waves in the 1st tower bending natural frequency for a soft-soft tower, it is more sensitive to a shift of the 1st tower bending natural frequency, which is why there is a bigger difference in fatigue damage between rigid model and flexible model than the original tower design.

Although from Sec 4.2.1.1 it shows that rigid model can estimate the 1st tower bending natural frequency with less error, from fatigue damage results here it shows that a soft-stiff design can be lack of strength to survive from waves load in the life time. Not to mention it also has higher chance of failing under extreme load case and having buckling issue.

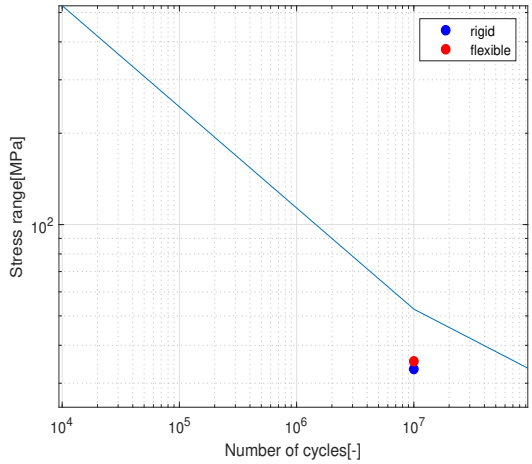

Figure 4.14: DEL and S-N curve(stiff-stiff)

	Rigid	**Flexible**	**Diff-**
Damage[-]	0.256	0.305	
DEL[MPa]	33.41	35.42	

Table 4.11: Fatigue damage and DEL of stiff-stiff tower

For the stiff-stiff tower design, because the 1st tower bending natural frequency for both models are all away from waves energy, the fatigue damage are much less as expected. In addition, the difference between two models are also less in spite of the larger difference in 1st tower bending natural frequency between two models

It should be noted that the stiff-stiff tower design is made by having the 1st tower bending natural frequency slightly above 3P range based on rigid model and the 1st tower bending natural frequency from flexible model is still within 3P range, which means flexible model should have higher fatigue damage if 3P wind load is included.

Therefore, from the fatigue damage estimation study performed in this thesis, one can only conclude that the model with rigid hull tends to underestimate the fatigue damage **under waves load** but not necessarily true if other excitation sources are included. In addition, the magnitude of the difference in fatigue damage under waves load between rigid model and flexible model depends on where the designed 1st tower bending natural frequency is.

4.3 Limitation of the Developed Model

Hydroelasticity

Although from previous work by de Souza[50] it is concluded that the inclusion of hull flexibility in hydrodynamic calculation may not to be important in a dynamic analysis, the conclusion is based on a TLP concept with small size(5MW) wind turbine, and it does not necessarily applied to a spar-buoy with large size(10MW) wind turbine. However, in this thesis, hull flexibility is neglected in the hydrodynamic load calculation.

Tower-Spar Interface

It is assumed that the tower and the spar are rigidly connected and the interface condition is described by only compatibility of the displacement. In other words, force equilibrium at the interface is not included in the model and it might result in different dynamic properties(i.e. natural frequency) of the system.

Modeling of the Blades

In the developed FEM model, the flexibility of the blades are modeled as beam elements with sectional varied flapwise bending stiffness. However, a blade has complex 3-D geometry which results in high coupling between flapwise, edgewise and torsional stiffness. These coupling effect cannot be captured by the developed model. Furthermore, when a wind turbine is operating, the centrifugal force from blades rotation and wind load can lead to stiffer blades, which is not taken into account in the analyses either.

Modeling of the TLP

In the developed rigid model, the TLP concept is modeled in the same way as other concepts with catenary mooring system, which the platform is modeled as a point mass attached to springs. However, a TLP system is very stiff and the flexibility of the tendons can have huge influence on the dynamics of the system, which the developed rigid model cannot capture.

Hydrostatic Stiffness

In the developed rigid and flexible model, structural flexibility(tower and spar) is neglected in hydrostatic stiffness calculation, meaning the restoring moment is modeled as a concentrated force at MSL.

Aerodynamic Damping

In fatigue damage estimation the linearized aerodynamic damping is based on the 1st tower bending mode of an onshore wind turbine in order to be comparable, which means the difference in aerodynamic damping between a rigid hull model and a flexible hull model is missing.

Chapter 5

Conclusion and Future Work

5.1 Conclusion

In order to answer two research questions **"What is the difference in tower design with a floating foundation?"** and **"What is the effect of hull flexibility on tower design?"**, two separated analyses are implemented.

Tower Design with a Floating Foundation

The first research question is answered by implementing structural analysis on four different floating concepts. The tower dynamic properties of four floating concepts(1 spar-buoy, 2 semi-subs and 1 TLP) are compared with the case of having a fixed foundation. The results based on floaters with catenary mooring system(spar-buoy and semi-subs) indicate that **the 1st tower bending natural frequency can increase significantly**(approximately 40%) from a fixed foundation to a floating foundation, and the results also show that the 2nd tower bending natural frequency is barely affected by the floating foundation. The significant increase in the 1st tower bending natural frequency implies the fact that a soft-stiff tower design is more difficult to achieved for a floating foundation(with catenary mooring system).

On the other hand, for a TLP concept, the 1st tower bending natural frequency barely changed from fixed foundation to floating foundation, but the 2nd tower bending mode is found highly coupled with thr platform pitch motion. From a tower design view point, using a land-based tower design for a TLP floating concept could be less problematic. Admittedly, due to the limitation of the developed rigid model, the full dynamic properties of a TLP system(includes tendons vibration) is not captured.

Effect of Hull Flexibility

The second research questions is answered by implementing structural analysis and fatigue damage estimation based on a large size spar-buoy concept.

The results from structural analysis indicate that hull flexibility can lead to **decrease in the 1st tower bending natural frequency**, and the magnitude **depends on the relative stiffness** between the tower and the spar. Based on the two tower design cases from this thesis, it is shown that hull flexibility leads to 7% decrease in the 1st tower bending natural frequency for a soft-stiff tower and 22% decreas for a stiff-stiff tower. In addition, the inclusion of hull flexibility **results in a 2nd system bending mode**($\approx$ 1.5Hz), which is not captured in the rigid hull model. From the mode shape of the 2nd system bending mode it implies that the dynamic behavior at high frequency can be very different between a rigid hull model and a flexible hull model.

Furthermore, based on the design of Xue-10 spar, it is discovered that a stiff-stiff tower design is difficult to achieved by only increasing the tower thickness once hull flexibility is included in the model. In other words, **modification should be made for the design of Xue-10 spar** in order to have the 1st tower bending natural frequency within stiff-stiff range.

Lastly, the fatigue damage estimation shows that a soft-stiff tower design can lead to tremendous fatigue damage from waves load. Hence, **a soft-stiff tower is not realistic** for a large size floating wind turbine. However, a stiff-stiff tower design has high uncertainty in the 1st tower bending frequency without including hull flexibility. Therefore, it is concluded that **inclusion of hull flexibility is necessary** for large size steel-efficient spar-buoy floating wind turbines from a tower design perspective.

Overview of Tower Design for a Large Size Spar-Buoy Concept

Based on the results from the implemented structural analysis and fatigue damage estimation under waves load, a 1P-3P-6P diagram is plotted in Figure 5.1 as an overview of a tower design for a large size spar-buoy concept.

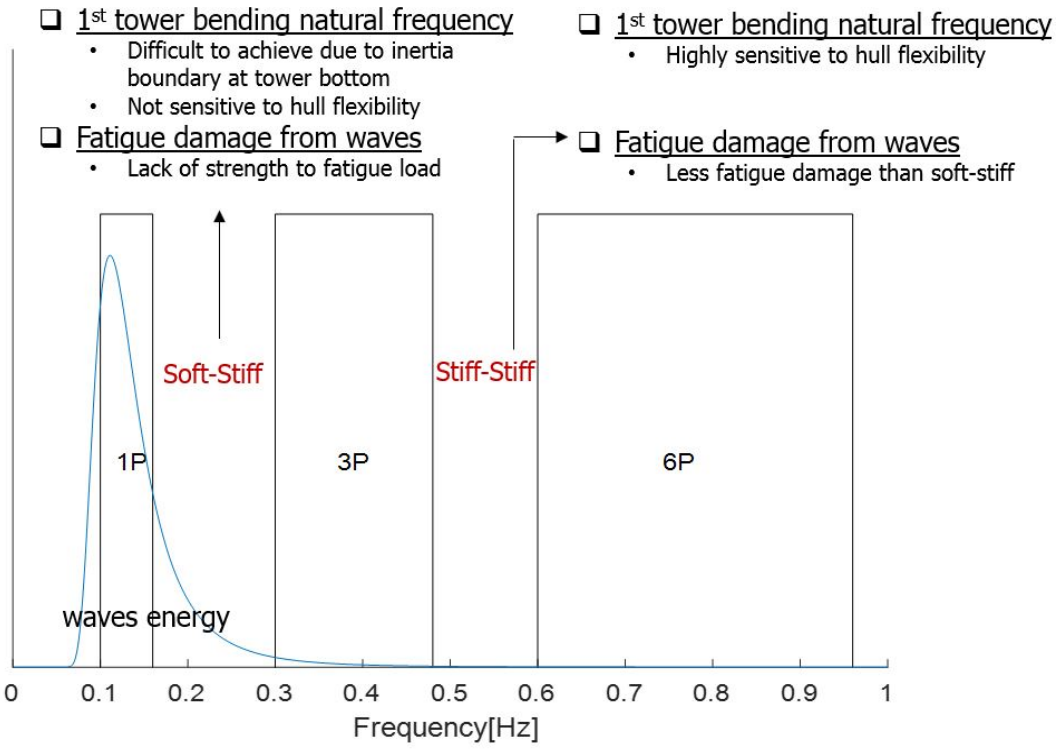

Figure 5.1: Tower design overview

5.2 Recommendation for Future work

Effect of hull flexibility on other types of floaters

The effect of hull flexibility in this thesis is studied based on a large size(10MW) spar-buoy concept. For the TLP concept, researches have shown that hull flexibility is already important even for a small size wind turbine(5MW). Prior work also investigates hull flexibility for a triple spar concept, but it does not address the possible influence from the tower design perspective. Until now, still very few concepts have been examined regarding the effect of hull flexibility. Therefore, it is recommended to implement similar study as done in this thesis for other large size floating concepts. For instance, two semi-submersibles in LIFES50+[35], OO-star and NAUTILUS-10, are two public available large size floating concepts which can also be investigated.

Include a full wind load model in the frequency domain

The implemented frequency domain fatigue damage estimation in this thesis only accounts for waves load. The only contribution from wind is a constant aerodynamic damping based on the 1st tower bending mode of the onshore DTU 10MW wind turbine. For more complete fatigue analysis, a full wind load model should be incorporated into the model. It can be achieved by either building a frequency domain wind load model, or directly utilizing an aero-elastic-servo time domain model to compute the wind load, and use Fourier transformation to convert the wind load to the frequency domain. In addition, the fatigue damage estimated from the frequency domain model should also be validated by a time domain model.

Similar study on even larger size wind turbines

In this thesis, the study on the effect of hull flexibility is based on a spar-buoy with a 10MW wind turbine. The same study can be applied to even larger sizes wind turbines(15MW to 20MW), and the effect of hull flexibility can be compared between different size of wind turbines. It could be interesting if one is able to quantify the effect of hull flexibility on the 1st tower bending natural frequency for different size of floating wind turbines.

Hydroelasticity study on large size spar-buoy concept

This thesis only investigates the influence of hull flexibility itself and does not include the hydroelasticity effect on hydrodynamics. Although from prior work by de Souza[50] it is indicated that hydroelasticity effect in dynamic analysis seems not to be important, the conclusion is based on a TLP concept with a 5MW wind turbine, and it does not necessarily apply to a large size spar-buoy floating wind turbine. Therefore, the significance of hydroelasticity for a large size spar-buoy should also be quantified.

Re-Design the large size spar-buoy concept Xue-10

From the case study of Xue-10, a large size steel-efficient spar-buoy designed by Xue[57], this thesis discovers that a stiff-stiff tower design for Xue-10 spar is a challenging task if one only modifies the tower without changing the spar. In other words, it is suggested that the design of Xue-10 spar should be modified in order to achieve a stiff-stiff tower design. Three possible options can be considered. The spar design can be improved by shortening the draft, choosing different material or using a hybrid solution.

A quantitative indicator for relative stiffness between the tower and the floater

This thesis indicates that the effect of hull flexibility on the 1st tower bending natural frequency depends on the relative stiffness between the tower and the floater. If the same floater is considered, the 1st tower bending natural frequency of a stiffer tower is affected more by hull flexibility than a softer tower. For simple beams with constant cross sections, bending stiffness may be a good indicator to identify such relative stiffness. However, it may be difficult to define one bending stiffness value for a tower or a floater. If a quantitative indicator for the relative stiffness between the tower and the floater can be defined, it may allow one to be able to expect the significance of hull flexibility beforehand, and such quantitative indicator can be useful during the design process.

Appendix A

Definition of Floaters

A.1 Xue-10 spar

A.1.1 Geometry and Properties

Xue-10 spar is the upscaled version of OC3Hywind spar. The definition of OC3Hywind spar can be found in OC3 project[28]. The geometry and properties of OC3-Hywind spar is shown in table A.1.

Dimension and Property	
Total Draft	120m
Distance to floater top above MSL	10m
Taper top to MSL	4m
Taper bottom to MSL	12m
Taper top diameter	6.5m
Taper bottom diameter	9.4m
Total mass, including ballast	7,466tons
Center of mass below MSL	89.92m
Pitch inertia about CM	4,229,000tons·m^2
Mooring fairlead below MSL	70m

Table A.1: Properties of OC3-Hywind

Figure A.1: Illustration of OC3Hywind spar[28]

Since the draft of OC3Hywind spar is 120m already, if the spar was upscaled directly it would become too long to install or even carry. Therefore, model scaling(non-dimensional approach) by size is not applicable due to the restriction of reality.

To upscale the spar from carrying 5MW wind turbine to 10MW wind turbine, some factors needed to be taken into account. For example, the thrust curve of two wind turbines are different and thus spar has to be upscaled such that it would remain within an ideal pitch range. Moreover, the spar can be upscaled based on the increased weight of the turbine.

The detail of upscaling method is not the main concern of this project and so the dimension of the 10MW spar is directly taken from the master thesis "Design, numerical modelling and analysis of a spar floater supporting the DTU 10MW wind turbine[57]".

However, due to the lack of information of three parameters in the paper, which are mass center of the spar z_s, inertia of the spar I_s, and inertia of the tower I_{tw}, they need to be reproduced.

Mass center of the spar z_s can be found by simple mass distribution calculation

$$z_s = \frac{M_{tot} \cdot z_{tot} - M_{turb} \cdot z_{turb}}{M_s} \tag{A.1}$$

where M_{tot} and z_{tot} are the mass and mass center location of the overall floating structure. M_{turb} and z_{turb} correspond to the wind turbine. M_s and z_s are spar mass and mass center.
The values found in the reference thesis are as follows

$M_{tot} = 13,405\text{tons} \quad z_{tot} = -74.6\text{m} \quad M_{turb} = 1,251\text{tons} \quad z_{turb} = 89.16\text{m} \quad M_s = 12,100\text{tons}$

which yields spar mass center z_s=-91.53m.

As for spar moment of inertia, it is calculated based on the total pitch inertia I = 1.27E+11kgm^2 found in the paper. The tower moment of inertia around its center of mass is calculated by finite element model.

$$I_s = 1.38\text{E+10 kgm}^2$$
$$I_{tw} = 4.97\text{E+8 kgm}^2$$

In addition, the upscaling of mooring system of Xue-10 spar is done by tripling the mass density per length of the lines. The overall properties of Xue-10 spar and wind turbine are listed in Table A.2 and A.3

Dimension and Property	**OC3Hywind**	**Xue-10 Spar**
Draft	120m	120m
Freeboard	10m	10m
Distance to taper top below MSL	4m	4m
Distance to taper bottom below MSL	12m	12m
Diameter above taper	6.5m	8.3m
Diameter below taper	9.4m	12m
Total mass, including ballast	7,466tons	12,100tons
Center of mass below MSL	89.92m	91.53m
Center of buoyancy below MSL	62m	62m
Pitch inertia about CM	4,229,000tons·m^2	13,776,000tons·m^2
Mooring fairlead below MSL	70m	70m
Mooring line mass weight per length	77.7kg/m	233.1kg/m

Table A.2: Spar platform properties

Dimension and Property	**NREL 5MW**	**DTU 10MW**
Tower density	8,500kg/m^3	8,500kg/m^3
Young's modulus	210GPa	210GPa
Tower bottom elevation	10m	10m
Tower top elevation	87.6m	115.63m
Hub height	90m	119m
Tower top diameter	3.86m	5.5m
Tower base diameter	6.5m	8.3m
Tower top thickness	19mm	20mm
Tower base thickness	27mm	38mm
Tower mass	249.7tons	574tons
RNA mass	350tons	677tons
Center of mass above MSL	70.6m	89.2m
Tower pitch inertia	121,700tons·m^2	497,400tons·m^2

Table A.3: Wind turbine properties

A.1.2 Mooring System

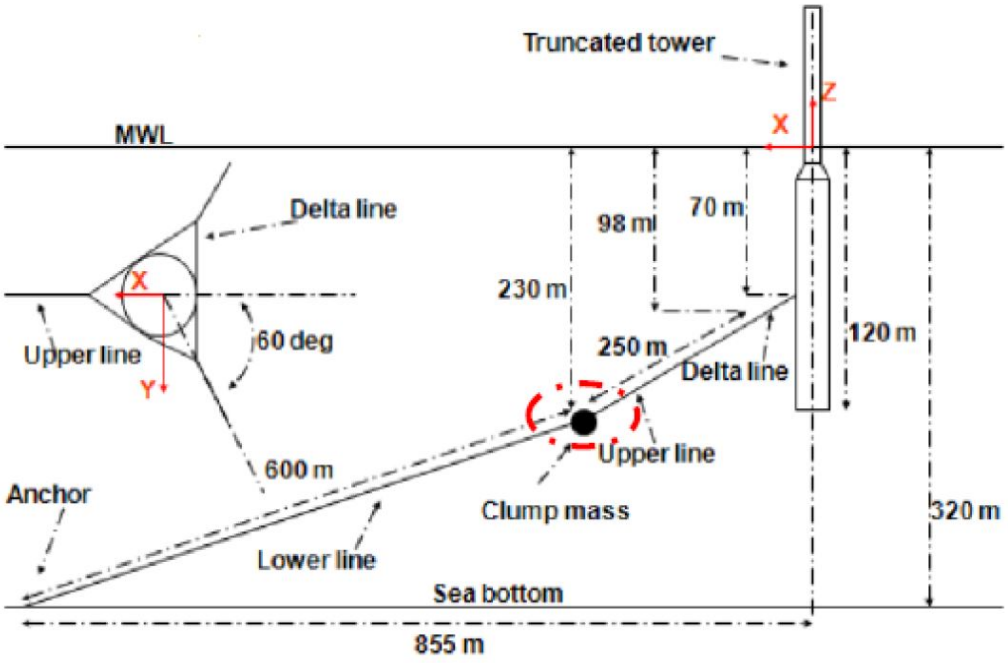

Figure A.2: Xue-10 mooring line arrangement

Dimension and Property	
Number of mooring lines	3
Angle between adjacent lines	120°
Water depth	320m
Depth to fairleads below MSL	70m
Radius to fairleads from spar centerline	6.5m
Radius to Anchors from spar centerline	855.17m
Unstretched mooring line length	902.2m
Mooring line diameter	0.09m
Equivalent mooring line mass density	233.12kg/m
Equivalent mooring line axial stiffness	384,243,000N

Table A.4: Xue-10 mooring line properties

A.2 OO-star Semi-Sub

A.2.1 Geometry and Properties

OO-Star semi-submersible consists of one center column and three outer columns. The definition and geometry are shown in Figure A.3, A.4, and the dimensions are listed in Table A.5. The tower does not entirely follow the definition of reference DTU 10MW[4]. The diameter and wall thickness have been modified. However, the tower top mass properties, namely RNA, hub and blades, remains the same as DTU 10MW turbine.

Dimension and Property	
Total Draft	22m
Distance to floater top above MSL	11m
Center column diameter(top)	12m
Center column diameter(bottom)	16.2m
Outer columns diameter(top)	13.4m
Outer columns diameter(bottom)	15.8m
Center to outer columns distance	37m
Total mass, including ballast	21,709tons
Center of mass below MSL	15.23m
Pitch inertia about CM	9,430,000tons·m^2
Displaced water volume	23,509m^3
Center of buoyancy below MSL	14.24m

Table A.5: Properties of OO-star

Figure A.3: Illustration of OO-star[35]

Dimension and Property	DTU 10MW
Tower density	8,500kg/m^3
Young's modulus	210GPa
Tower bottom elevation	11m
Tower top elevation	115.63m
Hub height	118.39m
Tower top diameter	5.33m
Tower base diameter	11.5m
Tower top thickness	29mm
Tower base thickness	75mm
Tower mass	1,257tons
RNA mass	676.7tons
Center of mass above MSL	73.81m

Table A.6: Wind turbine properties

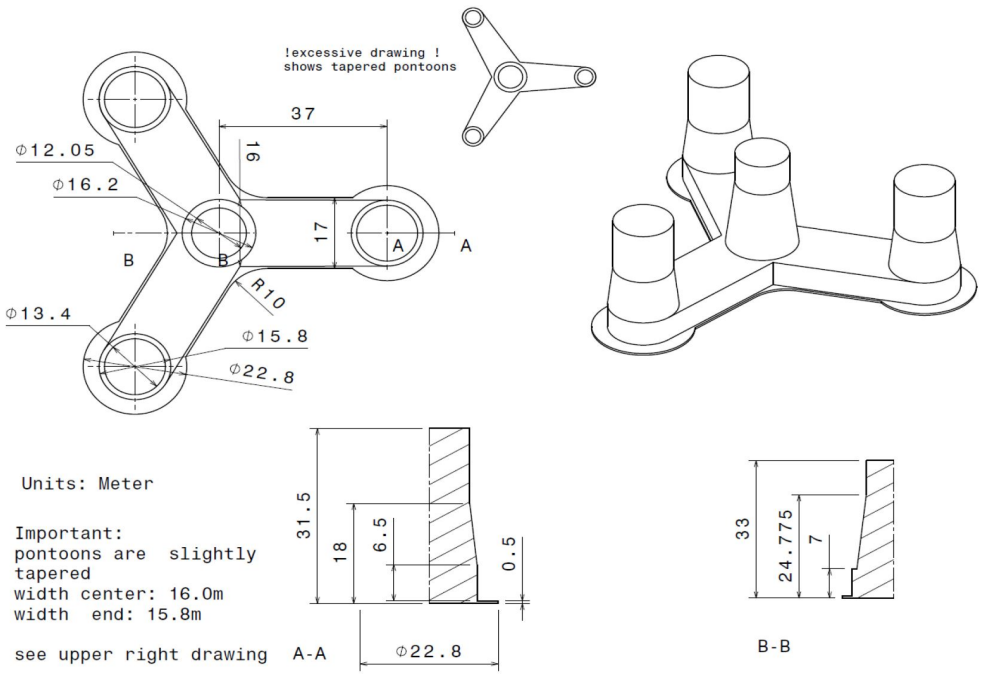

Figure A.4: Dimensions of OO-star semi-sub[35]

A.2.2 Mooring System

The mooring system of OO-star is a catenary system consisting of three chains. A clump mass is attached to each line. The layout and the property of mooring line can be seen from Figure A.5 and Table A.7.

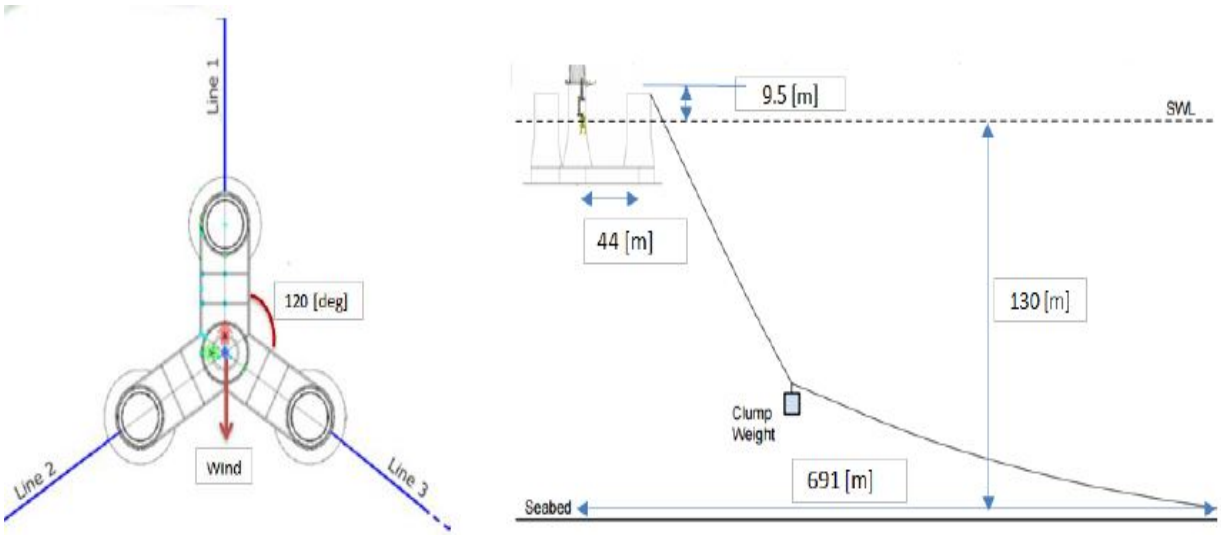

Figure A.5: OO-star mooring line arrangement

Dimension and Property	
Number of mooring lines	3
Angle between adjacent lines	120°
Equivalent total mass in water of the clump mass	500,00kg
Vertical distance to fairleads above MSL	9.5m
Radius to fairleads from platform centerline	44m
Radius to anchors from platform centerline	691m
Anchor position below MSL	130m
Unstretched mooring line length, upper part	118m
Unstretched mooring line length, lower part	585m
Initial vertical position of the clump mass below MSL	90.45m
Initial radius to the clump mass from centerline	148.6m
Pretension	1.67E+6N
Equivalent mass per length in air	375.4kg/m
Equivalent weight per length in water	3200.6N/m
Effective hydraulic diameter of the chain	0.246m
Physical chain diameter	0.137m
Equivalent mooring line axial stiffness	1.506E+9N

Table A.7: OO-star mooring line properties

A.3 NAUTILUS-10 Semi-Sub

A.3.1 Geometry and Properties

NAUTILUS-10 consists of four outer columns as shown in Figure A.6. The tower diameter and thickness are modified. However, the tower top mass properties, namely RNA, hub and blades, remains the same as DTU 10MW turbine.

Dimension and Property	
Total Draft	18.33m
Distance to floater top above MSL	7.67m
Outer columns diameter	10.5m
Distance between columns	54.75m
Total mass, including ballast	7,781tons
Center of mass below MSL	14.28m
Pitch inertia about CM	4,829,000tons·m^2
Displaced water volume	9,281m^3
Center of buoyancy below MSL	11.82m

Table A.8: Properties of NAUTILUS

Figure A.6: Illustration of NAUTILUS[35]

Dimension and Property	DTU 10MW
Tower density	8,500kg/m^3
Young's modulus	210GPa
Tower bottom elevation	7.67m
Tower top elevation	114.67m
Hub height	118.39m
Tower top diameter	5.5m
Tower base diameter	10.5m
Tower top thickness	37mm
Tower base thickness	40mm
Tower mass	879.4tons
RNA mass	676.7tons
Center of mass above MSL	54.9m

Table A.9: Wind turbine properties

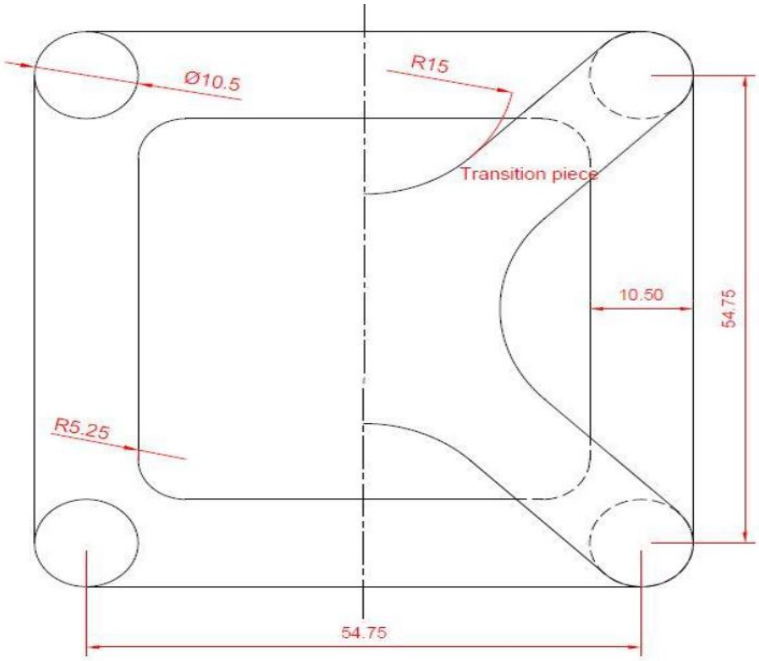

Figure A.7: Dimensions of NAUTILUS semi-sub[35]

A.3.2 Mooring System

The mooring line system of NAUTILUS-10 is a catenary system consisting of four chains.

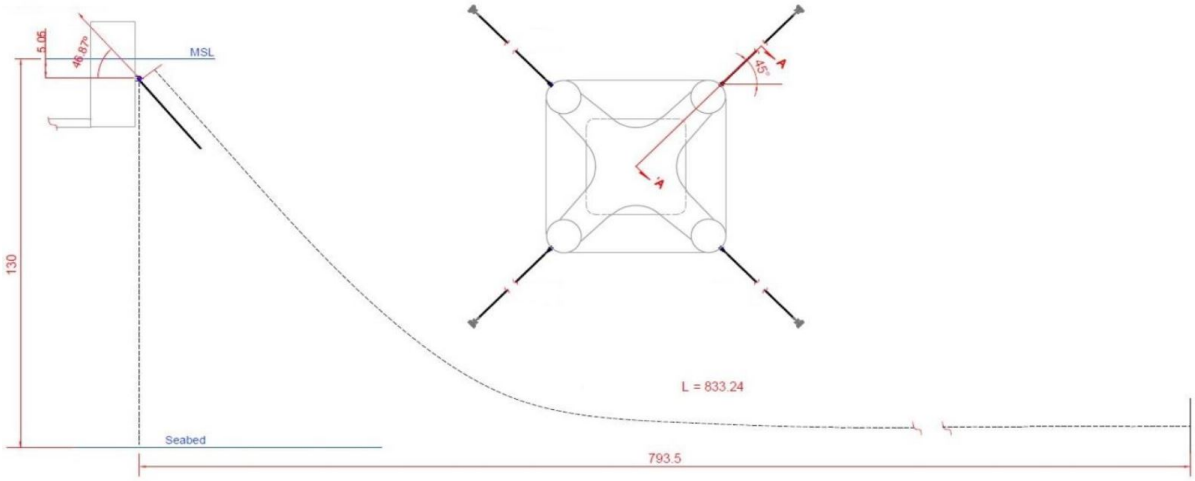

Figure A.8: NAUTILUS-10 mooring line arrangement

Dimension and Property	
Number of mooring lines	4
Angle between adjacent lines	90°
Vertical distance to fairleads below MSL	6.33m
Radius to fairleads from platform centerline	44m
Radius to anchors from platform centerline	837.5m
Anchor position below MSL	130m
Unstretched mooring line length	833.24m
Pretension	4.06E+6N
Equivalent mass per length in air	188.2kg/m
Physical chain diameter	0.097m
Equivalent mooring line axial stiffness	8.04E+8N

Table A.10: NAUTILUS-10 mooring line properties

A.4 Tian-10 TLP

A.4.1 Geometry and Properties

The selected TLP configuration is taken from Master thesis "Design, Numerical Modelling and Analysis of TLP Floater Supporting the DTU 10MW Wind Turbine[54]", which has the same platform geometry and mooring system as Phd thesis "Design and Dynamic Analysis of Tension Leg Platform Wind Turbines[1]", but the size is upscaled to support DTU 10MW reference turbine.

Dimension and Property	
Total Draft	35.3m
Distance to floater top above MSL	10m
Center column diameter	19.8m
Center column length h	45.3m
Spokes radius r_p	39.6m
Spokes height h_p	8.5m
Spokes width w_p	8.5m
Total mass, including ballast	8,121tons
Center of mass below MSL	26.87m
Pitch inertia about CM	tons·m^2
Displaced water volume	17,362m^3
Center of buoyancy below MSL	22.67m
Water depth	200m

Table A.11: Properties of TLP

Figure A.9: Illustration of TLP[54]

Dimension and Property	**DTU 10MW**
Tower density	8,500kg/m^3
Young's modulus	210GPa
Tower bottom elevation	10m
Tower top elevation	115.63m
Hub height	119m
Tower top diameter	5.5m
Tower base diameter	8.3m
Tower top thickness	21mm
Tower base thickness	42mm
Tower mass	605tons
RNA mass	676.7tons
Center of mass above MSL	89.98m

Table A.12: Wind turbine properties

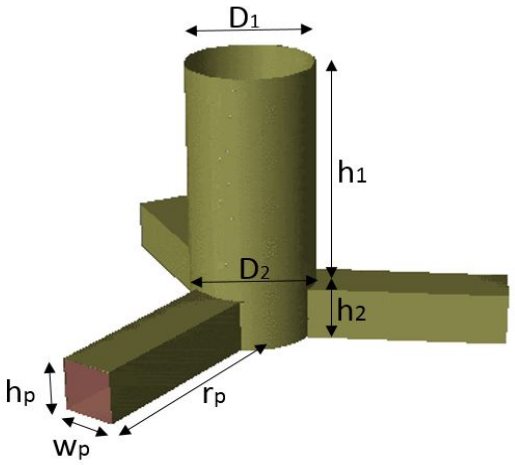

Figure A.10: Dimensions of TLP hull[54]

A.4.2 Mooring System

Dimension and Property	
Number of mooring lines	3
Outer radius	1.35m
Inner radius	1.26m
Density	7850kg/m^3
Area moment of inertia	0.623m^4
Young's modulus	2.11E+11Pa
Mass per unit length	5737kg/m
Tether stiffness	931.8MN/m
Unstretched tether length	164.7m
Pretension per line	28.1MN

Table A.13: TLP tether mooring properties

Appendix B

Numerical Linearization of Mooring Lines

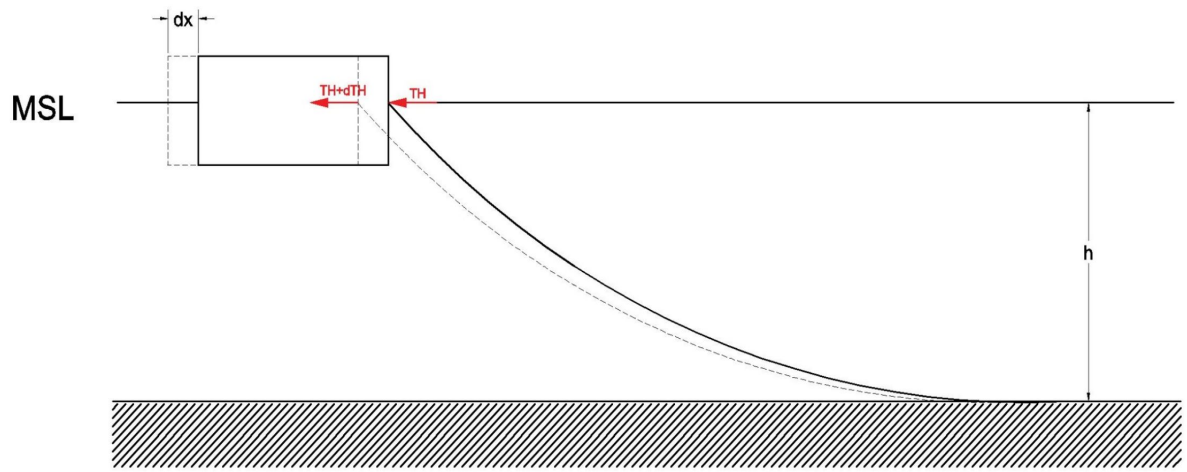

Figure B.1: Simple numerical test for mooring stiffness

The steps of estimating the equivalent stiffness is as follows

1. Set up mooring line configuration
2. Run static analysis and extract the horizontal tension T_H at the fairlead
3. Assign a small offset dx and run static analysis again

4. Extract new horizontal tension $T'_H = T_H + dT_H$
5. Calculate the slope $\frac{dT_H}{dx} = k_i$, which is the equivalent stiffness for one mooring line
6. Compute the overall equivalent stiffness by $K_{mr} = \sum_{i=1}^{n} k_i \cos^2\theta_i$ (equation 2.37)

The surge offset dx is set to 0.1m. The clump weight in OO-star mooring system is modeled by a concentrated mass.

The test results of three catenary mooring system (Xue-10, OO-star, NAUTILUS-10) are as follows

Xue-10 Spar

$$k_i = \frac{dT_H}{dx} \approx 60,000 N/m$$
$$K_{mr} = \sum_{i=1}^{3} k_i \cos^2\theta_i = 90,000 N/m$$
$$(\theta_1 = 0, \quad \theta_2 = \frac{2\pi}{3}, \quad \theta_3 = -\frac{2\pi}{3})$$

dx[m]	T_H[N]
0	2.063E+6
0.1	2.069E+6

Table B.1: Xue-10 mooring test results

OO-star Semi-Sub

$$k_i = \frac{dT_H}{dx} \approx 27,500 N/m$$
$$K_{mr} = \sum_{i=1}^{3} k_i \cos^2\theta_i = 41,250 N/m$$
$$(\theta_1 = 0, \quad \theta_2 = \frac{2\pi}{3}, \quad \theta_3 = -\frac{2\pi}{3})$$

dx[m]	T_H[N]
0	8.3982E+5
0.1	8.4257E+5

Table B.2: OO-star mooring test results

NAUTILUS-10 Semi-Sub

$$k_i = \frac{dT_H}{dx} \approx 22,300N/m$$
$$K_{mr} = \sum_{i=1}^{3} k_i \cos^2\theta_i = 44,600N/m$$
$$(\theta_1 = 0, \quad \theta_2 = \frac{2\pi}{3}, \quad \theta_3 = -\frac{2\pi}{3})$$

dx[m]	T_H[N]
0	3.9736E+5
0.1	3.9959E+5

Table B.3: NAUTILUS mooring test results

The equivalent stiffness of NAUTILUS can also be calculated analytically. The parameters required to calculate the equivalent stiffness are horizontal pre-tension T_H, mooring line weight per length in water w and the water depth h.
The computed equivalent stiffness k_i from analytical solution is 22,123N/m and the whole mooring line system $K_{mr} \approx 2k_i \approx$ 44,246 N/m, which are close to the result from numerical test.

Appendix C

Model Validation

C.1 Rigid Model

The model is validated based on natural periods calculated by modal analysis compared with the corresponding reference literature. The undamped natural periods from modal analysis can only tell whether the mass and stiffness of the system are described correctly.

Therefore, it has to be noted that the validation in this section does not validate the damping nor the external force and it only assures whether the dynamic properties of the structure is well described or not.
The results are listed in Table C.1, C.2, C.3, C.4 together with values from the literature.

Natural period[s]	**Rigid model**	**Xue's thesis**[57]	**Difference**
Surge	107.3	103.3	+3.8%
Pitch	38.07	38.97	−2.3%
1st Tower Bending	2.33	2.50	−6.8%

Table C.1: Natural period of Xue-10 spar

Natural period[s]	**Rigid model**	**LIFES50+**[36]	**Difference**
Surge	196.28	185.19	+6.0%
Pitch	30.09	31.65	−2.4%
1st Tower Bending	1.25	1.27	−1.6%

Table C.2: Natural period of OO-star semi-sub

Natural period[s]	**Rigid model**	**LIFES50+**[36]	**Difference**
Surge	116.25	117.65	−1.2%
Pitch	27.75	29.41	−5.6%
1st Tower Bending	1.86	1.90	−2.1%

Table C.3: Natural period of NAUTILUS-10 semi-sub

Natural period[s]	**Rigid model**	**Tian's thesis**[54]	**Difference**
Surge	43.98	45.23	−2.8%
Pitch/Bending	0.5	0.6	−16.7%
1st Tower Bending	3.31	3.49	−5.2%

Table C.4: Natural period of Tian-10 TLP

It can be found that in general the rigid model gives reasonable results with acceptable errors. For rigid body modes(surge and pitch), their accuracy depends mainly on mooring line stiffness and restoring hydrostatic stiffness respectively. For TLP system, the high pitch stiffness result in a high frequency pitch/bending coupled mode instead a rigid body pitch mode. In addition, the reason of the appeared high error in TLP pitch/bending mode might be due to that the natural period of pitch/bending mode in the literature was found by decay test in the time domain, which means it was damped natural period.

C.2 Flexible Model

The validation of the flexible model is done by having a high stiffness of the hull and compare the natural periods and mode shapes to rigid model. The name "stiff flexible"

is used to refer to the flexible model with a high stiffness of the hull. A high Young's modulus $E = 2.1\text{E+}5\text{GPa}$ is assigned for the stiff flexible case

Natural period[s]	**Stiff Flexible**	**Rigid**	**Difference**
Surge	108.4	107.4	+0.9%
Pitch	37.8	38.1	−0.8%
1st tower bending	2.33	2.3	+1.3%

Table C.5: Natural periods of stiff flexible and rigid model

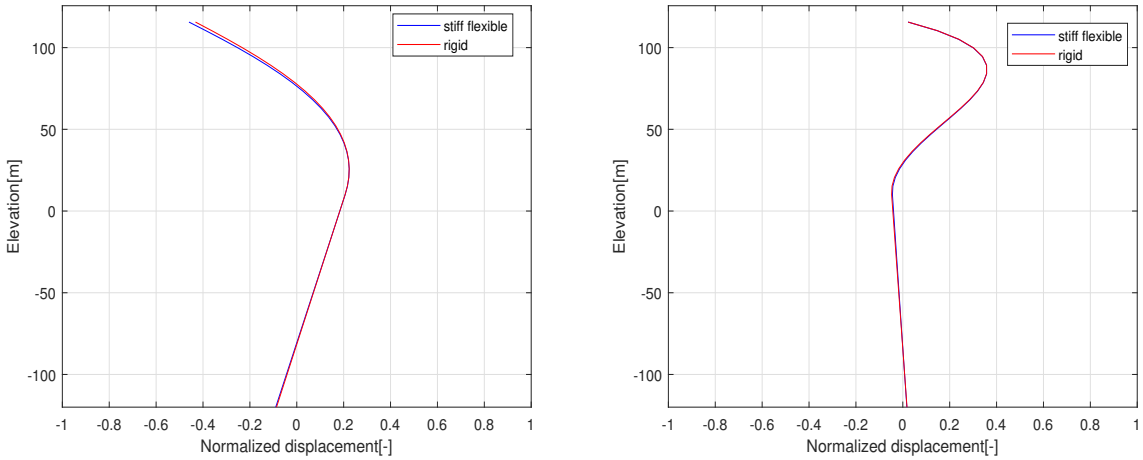

(a) 1st tower bending mode (MAC= 1) **(b)** 2nd tower bending mode (MAC= 1)

Figure C.1: Mode shapes from stiff and rigid model

It can be seen that both natural periods and mode shapes are agreed with the results from rigid model. It should noted that this way of validation can only check whether the mass distribution after including ballast and the recalculated added mass distribution are consistent with the rigid model.

Appendix D

Modal Approach

In addition to finite element method, another alternative to model a flexible spar is modal approach, which utilize generalized modes to describe the flexible deformation of the spar. The advantage of modal approach is a more compact model with less degree of freedoms. It is possible to include one bending mode of the spar as an additional DOF into the system and result in 3-DOFs for the floater.

The additional DOF ϕ is found by clamping the top end of the spar and extracting the first bending mode as shown in Figure D.1. The modal mass and modal stiffness of the third DOF of the spar and the coupled terms with surge and pitch can be formulated based on the spar bending mode shape[44][6]. Once the floater matrix is formulated, a master-salve transformation matrix can be used to couple the spar and the wind turbine

$$\begin{bmatrix} u_1 \\ u_2 \\ \phi \\ u_3 \\ u_4 \\ u_5 \\ u_6 \\ \vdots \\ u_{m+2} \end{bmatrix} = \begin{bmatrix} 1 & 0 & 0 & 0 & 0 & \cdots \\ 0 & 1 & 0 & 0 & 0 & \cdots \\ 0 & 0 & 1 & 0 & 0 & \cdots \\ 1 & h & 0 & 0 & 0 & \cdots \\ 0 & 1 & 0 & 0 & 0 & \cdots \\ 0 & 0 & 1 & 0 & 0 & \cdots \\ 0 & 0 & 0 & 1 & 0 & \cdots \\ 0 & 0 & 0 & 0 & 1 & \cdots \\ \vdots & \vdots & \vdots & \vdots & \ddots & \end{bmatrix} \begin{bmatrix} u_1 \\ u_2 \\ \phi \\ u_5 \\ u_6 \\ \vdots \\ u_{m+2} \end{bmatrix} \tag{D.1}$$

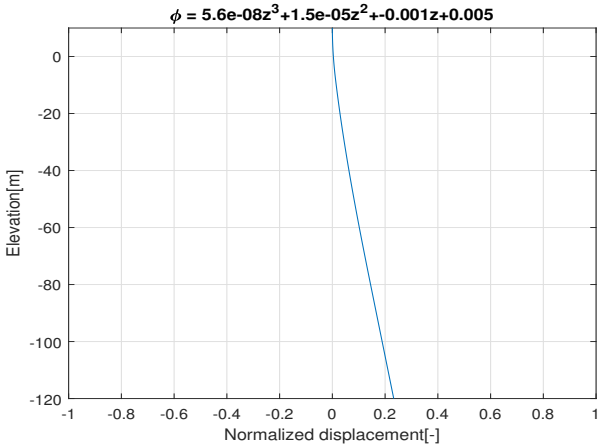

Figure D.1: Spar 1st bending mode

The resultant natural periods(Table D.1) and mode shapes(Figure D.2) are compared together with the results from finite element model. It is shown that modal approach gave good result for 1st tower bending. The larger difference in 2nd tower bending is expected because only the first bending mode of the spar is included into the model.

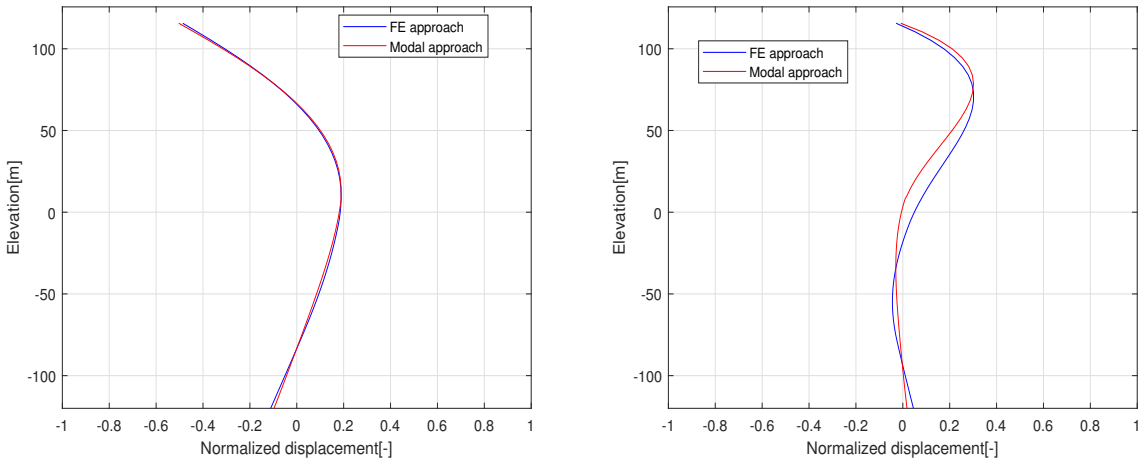

(a) 1st tower bending mode (MAC= 0.99) **(b)** 2nd tower bending mode (MAC= 0.91)

Figure D.2: Mode shapes from FE approach and modal approach

Natural Period[s]	**Modal approach**	**FE approach**	**Difference**
Surge	108.5	107.8	+0.7%
Pitch	38.7	38.4	+0.8%
1^{st} tower	2.73	2.82	−2.0%
2^{nd} tower	0.63	0.72	−13.0%

Table D.1: Natural period from FE and modal approach

References

[1] Bachynski, E., E., 2014. *Design and Dynamic Analysis of Tension Leg Platform Wind Turbines*. Phd thesis, Norwegian University of Science and Technology

[2] Bachynski, E., E., Kvittem, M., I., Luan, C., Moan, T. 2014. *Wind-Wave Misalignment Effects on Floating Wind Turbines: Motions and Tower Load Effects*. Journal of Offshore Mechanics and Arctic Engineering. NOVEMBER 2014, Vol. 136

[3] Bailey, H. et al, 2010. *Assessing underwater noise levels during pile-driving at an offshore wind farm and its potential effects on marine mammals* . Marine Pollution Bulletin 60 (2010) 888–897

[4] Bak, C. et al, 2013. *Description of the DTU 10 MW Reference Wind Turbine*. DTU Wind Energy Report-I-0092.

[5] Bir, G., Jonkman, J., 2008 *Modal Dynamics of Large Wind Turbines with Different Support Structures*. ASME 27th International Conference on Offshore Mechanics and Arctic Engineering (OMAE2008)

[6] Borg, M., Hansen, A., M., Bredmose, H., 2016 *Floating substructure flexibility of large-volume 10MW offshore wind turbine platforms in dynamic calculations*. DTU Wind Energy, Technical University of Denmark.

[7] Borg, M., Hansen, A., M., Bredmose, H., 2017 *Elastic deformations of floaters for offshore wind turbines: dynamic modelling and sectional load calculations*. ASME 36th International Conference on Ocean, Offshore and Arctic Engineering (OMAE2017).

[8] Bredmosea, H. et al, 2017. *The Triple Spar campaign: Model tests of a 10MW floating wind turbine with waves, wind and pitch control.*. 14th Deep Sea Offshore Wind R&D Conference, EERA DeepWind'2017, Trondheim, Norway.

[9] Butterfield, S., Musial, W., Jonkman, J., Sclavounos, P., 2007. *Engineering Challenges for Floating Offshore Wind Turbines*. NREL/CP-500-38776.

[10] *Carbon Trust*. Retrieved July 08, 2019, from https://www.carbontrust.com/offshore-wind/

[11] Chrysagis, G., 2016 *Comparison of coupled aero-hydro-servo-elastic simulations for floating wind turbines with model tests*. Delft University of Technology, the Netherlands.

[12] Cordle, A., Jonkman, J., 2011. *State of the Art in Floating Wind Turbine Design Tools* . 21st International Offshore and Polar Engineering Conference.

[13] DNVGL, 2010 *Environmental conditions and environmental loads*.

[14] DNVGL, 2011 *Fatigue Design of Offshore Steel Structures*.

[15] DNVGL, 2013 *Design of Floating Wind Turbine Structures*.

[16] Faltinsen. O., M., 1990. *Sea Loads on Ships and Offshore Structures*. Cambridge University Press

[17] Felippa, C., A., 2004. *Introduction to Finite Element Methods*. Aerospace Engineering Sciences Department of the University of Colorado at Boulder.

[18] Garrad, A., D., 1990 *Forces and Dynamics of Horizontal Axes Wind Turbines*. In: Freris, L., L., "Wind 422 Energy Conversion Systems". Prentice-Hall, New York, NY, 119-142.

[19] Hasselmann, K., et al, 1973. *Measurements of Wind-Wave Growth and Swell Decay during the Joint North Sea Wave Project(JONSWAP)*. Ergänzungsheft zur Deutschen Hydrographischen Zeitschrift, A(8) No.12.

[20] Hegseth, J., M., Bachynski, E., E., 2019. *A semi-analytical frequency domain model for efficient design evaluation of spar floating wind turbines*. Marine Structures 64 (2019) 186–210

[21] Hess, J., L., Smith, A., O., M., 1972 *Calculation of potential flow about arbitrary bodies*. Report No. MDC J5679-01, Douglas Aircraft Co., Long Beach, California.

[22] Huang, L., L., Riggs, H., R., 2000. *The hydrostatic stiffness of flexible floating structures for linear hydroelasticity*. Marine Structures 13 (2000) 91-106

[23] Jain, A. K., 1997 *Nonlinear coupled response of offshore tension leg platforms to regular wave forces*. Ocean Engineering, 24(7), pp.577-592.

[24] Johannessen, K., Meling, T., S., Haver, S., 2002. *Joint Distribution for Wind and Waves in the Northern North Sea*. International Journal of Offshore and Polar Engineering Vol. 12, No. 1, March 2002 (ISSN 1053-5381)

[25] Jonkman, J., M., Buhl, Jr., M., L., 2005. *FAST user's guide*. Technical Report NREL/EL-500-38230

[26] Jonkman, J., M., 2007. *Dynamics Modeling and Loads Analysis of an Offshore Floating Wind Turbine* . Technical Report NREL/TP-500-41958

[27] Jonkman, J. et al, 2009 *Definition of a 5-MW Reference Wind Turbine for Offshore System Development*. NREL/TP-500-38060

[28] Jonkman, J., 2010 *Definition of the Floating System for Phase IV of OC3*. NREL/TP-500-47535.

[29] Jonkman J., Musial, W., 2010. *Offshore Code Comparison Collaboration (OC3) for IEA Task 23 Offshore Wind Technology and Deployment, Chapter 5*. NREL/TP-5000-48191.

Jorgen, F., Mutlu, S., B., 2006. *Hydrodynamics Around Cylinder Structures, Chapter 4*. World Scientific Publishing Co. Pte. Ltd.

[30] Karimirad, M., Moan, T., 2011 *Extreme Dynamic Structural Response Analysis of Catenary Moored Spar Wind Turbine in Harsh Environmental Conditions*. Journal of Offshore Mechanics and Arctic Engineering, Vol. 133.

[31] de Klerk, D., Rixen, D., J., Voormeeren, S., N., 2008 *General Framework for Dynamic Substructuring: History, Review, and Classification of Techniques*. AIAA JOURNAL Vol. 46, No. 5.

[32] Langen, I., Sigbjörnsson, R., 1979 *Dynamisk Analyse AV Konstruksjoner*. Trondheim.

[33] Larsen, T., J., Hansen, A., M., 2007. *How 2 HAWC2, the user's manual*. Roskilde, Denmark: Risø National Laboratory. Denmark. Forskningscenter Risoe. Risoe-R, No. 1597(ver. 3-1)(EN)

[34] Larsen, T., J. et al, 2014. *Benchmark comparison of load and dynamics of a floating 5MW semisub windturbine, using three different hydrodynamic approaches*. DTU Wind Energy Report-I-0239, Technical University of Denmark.

[35] LIFES50+, 2015 *Qualification of innovative floating substructures for 10MW wind turbines and water depths greater than 50m. Deliverable D4.2 Public Definition of the Two LIFES50+ 10MW Floater Concepts.*

[36] LIFES50+, 2018 *Qualification of innovative floating substructures for 10MW wind turbines and water depths greater than 50m. Deliverable D4.5 State-of-the-art models for the two LIFES50+ 10MW floater concepts.*

[37] LIFES50+, 2018 *Qualification of innovative floating substructures for 10MW wind turbines and water depths greater than 50m. Deliverable D4.7 Models for advanced load effects and loads at component level.*

[38] Lomholt, A., K., 2019 *Numerical Study in BHAWC and Validation against Experimental Data of a Model Scaled 10MW Floating Wind Turbine with Active Pitch Control using the TetraSpar Floater.* DTU Wind Energy-M-0231.

[39] Lupton, R., 2014 *Frequency-domain modelling of floating wind turbines.* Doctoral thesis, Department of Engineering, University of Cambridge.

[40] MacCamy, R., C., Fuchs, R., A., 1954. *Wave forces on piles: a diffraction theory.* Beach Erosion Board

[41] MARINTEK, 2018. *SIMA User Guide.*

[42] Newman, J., N., 1994. *Wave effects on deformable bodies.* Department of Ocean Engineering, MIT, Cambridge, Massachusetts 02139, USA.

[43] Ormberg, H., Bachynski, E., E., 2012 *Global analysis of floating wind turbines: Code development, model sensitivity and benchmark study.* The 22nd International Ocean and Polar Engineering Conference. Rhodes, Greece: International Society of Offshore and Polar Engineers.

[44] Pegalajar-Jurado, A., Borg, M., Bredmose, H., 2018. *An efficient frequency-domain model for quick load analysis of floating offshore wind turbines.* Wind Energ. Sci., 3, 693–712.

[45] Price, W., G., Wu, Y., 1985. *Hydroelasticity of marine structures.* Elsevier Science Publishers B.V., 1985. p. 311-37.

[46] Robertson, A., 2014 *Offshore Code Comparison Collaboration Continuation Within IEA Wind Task 30: Phase II Results Regarding a Floating Semisubmersible Wind System.* NREL/CP-5000-61154.

[47] Roddier, D. et al, 2010 *Wind-Float: A floating foundation for offshore wind turbines*. Journal of Renewable and Sustainable Energy, 2(3):33104.

[48] SENJANOVIĆ, I., HADŽIĆ, N., VLADIMIR, N., 2011. *Restoring Stiffness in the Hydroelastic Analysis of Marine Structures*. BRODOGRADNJA 62(2011)3, 265-279

[49] Shim, S., Kim, M., H., 2008 *Rotor-Floater-Tether Coupled Dynamic Analysis Of Offshore Floating Wind Turbines*. The Eighteenth International Offshore and Polar Engineering Conference, 6-11 July, Vancouver, Canada.

[50] de Souza, C., E., S., Bachynski, E., E., 2018. *EFFECTS OF HULL FLEXIBILITY ON THE STRUCTURAL DYNAMICS OF A TLP FLOATING WIND TURBINE*. OMAE2018-77310.

[51] Stiesdal, H., 2017 *TetraSpar Industrialized Floating Foundation*.

[52] Svendsen, K., 2016 *Structural Design and Dynamic Analysis of a Tension Leg Platform Wind Turbine, Considering Elasticity in the Hull*. MSc Thesis. European Wind Energy Master Program.

[53] Tempel, J., van der., 2006. *Design of Support Structures for Offshore Wind Turbines*. Phd thesis

[54] Tian, X., 2016. *Design, Numerical Modelling and Analysis of TLP Floater Supporting the DTU 10MW Wind Turbine*. MSc thesis, Norwegian University of Science and Technology.

[55] *Vindeby offshore wind farm, 4C Offshore*. Retrieved June 30, 2019, from https://www.4coffshore.com/windfarms/vindeby-denmark-dk06.html

[56] WAMIT, Inc. *WAMIT user manual Version 7.3*.

[57] Xue. W., 2016. *Design, numerical modelling and analysis of a spar floater supporting the DTU 10MW wind turbine*. MSc thesis, Norwegian University of Science and Technology.

TU Delft NTNU SIEMENS Gamesa RENEWABLE ENERGY